Performance Assessment of Rotating Detonation Engines

Development of a Thermo-Chemical Analysis Model

M. N. Lengkeek

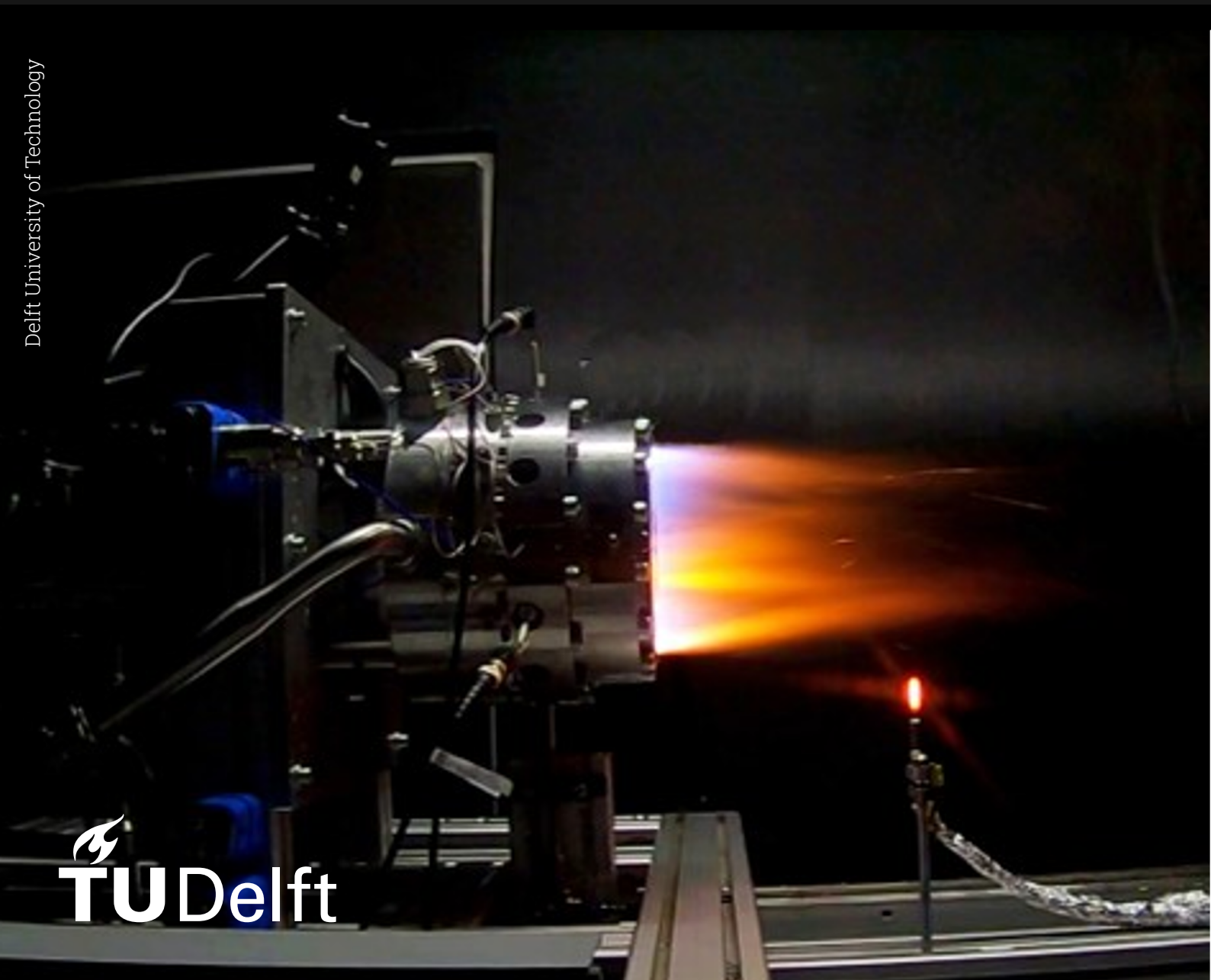

Delft University of Technology

TU Delft

Performance Assessment of Rotating Detonation Engines

Development of a Thermo-Chemical Analysis Model

by

M. N. Lengkeek

to obtain the degree of Master of Science at the Delft University of Technology,
to be publicly defended on Thursday, 5 December 2024 at 8:30.

TU Delft Supervisor:	Dr. B.V.S. Jyoti
TNO Supervisor:	Dr. Tim Roos
Project Duration:	April 2024 - December 2024
Faculty:	Faculty of Aerospace Engineering, Delft

An electronic version of this thesis is available at `http://repository.tudelft.nl/`.

Cover: Rotating Detonation Engine test performed by DefendTex/RMIT, Australia

TU Delft

Preface

This thesis marks the end of my studies at the TU Delft. Over the past few years, I have had the privilege of delving deep into the field of aerospace engineering, a journey that has been both challenging and immensely rewarding. My work in the student rocketry club DARE in particular provided me with a wealth of experience in the field of rocketry, propulsion systems and management. These experiences have not only broadened my technical skills but also ignited a passion for innovation and problem-solving in the field.

Being an engineer, to me, means being a life of learning and problem solving. Although I am leaving the university behind me, I will continue the cycle of trying, doing, and learning that has become so familiar to me over the past few years. I've found that engineering is rarely a solitary endeavour; it requires teamwork and effective communication. This realization has shaped my approach to both academic and professional challenges, and I would like to recognise everyone I've worked with over the last few years, in DARE, in my studies, and in my forays into professional life.

My journey with this research topic started with the proposal for a test setup for Rotating Detonation Engines, my internship. And it grew from there to my thesis: developing a fully validated performance assessment tool for these Rotating Detonation Engines. I would like to extend my heartfelt thanks to Tim for bringing this topic to the Netherlands, and allowing me to be part of it from the start. His boundless knowledge and enthusiasm on the topic, and his exceptional supervision have significantly augmented the quality and depth of my thesis.

The support and guidance I received from my colleagues at TNO were invaluable, and I am particularly grateful to Wolter Wieling and Jos van den Brand, alongside Tim, for their help and support with the test design, set-up and execution. I would also like to thank the remainder of my colleagues at TNO for their mentorship and encouragement.

I would also like to thank my supervisor, Jyoti, for her support and the freedom she granted me during this project.

Finally, I want to express my gratitude to my family and friends for their unwavering support. A special thanks to my partner, Martijn, for his patience and encouragement throughout this process, and his uncanny ability to stand-in as a rubber duck. Your belief in me has been a constant source of motivation.

As I look forward to the next phase of my life, I am excited about the opportunities and challenges that lie ahead. This thesis is not just the culmination of my studies but the beginning of a new chapter in my journey as an engineer.

M. N. Lengkeek
Delft, December 2024

Summary

The purpose of this thesis is to explore the development, validation, and usage of a thermo-chemical performance assessment model for a Rotating Detonation Engine (RDE). This research addresses a knowledge gap in the development of performance models of RDE's, and will allow the client to make rapid prototyping performance assessments.

A RDE is a type of propulsion system that uses continuous detonation waves travelling around an annular combustion chamber to produce thrust. This method of generating propulsion is up to a theoretical 20% more efficient than a deflagration engine due to the nature of the detonation reactions taking place. The detonation reaction results in a lower entropy release for the same amount of heat addition, enabling the production of a greater amount of work.

The higher efficiency of the engine reduces the consumption of harmful fuels, enabling the use of less efficient but cleaner alternatives. This shift not only lowers emissions but also promotes a more sustainable alternative to rockets, thrusters and other space-based applications.

The objective of this thesis is to develop a thermo-chemical analysis model of an RDE, and use this to investigate the impact of geometries and operating conditions on the performance of this RDE. The objective is split into three research questions, regarding the creation, validation, and usage of the thermo-chemical analysis model. This research is conducted in collaboration with TNO, aiming to provide a well validated model for further development of RDE's in the future.

The model is created using a combination of RDE-specific and general techniques found in literature, combined in a novel manner to limit the number of input parameters required. The time- and space-dependant processes within an RDE have been translated into a steady 1-dimensional (1D) model. At each thermodynamic station defined in the RDE, the flow properties are derived, in addition to the full RDE performance parameters: pressure gain, thrust, specific impulse (Isp), combustion efficiency, and detonation velocity. The implementation of losses originating from non-premixed propellants and non-ideal combustion in a full RDE model are among the two most significant contributions to the model and field of research.

The validation of the model is performed using data gathered from a test campaign performed at TNO, using an RDE with modular geometry and mass flows varying from 0.3 to 1.5 kg/s. In total the data of 82 different RDE tests was used in the model validation. The validation results show a promising maximum mean deviation of 6% in one of the selected validation parameters, with the remainder mostly remaining below 5% variation. In comparison, models from literature require a larger degree of test or computational Fluid Dynamics (CFD) data and have an accuracy of 2-30%, underlining the excellent accuracy of the model developed in this thesis.

The model was used in an assessment of the impacts of various inputs on RDE performance. Here it was found that the main geometric feature of RDE's, the injector to throat area ratio has a significant impact on pressure gain, while the mass flow and equivalence ratio have a larger impact on the detonation velocity, specific impulse and thrust. Additionally it was found that peak combustion efficiency occurs not at stoichiometric propellant ratios, but just before.

Lastly, three recommendation are shared for the improvement of this model; the addition of new propellants including liquid fuels, an investigation into the impact of the single detonation wave assumption, and the potential addition of more RDE phenomena. In addition, it was recommended that the performance assessment undertaken a part of this thesis be further expanded upon as a follow-up study on RDE performance parameters.

Contents

List of Figures

List of Tables

Nomenclature

Abbreviations

$C-J$	Chapman-Jouguet
CFD	Computational Fluid Dynamics
$CTAP$	Capillary Tube Attenuated Pressure
DDT	Deflagration to Detonation Transition
$DRDE$	Disk-shaped Rotating Detonation Engine
Isp	Specific Impulse
LHV_{fuel}	Lower heating value of fuel
MCF	Mass Capture Fraction
OF	Oxidiser to Fuel (ratio)
OFR_{stoich}	Stoichiometric oxidiser to fuel ratio
PDE	Pulse Detonation Engine
PGC	Pressure Gain Combustion
PGC	Pressure Gain Combustion
$PreDet$	Pre-Detonator
PRF	Pressure Recovery Fraction
RDE	Rotating Detonation Engine
SPY	Entropy, Pressure, Composition
TNO	Nederlandse Organisatie voor Toegepast-Natuurwetenschappelijk Onderzoek
TPY	Temperature, Pressure, Composition
TRL	Technology Readiness Level
ZND	Zeldovich-von Neumann-Doring

Symbols

ΔP	Pressure gain
Δ	Radial thickness of the combustion chamber
A	Cross-sectional area
D_{min}	Minimum chamber diameter
H	Enthalpy
H_{min}	Minimum chamber height
L	Length of the combustion chamber
L_{min}	Minimum chamber length
M	Mach no.
M_{act}	Mach number of the real detonation wave

M_{CJ}	Mach number of CJ detonation wave
P	Pressure
P	Pressure
P_{crit}	Critical pressure for throat choking
P_{decay}	Decay pressure
P_{det}	Detonation pressure
Q_{CJ}	Heat added in a CJ detonation
R_g	Gas constant
U	Internal energy
V	Specific Volume

χ	Heat lost in detonation wave when compared to CJ
$\dot{m_{diff}}$	Difference between input and actual mass flow
$\dot{m_{input}}$	Mass flow given as input to RDE model
$\dot{m_{lost}}$	Mass flow lost in buffer zone
$\dot{m}$	Mass flow
ϵ	Turbulent dissipation rate
η_c	Combustion efficiency
γ	Ratio of specific heats
ω	Non-reacting volume fraction of PaSR
ϕ_g	Global equivalence ratio before the buffer zone
ϕ_{comb}	Equivalence ratio after the buffer zone
ψ	Buffer zone equivalence ratio factor
τ	Non-dimensionalised time in the combustion chamber
τ_c	Turbulent chemical time scale
τ_m	Turbulent mixing time scale
$\tau_{f_{rec}}$	Time of fuel injector recovery
$\tau_{ox_{rec}}$	Time of oxidiser injector recovery
c^*	Characteristic velocity
c_0	Speed of sound in gas mixture
d_c	Diameter of outer combustion chamber wall
h_c	Critical height of the detonation wave
h_d	Height of the detonation wave
h_{min}	Critical chamber height
k	Pressure decay factor
n	Value assigned to the progress of the chemical reaction
n	Value assigned to the progress of the chemical reaction
s_u	Laminar flame speed

v	Kinematic viscosity
v_{eff}	Effective viscosity

Subscripts

2	Plenum station
4	Combustion chamber exit station
s	Static conditions
t	Total conditions

1

Introduction

The world, as we know it, went through a significant fundamental shift when combustion engines were first developed; allowing for the first time for work to be produced using means other than the internal energy in the bodies of us or our animals, or the natural force of gravity. In fact, it is these combustion engines that allowed us to overcome that very same force of gravity and take to the skies and beyond the limits of our planet. However, the usage of those combustion engines will, in many cases, soon be fading away to be replaced by the next innovation; electric engines which can run on greener electricity and reduce the harm to the environment.

One avenue where the combustion engine cannot yet be replaced is in the overcoming of gravity, and the travel to beyond our terrestrial environment. Rocket engines are a form of combustion engine that require such a high thrust to weight ratio they cannot easily be replaced by the heavier electric engines and battery systems. Most basically, these engines function through the principle of momentum in a low friction environment; throwing mass out the back of the rocket to allow it to travel forwards. This principle requires either a large amount of mass, or a large velocity at which it is expelled, achieved by the combustion of a fuel and oxidiser element in a combustion chamber, and the acceleration of this hot, high pressure flow by means of a nozzle. Due to the limited chemical energy stored in these propellants, there is at some point a limit to the rocket acceleration that can be achieved using certain propellant combinations.

Unfortunately, the most well-known propellant combinations which provide sufficient energy to accelerate orbital rockets are either toxic to the environment, or non-renewable fossil fuels. To reduce the harm on the environment and the usage of non-renewable resources, the rocket engines must be made as efficient as possible. While higher efficiency engines can lead to a reduction in fuel used, it can also lead to a higher chemical energy extraction, and hence a higher maximal acceleration that can be achieved with a propellant combination, thereby allowing the usage of less toxic, more renewable fuels for these engines.

A form of rocket engine on which research is just starting to pick up is the Rotating Detonation Engine (RDE). This is a combustion engine which works on the principle of detonation instead of the more common deflagration, thereby running with a almost 25% increase in theoretical efficiency. Research on Rotating Detonation Engines is currently being conducted in many places around the world, with the highest Technology Readiness Level (TRL) research being performed on the in-space test of a RDE by the Japanese Space Agency (JAXA). With current state-of-the-art research, a large gap still remains on the ability to determine the performance of an RDE without using data from tests as an input.

This thesis on Rotating Detonation Engines (RDE's) aims to produce a validated theoretical thermo-chemical analysis model of RDE performance, and to assess how variations in engine geometry affect the performance of this type of engine.

1.1. Rotating Detonation Engines

Rotating Detonation Engines (RDE's) offer the possibility of a substantial increase in thermodynamic cycle efficiency of a combustion engine, shifting from the traditional deflagration-based systems to a more efficient detonation-based approach. In a comparison of detonative and deflagrative combustion, detonation yields a lower entropy increase for an identical heat release, thereby allowing more of the released chemical energy to transform into work performed by the engine.

RDE's can be used in a variety of applications where combustion engines are used, but this thesis will specifically investigate their usage as rocket engines, replacing the solid, liquid, or hybrid engine used in many rocket applications today.

The idea of harnessing the unsteady detonation process as a means of powering the combustion engine idea was first proposed in 1940, and later implemented in the building of the first Pulse Detonation Engine (PDE), an early precursor to the modern RDE. Work on this topic stagnated somewhat in the following years, but has picked up again with the near simultaneous revival of continuously rotating detonation propulsion by researchers in Russia, Poland, and France in the early 2000's. Nowadays, work on RDE's and related branches of detonative propulsion continues in many countries and research institutes, with the first firing of an RDE in The Netherlands in late 2023 at the Nederlandse Organisatie voor Toegepast-Natuurwetenschappelijk Onderzoek (TNO).

1.2. Cooperation

This thesis is undertaken with TNO as client, and is part of the larger set of work on RDE's started in 2023. The aim of the RDE research at TNO is to create an extensive test set-up and simulation suite, allowing The Netherlands to become one of the forerunners on research into RDE's. The work requested by TNO for this thesis involves the creation and validation of a comprehensive performance model of an RDE.

The larger set of work on RDE's by TNO this year encompasses a test campaign on the current TNO RDE engine, performed at the location in Ypenburg. Work for this thesis also includes aiding in the remainder of the preparations and the operation of the test campaign, as the data gathered here is also used for the validation aspect of this thesis.

1.3. Report Structure

The initial part of this thesis is a literature study into the relevant background knowledge. This involves research into the different between detonative and deflagrative combustion presented in chapter 2. Once the required background knowledge of detonation combustion is presented, the literature study delves into the workings and state of the art of Rotating Detonation Engines itself, presented in chapter 3.

It is only after the completion of the literature study, when the reader has the required background information, when the research objectives for this thesis are presented. These, along with the requirements set on the thermo-chemical analysis model, can be found in chapter 4.

The process and the final result in the creation of the thermo-chemical analysis model simulation software is described next in chapter 5. Within this chapter, the structure of the model is first described, followed by the detailed implementation of the relevant fidelity levels of the model. Lastly, a section on the usage of the model is presented.

The TNO test campaign, and the resulting that that will be used in validation is described in chapter 6. The verification and validation of the model is described in chapter 7. This is accompanied by a sensitivity analysis of a number of model input parameters, and an assessment of model accuracy using various test results from literature.

The model is then used to determine the impact of different engine geometries on the performance metrics identified. This is described in chapter 8. Finally, the conclusions of this report are presented, and a number of recommendation for future work on this topic are described in chapter 9.

2

Detonation Combustion

Detonative combustion is a subset of combustion that occurs when flame front velocities are faster than the speed of sound. It is typically used in explosives, however it can also be harnessed and used as a combustion mechanism to drive a propulsive device.

This chapter will first explore the history of detonative combustion, as well as highlight the difference between detonation and deflagration combustion. Additionally, this chapter will explore some thermodynamic cycles that approximate detonative combustion behaviour. These cycles help understand the energy conversion processes involved and provide insights into designing efficient engines

2.1. Detonation vs. Deflagration

When the word 'combustion' is mentioned one typically thinks of the deflagrative kind; a flame of a candle, or a log in a fire. This type of combustion is characterised by a relatively slow flame front, travelling at velocities lower than the speed of sound. The other type of combustion is what typically comes to mind when one mentions the word 'explosion'; detonative combustion. Here the detonation front travels at velocities higher than the speed of sound, and is hence accompanied with a shock wave. In thermodynamic analysis, deflagrative combustion is typically seen as a constant pressure process, while detonation is a constant volume process. In this section the history of, and the phenomena behind, detonation are explained.

The existence of detonations in gaseous mixtures was first shown by Berthelot and Vieille in the early 1880's [1, 2], with the systemic measurements of combustion velocity in a number of gasses. The theory of detonation was further expanded on by the works of Chapman and Jouguet with the proposal for qualitative theories that predicts the detonation velocity of a gaseous mixture [3–5]. These independent theories would later become known as the Chapman-Jouguet detonation theory.

All possible solutions within nature must conform to a solution of the three balance equations: the conservation of mass, momentum and energy. This can be modelled by the combination of the Rayleigh line and the Hugonoit curve [6, 7]. The Rayleigh line is the combination of the mass and momentum equations, and describes the locus of quasi-static thermodynamic state points traced during the flow. In comparison, the Hugoniot curve is based on the conservation of mass, momentum and energy, and establishes the relation between pre- and post-shock combustion flow. Any possible real solutions to combustion must therefore lie on the intersection of these two lines.

Two branches of the Rayleigh line are possible, an upper one corresponding to detonation, and a lower one corresponding to deflagration. These two Rayleigh lines, and the Hugonoit curve can be seen in Figure 2.1 [8].

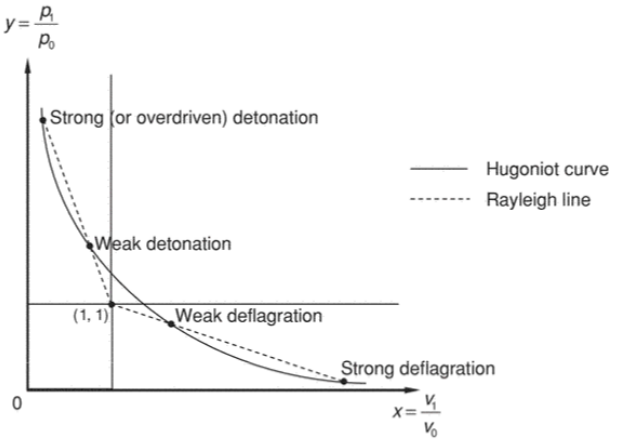

Figure 2.1: The convergence of the Hugoniot curve and the Rayleigh line to form the strong and weak detonation solutions. Taken from *The Detonation Phenomenon* [8]

As can be seen, any Rayleigh line will have two possible intersection points with the Hugonoit curve; corresponding to a so called strong and weak detonation solution. The strong detonation has a much greater pressure and density differences, as well as subsonic product flow, relative to the wave. In contrast, the weak solution has much smaller differences in density and pressure over the detonation wave, and a supersonic product flow relative to the wave [8]. This weak solution is most often seen in nature.

Here both Chapman and Jouguet used similar reasoning to come to the same solution. Chapman argued that the solution with the minimum entropy must be the solution found in nature, while Jouguet argued it must be the minimum velocity solution [3–5]. In this case, both proposals correspond to the steepest possible line in the deflagration, and the most shallow line in the detonation, occurring where the strong and weak solutions converge on each other. This can be visualised in Figure 2.2 as the C-J solution, and this condition is named the tangency condition, representing the idea detonation case [8].

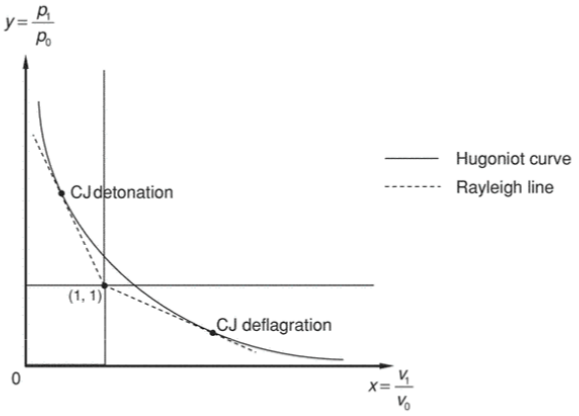

Figure 2.2: The minimum velocity, C-J solution. Taken from *The Detonation Phenomenon* [8]

While this C-J theory provides the link between the equilibrium states between the upstream and downstream flows, it does not yet give the complete picture. Many years later, Zeldovich [9], Von Neumann [10], and Döring [11] described the largely accepted, physical model of the detonation front. This model consists of a leading shock wave, followed by an induction zone where free radicals start appearing, and finally a reaction zone where the recombination of molecules occurs. This model is shown in Figure 2.3, with the shock travelling to the right [8].

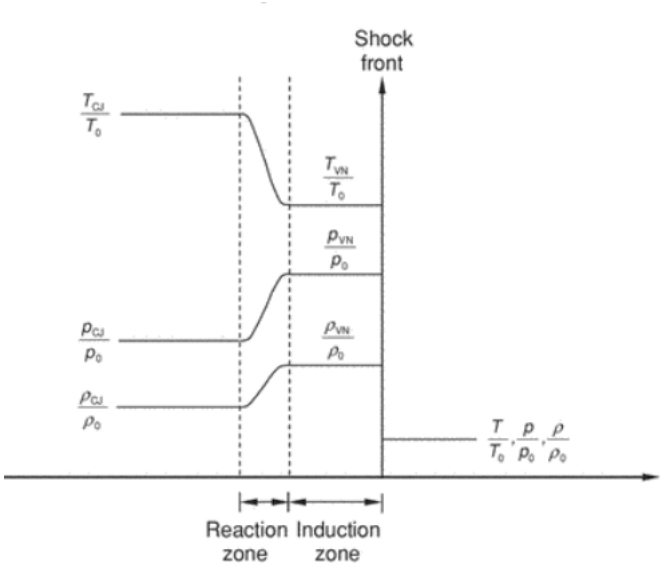

Figure 2.3: The Zeldovich-von Neumann-Doring (ZND) model of a detonation wave. Taken from *The Detonation Phenomenon* [8]

The additional theory for what occurs within the detonation is described by the Zeldovich-von Neumann-Doring (ZND) theory, based on their proposed model of a detonation wave. This theory both incorporates heat and momentum losses, lowering the detonation velocity from that of the C-J theory, as well as introduces intermediate solutions. This is done with the use of a value assigned to the progress of the chemical reaction, n. At each value of n, an intermediate Hugoniot curve can be produced, and thus the thermodynamic states are known at each step of the reaction [8].

This additional theory also introduces the concept of detonation cells. Due to the micro-structure of the detonation wave, the shocks tend to arrange themselves in a grid-like structure, pictured in Figure 2.4 and called detonation cells. The size of these structures is dependant on the propellant combination, and the pressure and temperature [8].

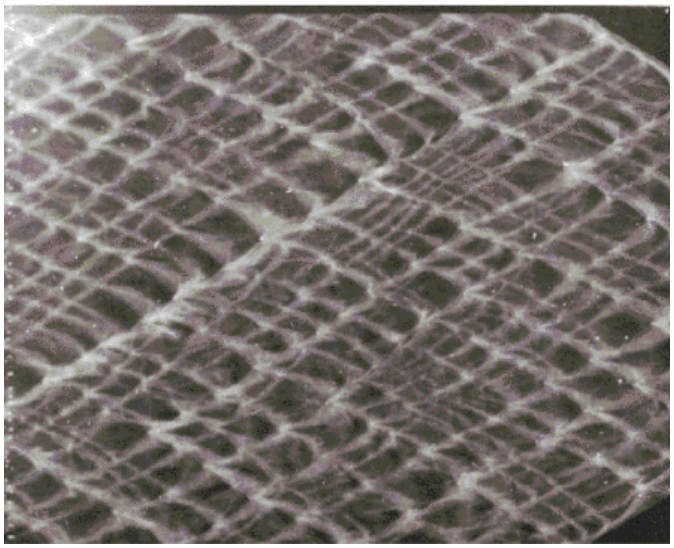

Figure 2.4: An open-shutter photograph of the detonation cell structure in a thin channel. Taken from *The Detonation Phenomenon* [8]

2.2. Thermodynamic Cycles

The classical thermodynamic cycle analysis is one of the fundamental tools for analysing and understanding combustion engines. As this type of approach is typically used for everything from the idealised car engines (the Otto cycle), idealised steam engines (the Rankin cycle), to more complex engine types, it is a useful exercise to compare the cycles that may be relevant to the process occurring with an RDE. This section will highlight a number of the documented cycles shown to be relevant to detonation propulsion, and analyse their value in the understanding of processes within an RDE.

There are four main cycles to be considered here; first the Brayton cycle discovered in 1872 [12] is the cycle used for analysis of turbojets or ramjets. This is a common constant pressure cycle hat gives a good indication of deflagrative behaviour, and provides a baseline as to which the remainder of the cycles can be compared.

Compared to the Brayton's constant pressure process, a detonation can be approximated by a constant volume process, giving the reason for the second cycle. The Humphrey cycle is a modification of the Brayton cycle, where the constant pressure heat addition is replaced by a constant volume process in an attempt to model the detonative nature of the combustion [13]. The Humphrey cycle is relatively simple to implement, however it does not capture the physics behind the detonation combustion, and hence cannot provide an accurate representation of the work performed [14]. Due to its simple implementation, it is often cited as a good representation of the cycle thermal efficiency of detonation engines [13].

Thirdly, the Fickett-Jacobs cycle allows one to compute the work obtained from an unsteady detonation cycle in slightly more detail. It is a more sophisticated model made to account for the pressure risen in a detonation, based on the C-J detonation model which can be approximated using Rayleigh heating in the compression stage. Unfortunately as the model fails to account for the physical processes occurring within the ZND model of detonation, this cycle also underestimates the work performed. [14]

Lastly, the ZND cycle (or PDE cycle as is it often called) captures the physical nature of a one dimensional detonation wave. It is in many aspects identical to the Brayton cycle first discussed, however the process of heat addition is significantly different. First the passing shock wave compresses the gasses to a pressure called the von Neumann spike. Next the reactions involved in the detonation wave are modelled by a constant area heat addition process, before the adiabatic, isentropic expansion process occurs in the same manner as the Brayton cycle. [13, 14]

Each of these thermodynamic cycles are pictured in Figure 2.5. As is common in these types of diagrams, the area within the curve represents the work extraction of the cycle.

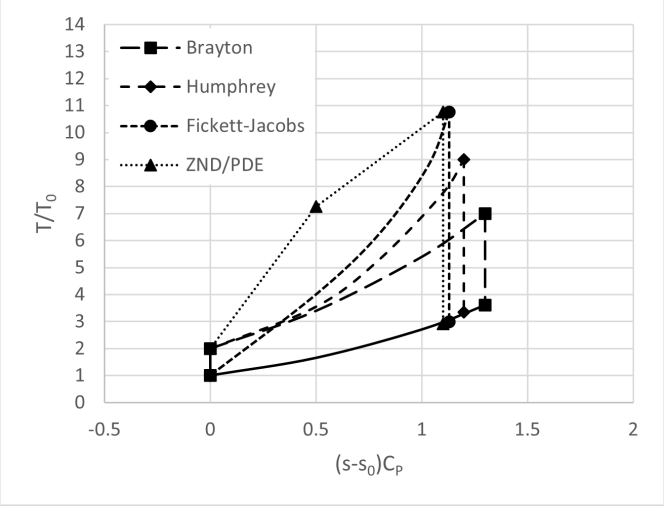

Figure 2.5: A comparison of the four thermodynamic cycles discussed. Adapted from [14] and [13]

The ZND cycle is the current best closed cycle representation of an RDE. It can be seen that this cycle is more efficiency than the Brayton cycle (due to the larger amount of work extracted),and that higher

temperatures are reached within the detonation when compared to the deflagration. This increase in efficiency is the large benefit of RDE's over conventional engines, however this increase in temperature proves a challenge for implementing this engine outside of a short-duration test set-up. Recent research [15–18] has delved into the thermodynamic analysis of an RDE, however there is no agreed cycle definition as of yet.

3

Rotating Detonation Engines

The Rotating Detonation Engine (RDE) is an engine full of complex phenomena; not only is the combustion a detonation as opposed to a deflagration, the entire process is unsteady in both time and space. Combined, these factors make it a difficult engine to numerically or thermodynamically model. However, in comparison to traditional deflagration based engines, RDE's offer a significant potential improvement in combustion efficiency.

This thesis involves the creation of a model to accurately represent the performance of an RDE, and uses that to distinguish key flow and geometry factors that impact the performance. The literature study undertaken as a part of this thesis investigates what is already known about RDE flow parameters, followed by modelling approaches. Lastly, a form knowledge gap in RDE work is identified, and narrowed down with the aid of user requirements developed with TNO as client (see chapter 4). This chapter shares the results of the literature review specifically into RDEs, with a focus on aspects required to model their phenomenon.

First, the operating principles and the various flow phenomena within an RDE are explained. Next, the most important performance characteristics of the RDE are identified, and the effects of these are analysed. The following section provides a brief explanation of the various parts found within a RDE. Subsequently, the state-of-the-art of RDE models is explored, and the advantages and disadvantages of various approached are compared. Finally, a knowledge gap within the field or RDE modelling is identified, based on this state-of-the-art, and some pre-identified user requirements.

3.1. RDE Operating Principles

Rotating Detonation Engines (RDEs) can be divided into two modes of operation; in rocket-mode or airbreathing. The first is typically used in applications where a separate oxidiser tank is required, with space-based or launcher applications coming to mind. An example of a higher performance oxidiser used in rocket-mode operation and testing of RDE's at the current Technology Readiness Level (TRL) is gaseous oxygen [15, 16, 19, 20]. In contrast, airbreathing operation of an RDE involves using the surrounding air as the oxidiser. This is typically used in flight operations staying within the atmosphere, and removes the need for a large oxidiser tank.

A RDE typically consists of a annulus shaped combustion chamber. The propellants, either premixed or non-premixed, are injected at one end (the head-end) and some form of nozzle is attached to the other end (nozzle-end). During operation, one or more detonation waves typically travel in azimuthal direction along the head-end of the chamber, while the propellants predominately have axial velocity. A schematic of a conceptual RDE can be seen in Figure 3.1.

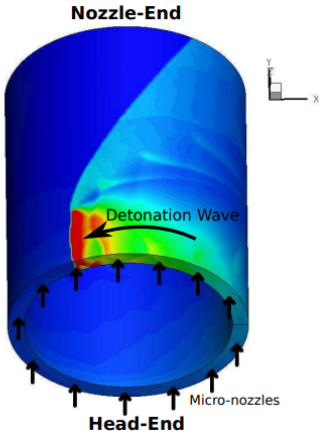

Figure 3.1: Schematic of three-dimensional RDE showing detonation wave. Image from *Schwer and Kailasanath* [21]

As the radial thickness of the cylindrical annulus is typically small compared to the chamber diameter and axial dimension, the flow is typically assumed to have no radial variation. This allows one to 'unwrap' the three dimensional cylinder into a two dimensional plane. Unless stated otherwise, this assumption will also be made for all further discussion on the dynamics within an RDE. This 'unwrapped' flow field can be seen in Figure 3.2 in the form of a temperature solution of a numerical RDE simulation performed by *Schwer and Kailasanath* [22].

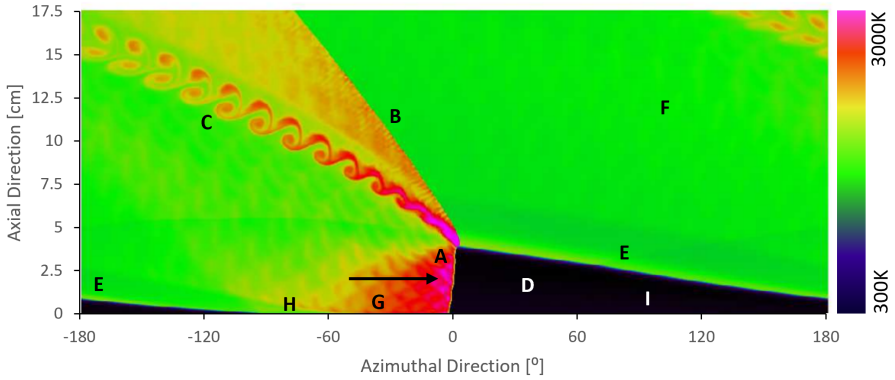

Figure 3.2: Temperature gradient solution of 'unwrapped' RDE solution, showing relevant flow features. Adapted from *Schwer and Kailasanath* [22]

There are a number of important flow features seen in Figure 3.2, these are indicated by the labels. The detonation front is seen at A, it propagates in the positive azimuthal direction (from left to right), and the red-pink area behind the wave indicates the presence of the hot detonation products. The line at B indicates the trailing oblique shock wave caused by the freshly detonated expanding products. If the chamber is sufficiently long, particles may encounter this oblique shock multiple times [20]. The slip line between the freshly detonated and the detonation products one cycle older can be seen at C. The freshly detonated products are less expanded and have a higher temperature, causing the formation of this slip line. Additionally, Kevin-Helmholtz instabilities occur at this slip line due to the large azimuthal velocity differences between these layers [23]. The freshly injected (premixed) reactants are shown in region D. It can clearly be seen that all non-combusted propellants are at the original plenum temperature. Deflagrative burning may spontaneously occur where the fresh propellant comes into contact with the hot detonation products. The propellants that have combusted via deflagrative combustion, and hence have not passed through the detonation wave, can be seen in region E. Region F shows the expansion region with the detonated products.

Regions G, H, and I show the three different propellant injection scenarios. Due to the significant pressure increase with the detonation wave, the injectors are temporarily blocked in region G. As the wave moves from left to right, the detonation products expand and their pressure decreases. This can be seen in region H, where the pressure is less, allowing propellant to flow into the combustion chamber, but still sufficiently high to ensure subsonic flow. Finally in region I, the pressure in the combustion chamber is less than the critical injection pressure, and the combustor inlet is once again sonic [23, 24].

Alongside the general flow field simulations, research has also been performed on the flow of particular particle paths within an RDE. The flow paths of five particles can be seen in Figure 3.3, displayed over the temperature solution adapted from *Schwer and Kailasanath* [22]. In this image, the particles appear in a reference frame attached to the detonation wave, and appear to move from right to left.

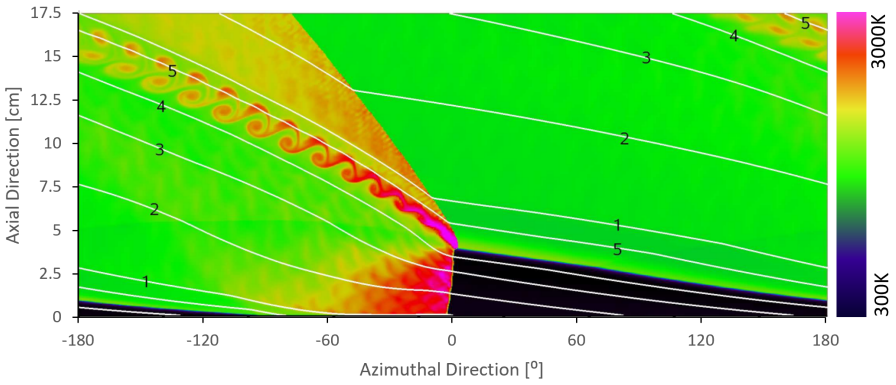

Figure 3.3: Temperature gradient solution of 'unwrapped' RDE solution, showing fluid particle paths in white. Adapted from *Schwer and Kailasanath* [22]

In the analysis by *Schwer and Kailasanath* [22] the particles can be grouped by three types; those that pass through both the detonation wave and the oblique shock wave, those that only pass through the detonation wave, and those that only pass through the oblique shock wave. In the last case, the combustion occurring is deflagration, not detonation. The following explanation of the paths these particles take within the engine is in a wave-fixed reference frame, thus given from the perspective of the particle itself travelling along one of the lines indicated in Figure 3.3.

Particles going through the detonation front are indicated by flow paths two, three and four in Figure 3.3. In this particular case, only those along flow path two also travel through the oblique shock. However this distribution changes with a changing combustion chamber length [23]. After passing through the inlet to the combustion chamber, the detonation front travels over these fresh propellants, moving due to pressure from the expansion of the combustion products behind the detonation front. As they are passing through the detonation front, the density, pressure, temperature and azimuthal velocity of the particles increases rapidly, while the axial velocity decreases. Behind the detonation front the flow will expand, and during the expansion the particle's azimuthal velocity, pressure and density decrease rapidly, while the temperature decreases slightly. The axial velocity significantly increases again due to the expansion process. [22, 25] The flow can then be further expanded through a nozzle or similar process to generate thrust.

In addition to the detonation wave, a portion of particles also goes through the oblique shock wave. An example of such a flow path can be seen in for flow path two in Figure 3.3. The process of going through the oblique shock is similar to the detonation front; the density, pressure, temperature and azimuthal velocity all increase during the passage of the shock, however this increase is significantly less than after the passage of the detonation wave. There is also no heat addition through this shock. These properties decrease and stabilise shortly after due to the mixing with the expanding flow of the detonation process. Only the axial velocity once again increases after the oblique shock wave. [25]

The last case refers to particles which do not pass through the detonation wave, only the oblique shock. This path is shown along flow path five in Figure 3.3. Deflagration of the particle occurs due to the

proximity of the hot combustion products from the previous round. After combustion, the particle encounters the oblique shock wave in the same manner as the other particles, and experiences the same changes in thermodynamic properties. The maximum pressure achieved in this case is also significantly less, and hence the main performance of the RDE is due to the flow particles undergoing the detonative combustion. [22, 25]

There is also another path identified by *Zhou and Wang* [25]. In this case, the particle passes through the detonation front at the very head-end of the chamber, along line one in Figure 3.3, and undergoes a slightly different form of detonation. As this particle is injected just before the detonation wave passes, it passes through the region of detonation wave closes to the head-end of the chamber. A close-up of this structure can be seen in Figure 3.4, and the type of detonation described here occurs at label 1. Here, the particle undergoes combustion just before the induced shock wave, and while the temperature reaches the same maximal level as with the other form of detonative combustion, the pressure only reaches at most 44% of the peak pressure, reducing engine efficiency [25].

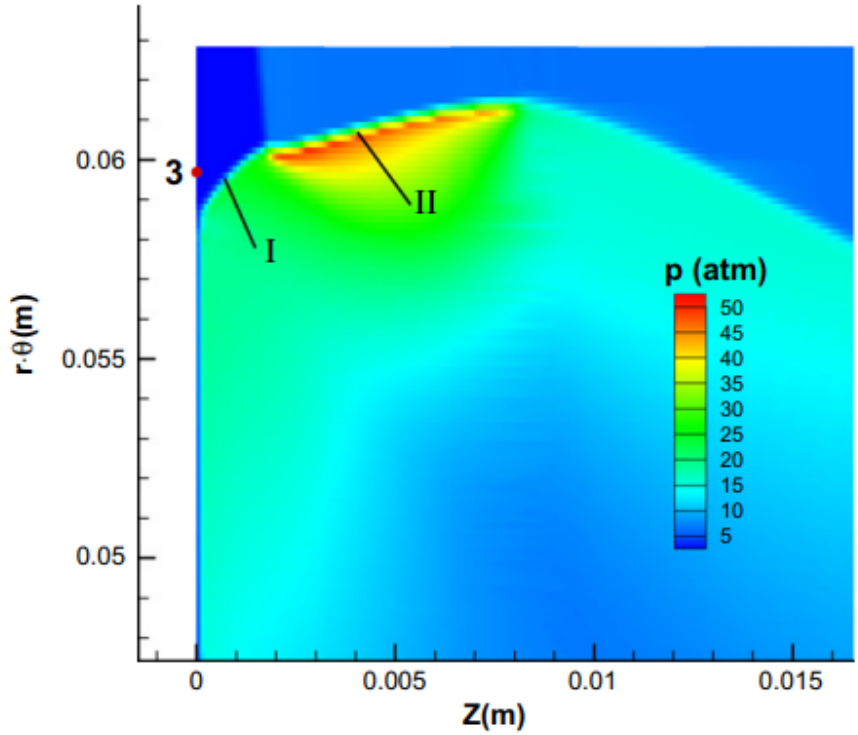

Figure 3.4: Enlargement of a pressure distribution simulation over a detonation front (travelling vertically up) showing the two structures within the detonation front. Image from *Zhou and Wang* [25]

In the simulations run by *Zhou and Wang* [25], it was found that approximately 24% of the particles are burnt by deflagration. However, the simulations run by *Schwer and Kailasanath* a year earlier estimate this figure at a much lower 10% [26]. A more recent study by *Lau-Chapdelaine et al.* in 2024 was found to agree with the study by *Zhou and Wang*, with a value of 25% [24]. The burning of the propellants by deflagration instead of detonation is called parasitic deflagration, and reduces engine efficiency [27].

The particle traces by *Zhou and Wang* also highlight interesting phenomena in the flow velocity of particles within the combustion chamber. The axial and azimuthal particle velocity can be seen in Figure 3.5. It is interesting to note that the detonation wave causes the axial velocity to decrease, while the azimuthal rapidly spikes. This reverses again during the expansion after this detonation wave, where the azimuthal velocity rapidly decreases while the axial velocity slowly increases. [25]

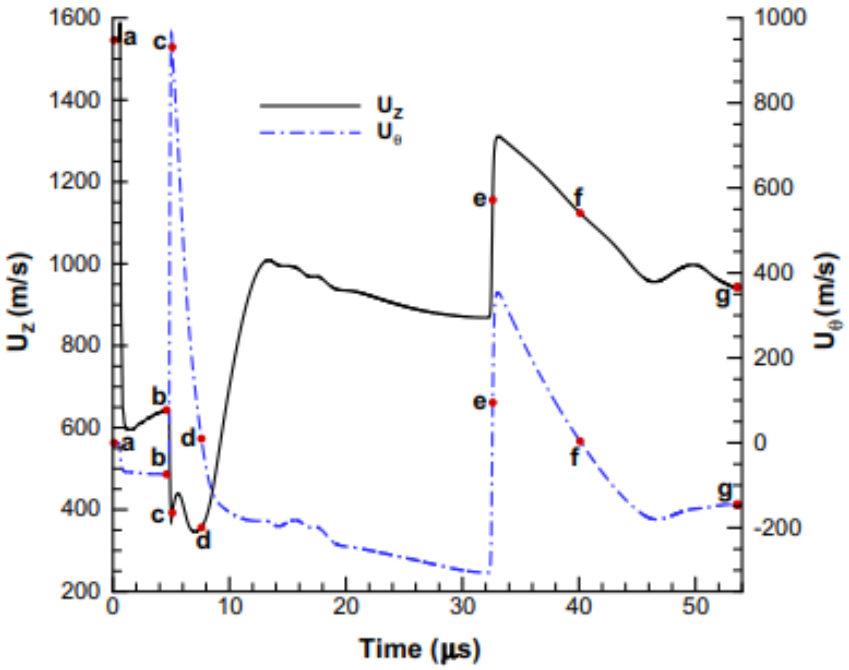

Figure 3.5: The axial and azimuthal flow velocity of particles within the detonation front. Image from *Zhou and Wang* [25]

3.2. Performance Characteristics

The general operating principles and flow field within an RDE was described in the previous section. This section will delve into the main performance characteristics of an RDE; what they are and what parameters may affect these performance characteristics.

Pressure gain: Total pressure is an important measure for the performance of an engine. With an ideal deflagration combustion process, no total pressure is lost during combustion, and hence in a real deflagration a total pressure loss is measured. However, detonation combustion is an unsteady, constant volume process and because of these two attributes it is possible to gain total pressure over the course of the combustion. As total pressure can be considered a measure of a fluid's ability to do work, the more total pressure at the end of the combustion process (i.e. the higher the pressure gain or the lower the total pressure loss), the more work an engine can do for a given amount of fuel. Pressure gain as a percentage is defined by the ratio of total combustor exit pressure to total plenum pressure, as seen in Equation 3.1 [28, 29].

$$\Delta P = \left(\frac{P_{2,t}}{P_{4,t}} - 1 \right) \cdot 100\% \tag{3.1}$$

However, an increase in total pressure in an RDE is a significant achievement in today's experimental world due to a number of typical loss factors; mainly mixing and injection total pressure losses. Both of these should be minimised to maximise the pressure gain of an RDE [30, 31]. The typical maximum pressure gain obtained by parties currently testing is approximately at -5% [32, 33]. The state-of-the-art in pressure gain lies at marginal pressure gain presented in early 2024 [33].

Thrust and specific impulse (Isp) are traditional performance parameters of a rocket engine, and are also of use to the performance analysis of an RDE. In most RDE simulations or tests, the effect on thrust has been analysed from the viewpoint of a constant mass flow, making the definition very similar to the specific impulse. Hence, they will be treated as one for this analysis. A number of interesting parameters were found to have an effect in the Isp of an RDE; the Isp has been found to increase when the ratio of plenum stagnation pressure to chamber back pressure increases [22]. It additionally increases when a smaller percentage of the propellants combust deflagratively [15]. Lastly it was found that a lower initial

propellant temperature will yield a higher pressure gain, but a lower Isp [20]. This indicates that the optimisation of RDE performance is not straightforward, and choices must be made which performance parameter to optimise for.

Detonation velocity: A performance parameter specific to detonative propulsion is the detonation wave velocity. This is often reported as a percentage of the ideal C-J velocity, described in chapter 2. Average experimental results typically place the detonation velocity anywhere between 60-90% of the C-J velocity, and a large number of factors impact it. This loss is typically attributed to two main factors; propellant burning deflagratively due to improper mixing and similar parameters, and heat losses to the walls. [15] There is another factors that is less often attributed, mostly because there is little known about the process. This factor is called lateral relief, and it refers to the fact that the detonation wave is only restricted at the head end of the chamber, while the ideal detonation wave used to calculate the C-J velocity is restricted at both ends. This factor could potentially influence the detonation velocity by up to 20% [17]. Lastly, relatively recent experimental work has sown that the changing of wave modes within the RDE can also have an influence on the detonation velocity. *Bigler et al.* found a 12% decrease in detonation velocity when transition from two to three waves in the chamber with the same testing set point [27].

Combustion efficiency: The last relevant performance parameter is the combustion efficiency, which is a measure of how effectively the heat content of the propellants is output as usable heat. This can be defined in a number of ways, although the most common is based on the characteristic velocity. This definition is shown in Equation 3.2, and can also be easily measured in experiments. In theory, when defined as stated here, detonative combustion has a higher combustion efficiency than deflagrative combustion, hence, the presence of parasitic combustion leads to a reduction in combustion efficiency. [27]

$$\eta_c = \frac{c^*_{real}}{c^*_{ideal}} \tag{3.2}$$

3.3. Geometry

The geometry of an RDE has a large influence on the performance characteristics. The following sections will give an overview of the main types of geometries using in testing, and how variations in these may cause changes in the performance of the RDE.

Firstly the injector design is discussed, followed by a description of the annular, and as alternative, disk-shaped combustion chamber. Next the types of nozzles typically used on RDE are explained, and the common ignition mechanisms are presented. These elements can be seen in the RDE cross-section shown in Figure 3.6.

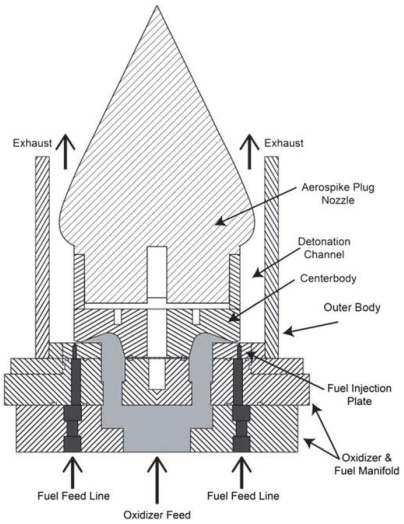

Figure 3.6: The cross-section of an RDE with an annular combustion chamber and an aerospike noxxle. Image from [34]

3.3.1. Injector

The injector design process of an engine is a well-known process to many propulsion engineers. However, there are a number of RDE specific considerations and flow phenomena that need to be taken into account. This section will explain three critical aspects of RDE injector design, and how they impact the performance of an RDE.

Firstly, the ability of an injector to provide propellant to the RDE depends on the pressure ratio between the injector stagnation pressure and the variable chamber pressure. As a detonation wave passes an injector nozzle, the local chamber pressure rises to that above the plenum pressure. This means that the inflow of propellants to the chamber is temporarily blocked, and in some cases it can mean a flow of detonated propellants back into the plenum. This behaviour of the injector is greatly dependant on the design of the injector itself. A higher pressure gain is achieved when a larger injector is used, as this lowers the plenum pressure required to achieve a certain mass flow, however this means a higher chance for injector backflow. As the detonation wave moves on, the chamber pressure decreases, and the propellant can once again flow into the chamber. This process can be seen in Figure 3.7, where the propellant flow in both combustor and the propellant feed system have been modelled with a 2D numerical simulation. The blue indicates fresh propellant, yellow indicates the detonation wave, and the upper white line shows the injector throat, while the second white line indicates the degree to which backflow occurs.

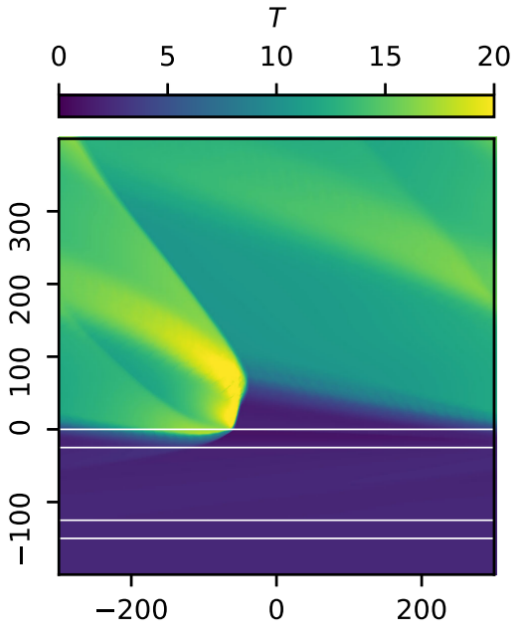

Figure 3.7: 2D numerical Temperature simulation results of an unwrapped combustion chamber and propellant feed system showing the temporarily injector blocking and flow reversal due to the passing detonation wave. Image from *Lau-Chapdelaine et al.* [24]

This injector blockage can result in a reduced average mass flow, and must be compensated for. The reduction in mass flow can be calculated by knowing what portion of the injector is blocked at a given time, a method proposed by *Braun et al.* [35]. By knowing the stagnation pressure of the injector, the location at which this matches the chamber pressure can be identified. Naturally, it is possible that with a difference in fuel and oxidiser injection pressures, the Oxidiser to Fuel (OF) ratio may be slightly different from the operating point. Additionally, this can lead to pockets of unmixed fuel or oxidiser in the combustion chamber, lowering the combustion efficiency of the engine. [36] When the propellant injection occurs below sonic velocities, the pressure oscillations occurring due to the detonation front in the chamber can be transmitted to the plenum, and further up the propellant feed system. [37]

The area ratio of inlet nozzle to chamber throat is of particular importance in the injector design, and there are two factors related to this. A larger area ratio will result in the potential for a larger mass flow,

which is desirable as this results in better chances for good mixing. However, this would lead to a larger supply pressure due to the injector blockage described above. However, this leads to a very large supply pressure requirement due to an increase in detonation pressure, which is difficult to achieve in a real system and typically leads to low pressure gain values. Hence, a balance must be found between these two contradicting factors. The difficulty in finding this balance is one of the reasons for the difficulty in designing an RDE.

A very similar factor, the injector stiffness, is the ratio of plenum pressure over combustor pressure, and hence as the area ratio between the two increases, the stiffness typically decreases, and the inlet becomes less restrictive [33, 38]. Typically, a stiffer injector means the pressure oscillations in the plenum are weaker, but conversely reduce the performance of the RDE by weakening the detonation front [18, 21, 37, 38]. However, recent work by *Brophy and Thoeny* shows opposing phenomena, in their tests the stiffer injector yields strong, but very high frequency, oscillations [33].

Lastly, the design decision must be made between a premixed and non-premixed injector. Currently, most experiments have been performed with non-premixed injectors, and most simulations have assumed the propellants are perfectly mixed, as this simplifies the simulations significantly. However, research into the effect of premixing on RDE performance has shown that this can have a significant performance impact. *Ayers et al.* found that successful experiments with premixed propellants has a detonation velocity close to the CJ velocity, while non-premixed experiments lay around 60% of CJ velocity. However, they also found that premixing can have a negative impact on other aspects of performance, most notably the structural integrity of the engine, due to the pressure oscillations igniting the premixture in the plenum [39, 40]. In addition, pre-mixing is not possible in a physical system, as the chance of an unexpected combustion in the supply lines is too large.

3.3.2. Combustion Chamber

The shape of the combustion chamber plays a large role in determining the performance of an RDE [21, 23, 41]. The majority of the RDEs in current research have an annular combustion chamber, with a flow field as explained above. Hence this section will first focus on the characteristics of such a combustion chamber. However, there has also been a not insignificant portion of research performed on Disk-shaped RDEs (DRDE) [36, 42–45], and hence this topic will also be touched upon.

Annular Combustion Chamber Characteristics

There are four main dimensions of the annular combustion chamber; the length of the combustion chamber, L, the diameter of the outer chamber wall, d_c, the radial thickness of the chamber, Δ, and the height of the detonation wave within the chamber, h_d. Each of these are also displayed in Figure 3.8.

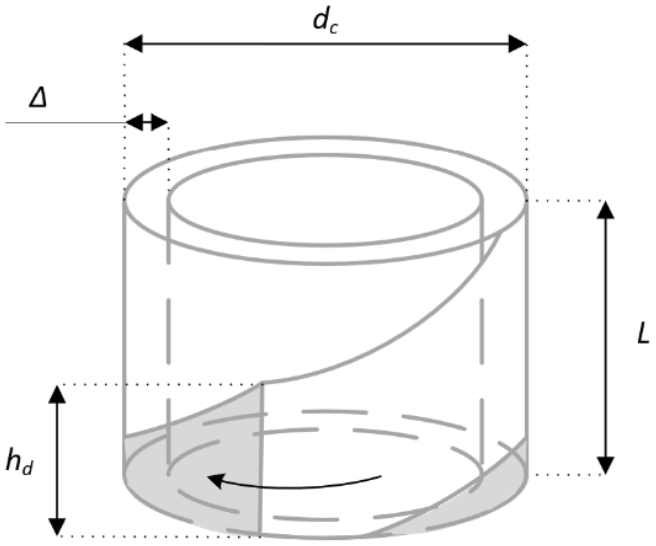

Figure 3.8: The four main dimensions of the annular RDE combustion chamber

Of these main dimensions, the height of the detonation wave is often equated with the height of the propellant fill zone, which in turn mainly depends on the propellant injection parameters, and detonation wave velocity. Higher propellant injection velocity will naturally cause a longer propellant fill zone, and similarly lower velocities will create a smaller zone. In addition, a faster detonation wave will allow for less time for the propellants to replenish, while a slower wave will allow for more propellant filling time. A large filling time will naturally lead to a larger propellant fill zone. [23]

There is an ideal propellant fill height defined as the critical height, h_c. This critical height is the minimum propellant fill height required to sustain one stable detonation wave in the engine. A larger fill height can lead to more propellant being available in the combustion chamber, and hence multiple waves will often occur, especially at higher operating mass flows. Smaller fill heights can lead to instabilities in the detonation, such as galloping detonation, or failure in forming a detonation wave. The critical fill height is mostly dependent on the size of the detonation cells, and hence the propellants used in the RDE. [23, 41]

The minimum size of the other three engine dimensions are dependent on this critical fill height. The length of the combustion chamber should be at least $1.5 - 2$ times larger than the critical height. If this is too small, detonation wave instabilities can occur due to pressure losses ahead of the wave. [41] However, the chamber should not be too long, as this means the particles will encounter the oblique shock too many times, leading to poor pressure gain performance. [20, 30] In this sense, the minimum chamber length is often also the optimum length.

There are two important factors to consider with the diameter of the outer chamber wall; firstly, in conjunction with chamber radial thickness, a small diameter means the detonation wave will travel a more circular path, promoting instabilities and generating larger losses. [38] Secondly, *Schwer and Kailasanath* [21] found a correlation between the chamber diameter and detonation wave height; as the diameter increases, there is more fill time, and this height also increases. Based on similar reasoning, *Bykovskii et al.* [41] defined a relation for minimum chamber diameter.

Lastly, the minimum radial thickness of the combustion chamber is largely dependent on the size of the detonation cells; making the chamber too thin will ensure the detonation does not get sufficient room to propagate. As both are based off the detonation cell size, this minimal thickness is 0.2 times the critical height. [41]. When increasing the chamber thickness from this minimal size, the flow becomes more 3D, meaning the quasi-2D flow simulations where the chamber is unwrapped as in Figure 3.2 start to no longer become representative. Additionally, the number of transverse shocks within the combustor also increases, lowering the pressure gain performance. [21, 23]

Disk-shaped Combustion Chamber Characteristics

The disk-shaped RDE is not fundamentally different than the typical annular combustion chamber configuration. This type of combustion chamber consists of a hollow disk, with an annular exhaust, as can be seen in the flow and hardware shown in Figure 3.9. The propellants can either be injected at the center of the disk, with the exhaust at the outer edges (radial outflow), or in opposite configuration as a radial inflow chamber. Most designs use the radial inflow configuration, as this reduces the required nozzle size. [43]

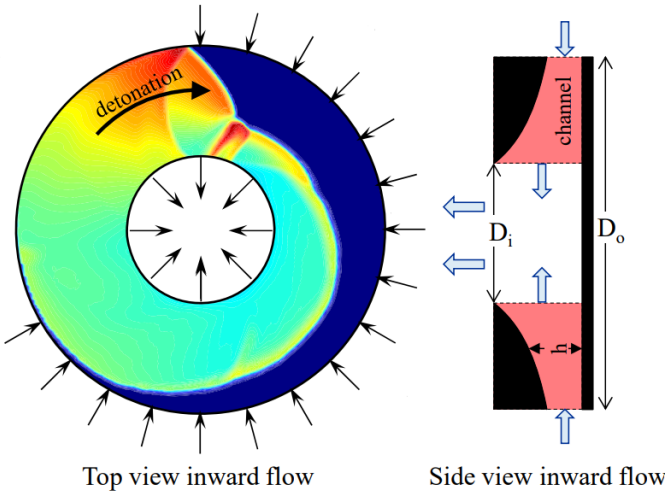

Figure 3.9: A top view flow simulation, and a side view of the channel configuration of a Disk-shaped RDE. Image from *Paxson* [46]

In the DRDE, the detonation wave propagates in the radial plane, and as a consequence, the flow must be turned in the axial direction before reaching a nozzle. This turning often involves heat losses and a large heat load on the parts involved. Hence, the DRDE is less suited for propulsion applications. This radial flow can be desired in energy generation applications however, as this allows the use of radial inflow turbines. [44]

Although the detonation stability of a DRDE is often lower than that of an annular RDE [36, 43, 47], when the right operating conditions are achieved, the specific impulse was found to lie much closer to the theoretical value. Additionally, large mass savings may be achieved in with a DRDE as compared to an annular RDE. [45]

Depending on the application, the DRDE may be the appropriate choice for combustor shape. However, as it has been less widely researched, and due to the limited compatibility for propulsion applications, this thesis will continue by considering only the annular combustion chamber shape.

3.3.3. Nozzle

Experimental RDEs are typically operated either without a nozzle (unconstricted), or with either a traditional converging-diverging or aerospike nozzle (constricted). The aim of this section is to provide some background on the details of the nozzles used, and the performance effect of a constricted versus unconstricted RDE.

Converging-diverging nozzles are most commonly used in rocket propulsion applications. However, due to the annular nature of the RDE outflow, aerospike nozzles are the favoured nozzle in this case. Aerospike nozzles consist of a conical protrusion in the centre of the flow, while the ambient pressure provides a flow director on the outside. As the ambient pressure changes, the aerospike nozzles compensate for this, and are continuously altitude adapted. [48] An example of both a converging-diverging and an aerospike nozzle on an RDE can be seen in Figure 3.10.

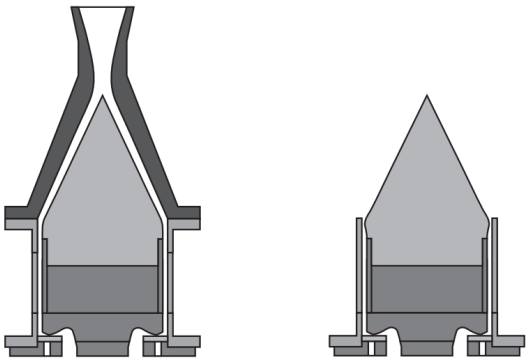

Figure 3.10: An example of a converging-diverging nozzle (left) and an aerospike nozzle (right) on an RDE. Image adapted from *Fotia et al.* [49]

In both simulations and experimental tests, it was found that an RDE with a nozzle performs better than one without. The thrust of the RDE is 2-3% greater will converging-diverging nozzle, and an additional 7% greater when using an aerospike nozzle. [20, 50]

However, it has also been found that the constriction of the RDE combustion chamber has detrimental effects on the detonation process. *Bykovskii et al.* [41] finds that the constriction weakens the detonation waves, while *Codoni et al.* [51] and *Ge et al.* [52] both found that transverse shocks can be reflected back into the chamber due to the constriction. Lastly, the presence of constriction increases the chamber pressure, and hence also greatly affects the number of waves present in the detonation chamber. Restriction does also improve the pressure gain performance of an RDE, and in some test cases is required for the start-up phase of operation [32, 53, 54]. Hence, a balance must be found between the positive and negative aspects of the restriction on an RDE.

3.3.4. Ignitor

Initiation of a detonation occurs due to a spontaneous energy increase. This can be in the form of a shock wave, or a local energy source [8]. In experiments this is typically realised in the form of a Pre-Detonator (PreDet), consisting of an energy source such as a spark plug attached to a long thin tube filled with detonable gasses. The spark plug will ignite a deflagration in the gasses, which will then travel down the tube and undergo a Deflagration to Detonation Transition (DDT), ensuring a detonation wave arrives in the combustion chamber of the RDE and is able to ignite the propellants. [55]

Other forms of RDE ignition methods include the usage of a spark plug in the wall of the detonation chamber. This has the advantage of not requiring an additional, and often bulky, component to the system, but does require an increase in energy needed to ignite the RDE. Additionally, the energy that can be deposited is more limited than with a pre-detonator. This method was employed in the only space environment test of an RDE to date, on the second stage of a JAXA mission. [56]

Both these methods are forms of indirect ignition. Direct ignition of the detonation wave is also possible, however this requires a much greater initiation energy, and hence is not commonly used. This direct initiation causes an overdriven detonation wave, which then decays to the normal detonation wave and results in stable RDE operation. [55]

3.4. State-of-the-Art in RDE Models

In recent years, the modelling and simulation of detonative propulsion, and specifically RDEs have come to complement the efforts on experimental testing. These modelling efforts aim to predict the RDE flow field, performance, and optimize design parameters. They additionally aim to address critical challenges related to heat loads, combustion efficiency, and detonation characteristics. In general, these modelling efforts can be grouped into two categories; modelling using time-based numerical methods, and modelling based off the flow properties at various points in the engine. The first type of model is grouped under the heading of Computational Fluid Dynamics (CFD) models, while the second type are thermodynamic models.

In this section, the state-of-the-art, and their contribution to general RDE knowledge, will be discussed for both these modelling methods. In addition, the advantages and disadvantages of either method will be discussed.

3.4.1. CFD Models

Computation fluid dynamics models are the best known method to create a visualisation of the complex flow field in the RDE combustor. Due to the recent advancements in computing technology, and the complexity of RDE simulations, this field developed relatively late. The first CFD models started appearing in the late 2000's, with *Schwer and Kailasanath* at the forefront of this development. Their first model [22] focused on recreating the general flow field within an RDE, while subsequent additions allowed the investigations into engine geometry [21], variations of operating conditions, [26] and finally the effects of various fuels [57]. Figure 3.2 is one of the results of this first model by *Schwer and Kailasanath*.

The results of the variation of engine geometry validated the simple calculations made by *Bykovskii et al.*, and confirmed the description of combustion chamber geometry given in section 3.3. In the meantime, investigations into the flow path of various particles moving within an RDE combustor, were performed by *Zhou and Wang*, and *Guangyao et al.* among others [25, 41, 58]. These simulations resulted in the first confirmations that a portion of the propellants deflagrate rather than detonate within the chamber [25]. This was later visually confirmed through the use of more detailed models of gas species percentages within the flow by *Gaillard et al.* [59].

The previously described simulations were all performed under the assumption of an unwrapped 2D combustion chamber. The work performed by *Folusiak et al.* remains one of the early CFD simulations of three dimensional flows within the combustion chamber, investigating in particular the shape of the detonation wave at the head-end of the combustion chamber [60].

More recent CDF modelling efforts were focussed on modelling a specific section of the RDE combustor. *Lau-Chapdelaine et al.* investigated the effects of the detonation-injector interaction, and partial blockage of the propellant injectors [24]. *Guangyao et al.* implemented statistical particle tracking on the 3D simulations of a centreless RDE in the process of investigating possible performance benefits with mass reduction [58]. In addition, simple CFD simulations are used to select the most promising geometrical configurations to test in a physical experiment [33, 54].

Overall, these CFD models have contributed a great deal to the general knowledge and workings of RDE technology, helping understand how different aspects can be modelled in the thermodynamic models, or how to best perform data acquisition on experimental set-ups. They are exceptionally well suited for analysing the details in the flow, either surrounding the injector, and the expansion and shock interactions after the detonation wave. However, CFD models in general have long run times, and are computationally intensive, especially with an unsteady flow process such as in the RDE combustor. In addition, the kinetic processes involved with combustion add an additional level of complexity and computational time.

3.4.2. Thermodynamic Models

In contrast to CFD models, thermodynamic models do not result in a visual description of a flow field. Instead, these models are created to calculate the various thermodynamic properties (static and total temperature and pressure, enthalpy, entropy, flow velocities, etc.) at certain points, stations, within the RDE. In most applications, these thermodynamic models are made to capture the steady behaviour of propulsion devices and predict their propulsive performance, and hence can approximate the engine as a 1D system. Detonative propulsion however, is an unsteady process, and hence when modelled as such, unsteadiness in the flow can lead to inaccuracies in the modelling, or violation of the conservation laws. This unsteadiness that originates from the 1D approach must be dealt with in an appropriate manner [61]. In the case of an RDE, three typical approached are used; averaging over the period of a rotating detonation, following the particle flow paths identified using the above CFD models, and capturing the spatial unsteadiness in the flow by means of carefully considered station definition.

This first approach of averaging the flow properties over a rotating detonation period was used by *Ramanujachari et al.* [62], and *Nordeen et al.* [63]. In these models, the assumptions are made that the propellants are well mixed and fuel and oxidiser are supplied at a constant rate, as well as the

assumption of a steady flow when in a reference frame attached to the detonation wave. The analysis in such a steady frame, and later averaged over a period, allows the removal of the variation in the azimuthal direction, and the calculation of average performance properties. However particularly the approach of *Ramanujachari et al.* is not very detailed, and neglects a number of important factors [62]. Both *Shepherd and Kasahara* [64] and *Stechmann et al.* [20] created similar, though more detailed models that allowed for performance comparisons between different propellants and geometries. This type of approach can also be used in the removal of the unsteadiness of a RDE, and allow for direct modelling of the properties [61].

The second approach requires a thorough understanding of the physical processes occurring within the RDE, and the flow paths followed by propellant particles. This approach was used by *Kaemming et al.* to create a more accurate model, with emphasis on those processes that drive the performance in the RDE. Three possible particle flow paths are considered; those passing through both the detonation wave and the oblique shock, those passing only through the detonation wave, and those combusting deflagratively before passing through the oblique shock. The mass flows of each respective path are determined through the use of a CFD simulation. After the physical processes in each of these paths are calculated, the paths are mixed, and the spatial unsteadiness within an RDE combustor is hence removed [17]. They key difference with the previously described approach is that the amount of mass reacting in each different manner is required as a form of input, typically acquired from CFD. These separate mass streams can be modelled separately and as more of the main physical processes occurring within an RDE are modelled in this manner, this type of simulation is assumed to be a better reflection of reality than the period averaging mentioned above. However, division into the three flow paths does require some additional information, or empirical relations, making it potentially less versatile [17, 25].

Paulson et al. [16] and later *Burr and Paulson* [15] took the last approach in the creation of a thermodynamic model for an RDE. They defined five separate stations within the RDE combustor, and calculated the thermodynamic properties at each. The parasitic deflagration was assumed to be encountered first, after which both the remaining fresh propellants, and the deflagration combustion products undergo the detonation, as well as a rarefaction after. In this case, the detonation is first modelled as a von Neumann Shock, followed by a CJ heat addition, combining both the ZND and CJ models of detonation [15, 16]. This approach was also used by *Bigler et al.* in their model to investigate the effects of mode transitions on RDE performance. This model largely made use of the same station designation, but refrained from including the rarefaction wave [27].

It is difficult to determine whether the second or third approach results in a more accurate simulation. In both, ensuring a station designation representative of the physical processes is critical to the validity of the model. However, research has not yet been able to show whether the usage of different flow paths within the RDE combustor will lead to a better representation of the physical world.

There is a last category of thermodynamic models; those that do not calculate the full RDE, but parts of it. *Barnouin et al.* [65] produced a thermodynamic model to determine the heat loss due to incorrect mixing, parasitic deflagration, and heat loss to the chamber walls. This model deals purely with the combustion process, not the following expansion, and the output of this model is purely the combustion efficiency [65]. The aspects of several of these models such as this one can be combined into a single, mode detailed and realistic model of an RDE.

The accuracy of these models has been discussed by a number of parties. In an analysis of their own work and comparing the detonation velocity achieved, *Nordeen et al.* finds a residual between 31.7% and 0.5% when comparing their model to test values obtained by *Zhdan et al.* [63, 66]. In addition, they find their model has a residual of 2.23% when compared to the numerical simulations performed by *Schwer and Kailasanath* [22]. *Shepherd and Kasahara* provide an accuracy value of between the 5-10%, and a 30% error on the thrust, when comparing the Isp obtained from their model to a different set of simulation work by *Schwer and Kailasanath* [57, 64]. Although exact values are not defined, *Paulson et al.* states that although their work may be used as a framework for further work, it is not yet very accurate due to the lack of loss factors taken into account [16]. Lastly, *Kaemming et al.* shows graphs of Isp and specific thrust in comparison to test data obtained with the AFRL (Air Force Research Laboratory) RDE, where the Isp varies about 3% and the specific thrust varies about 5% [17].

3.5. RDE Models Knowledge Gap

In the above two sections the state-of-the-art and recent advancements in RDE modelling have been discussed. This section will elaborate on the aspects that remain less well developed, and present a potential knowledge gap for this thesis to cover.

The user requirements for the RDE model to be created during this thesis will be presented in section 4.2. However, of particular importance are the requirements that the model shall function as a 1D, thermodynamic cycle performance tool, and that the run time of the model shall be less than five seconds. The combination of these two requirements eliminates the usage of a CFD model, partly due to their typically long computation time. This means this thesis will create a thermodynamic model of the processes occurring in an RDE. Hence, only contributions possible by the creation of a thermodynamic model will be considered for the analysis of the knowledge gap within the modelling of RDEs.

In the experimental work performed to date, one of the largest challenges to achieving positive pressure gain is the pressure loss over the injector and mixing phases [28, 29]. However, in most thermodynamic simulations, the simulation starts at the combustor head-end, and assumes the propellants are well mixed [15–17, 20, 62–64]. It is only the work performed by *Barnouin et al.* [65] and to some degree *Bigler et al.* [27] that considered possible losses due to injector buffer zone creation, and improper mixing. The model by *Barnouin et al.* is additionally the only one to consider the effect of heat loss to the chamber walls, and assumes this loss to be a constant factor [65].

Moreover, only three of these models consider the full combination of combustion and flow processes as defined by *Zhou and Wang* [25], and *Schwer and Kailasanath* [22] as a result of their CFD models; the combination of parasitic deflagration, detonation, and passing through an oblique shock. These are the models by *Paulson* [16], *Burr and Paulson* [15], and *Kaemming et al.* [17].

Lastly, while this analysis is performed in a number of CFD models, only the thermodynamic model by *Stechmann et al.* considers variations in nozzle geometry, and assess the impact of these on the performance of the RDE [20].

The knowledge gap as identified in this analysis is a thermodynamic model consisting of a combination of the above mentioned points; the inclusion of losses due to injector buffer, mixing, and heat loss to the walls, as well as losses due to parasitic deflagration and the passage of the oblique shock, and the combination of different nozzle types. Including at minimum any two of these three points will result in a model that provides unique insights into the workings of an RDE, and allow for analysis in a manner that has not yet been performed.

In addition, the creation of such a model allows for the generation of a large amount of insight and knowledge into the performance of an RDE. Analysis using this tool will contribute directly to the general knowledge base, and additionally provide detailed insights for the client, TNO. Given TNO has only recently stated research into RDE's, this additional knowledge is a valuable addition.

3.6. Literature Study Conclusions

This section has illustrated the outcomes of a literature study into the subject of Rotating Detonation Engines, with a particular focus on the factors impacting performance and the modelling of RDE's. With this knowledge, and the more abstract background knowledge given in chapter 2, the reader should have sufficient topic-specific knowledge to follow the discussion regarding the RDE model and the remainder of this work.

This literature study first investigated the operating principles of an RDE, and found that these are quite different to that of a typical rocket engine. The detonation wave inside the combustion chamber is continuously fed a fresh supply of propellants, and while the supply lasts, will be sustained and continue rotating around the annulus shaped combustion chamber. The flow phenomena identified to be principal to the RDE behaviour are the backflow into the propellant plena, and the corresponding injector blockage, the deflagrative burning of propellants, the detonation wave itself, a slip line between combustion products of different cycles, and the trailing oblique shock coming from the detonation wave.

The performance characteristics were next to be presented, and each identified performance characteristic

includes a description of what it represents, and what parameters affect this performance characteristic. The identified performance characteristics are the pressure gain, the thrust, the specific impulse, the detonation velocity and the combustion efficiency.

The impacts of different geometries within the RDE was also investigated. The injector design has a large impact n the pressure gain performance, as well as an influence on the overall performance of an RDE due to the potential for injector blockage and backflow. A too large injector can also cause large pressure oscillations in the plena. The characteristics of two different combustion chamber shapes were discussed, the more common annular chamber, and the disk-shaped chamber. The geometry of the combustion chamber has a large impact on whether the engine will operate as an RDE, or as a traditional rocket engine. Both the aerospike and the converging-diverging nozzle were investigated as pertaining to RDE's. The aerospike was found to have higher performance results, as well as an easier degree of implementation due to the centerbody in the combustion chamber. Lastly, the ignition mechanism was discussed; most engines use a Deflagration to Detonation Transition (DDT) to provide the initial energy to ignite the RDE.

The state-of-the-are in RDE models was also a large aspect of this literature study, loosely divided into two categories: models based on a CFD-type approach, and models based more on the thermodynamic principles inside and RDE. The CFD-type models provide very detailed insights to the working of an RDE, however they tend to have a large computation time and require a large number of inputs from test data. In contrast, the models based off thermodynamic principles are not detailed enough to result in a flow-field description of the RDE combustion chamber. Instead they are typically 1D models, where the state and properties of the gas are known at various stations throughout the RDE. The large reduction in typical computational time, and less inputs required from test data comes at the cost of the detailed knowledge gained of the RDE flow field from a CFD model.

Lastly, after the analysis of the two different categories of state-of-the-art models, a knowledge gap that can be fulfilled by this thesis is identified. This is a thermodynamic model considering a number of flow phenomena, and the subsequent analysis of the RDE performance that can be completed using such a model.

4

Research Objective

An exploration of the fundamental background and current knowledge of RDE's was given in the preceding chapters. This review of the current literature highlighted a knowledge gap in the RDE field, which can be partially filled by this thesis; the creation of a thermodynamic model capable of deriving the flow and performance parameters of an RDE, using limited additional inputs.

This chapter focusses on the specific research objectives and questions that will form the backbone of this research on RDE's. It will first present the research objective and research questions, before following up on these with the requirements for the RDE model itself. A number of these requirements originate from TNO, as client of this research, and the remainder originate from the literature study and knowledge gap identified above.

4.1. Research Objectives

As a result of the client wishes, and the above mentioned literature study conducted into RDE's, the research objective defined for this thesis is:

To investigate the impact of different operating conditions on Rotating Detonation Engine (RDE) performance characteristics by developing a thermo-chemical analysis model for the combustion and mixing processes in RDE's.

This objective can be broken down into three sub-goals, each with their corresponding research question and sub-questions. The first research question encompasses the goals regarding the creation of the model as defined by the research objective. It is important to identify where this thesis fits in the scope of current research, hence the first step is to identify what the current state-of-the-art is with respect to RDE's, and how this can be modelled. Secondly, the phenomena needed for the thermo-chemical analysis model should be investigated, and the model itself should be created.

The second research question represents the validation of the model with data from an experimental test campaign conducted at TNO. To use this data, it is necessary to know both which design parameters can be altered to produce variations in engine geometries, and which performance metrics can be assessed as a result of the test data. Lastly, it is important to provide an estimation of how accurately the test data represents reality, and hence when the model is validated using this test data, how accurate the model is.

The last question details the usage of the model; the impact of different propellant combinations and geometries should be assessed at the level of a full propulsion system. This impact is determined based of key performance characteristics: engine thrust, specific impulse (Isp), pressure gain, and combustion efficiency.

This translates to the following three research questions, and their corresponding sub questions.

1. How can a thermo-chemical analysis model be formulated to accurately represent the detonation wave physics in an RDE?
   (a) What is the current state-of-the-art in the modelling of Rotating Detonation Engines?

   (b) What are the key performance metrics that need to be considered in a thermo-chemical analysis model of an RDE?
   (c) What are the key physical and chemical phenomena within an RDE?
   (d) How can the various physical and chemical phenomena within an RDE be modelled?
2. What is the accuracy of the thermo-chemical analysis model with respect to experimental data?
   (a) Which design parameters can be altered during the test campaign at TNO?
   (b) Which performance metrics can be established during a test campaign at TNO?
   (c) To what extent does the accuracy of the model depend on input parameters to the model?
3. What are the impacts of variations in geometry and operating conditions on the performance characteristics of RDEs?
   (a) How do variations in engine geometries affect the thrust, specific impulse, pressure gain and combustion efficiency of RDEs?
   (b) How do variations in operating conditions affect the thrust, specific impulse, pressure gain and combustion efficiency of RDEs?

As can be seen from the research questions, the thesis will be split into two parts. Firstly the creation of the model will be acted on, including many of the phenomena highlighted in the literature study above. The model will also be validated with the experimental data gained during the test campaign at TNO, as well as simulation and experimental data found in literature as a benchmark against this data set. Once this is completed, the model will be used to assess how the variations in engine geometries affect the performance metrics. This will allow the model to be tested on how the client wishes to use it, as well as provide examples for how to use the model.

4.2. Requirements

A proper systems engineering process is essential in designing a product that is functional, is able to be used as intended, and performs to the wishes of the client. An important first step in this process is the definition of user requirements, which have been agreed on both by the designer and the client. Requirements consisting of a 'shall' must be met in order for the product to be in accordance with the clients wishes, and those including a 'should' are the nice-to-haves of the client.

The following user requirements for the RDE model have been defined based on the wishes of TNO, and the aforementioned research objectives. These have been grouped into functional requirements, implementation requirements, and performance requirements.

4.2.1. Functional Requirements

The functional requirements describe the functionality of the model. These describe what the model should do.

REQ 01 The model shall calculate overall engine performance and local gas properties at relevant flow path stations, as a function of propellant chosen and engine geometry.

The minimum set of performance parameters to be calculated are:
- Pressure gain
- Specific impulse
- Thrust
- Combustion efficiency
- Detonation velocity
- Characteristic velocity

The minimum set of local gas properties to be calculated are:
- Static and total pressure
- Static and total temperature
- Static and total enthalpy

- Entropy
- Specific heat at constant pressure
- Specific heat ratio
- Gas composition
- Average molar mass
- Flow velocity
- Mach number

REQ 02 The model shall follow a defined station convention as defined by Brophy et al. in 2019 [29]

REQ 03 The model shall be applicable within the following ranges of operating conditions, and propellant types:
Chamber pressure: 0.5-200 [bar]
Equivalence ratio: Within detonability limits
Fuel types: H2, Methane, Ethylene
Oxidiser types: Air, O2

REQ 04 The model shall function as a 1D, thermodynamic cycle performance tool

REQ 05 The model shall perform a check to ensure the inputted geometry lies within the viable limits for RDE operation

REQ 06 The model shall function for an RDE in both airbreathing and rocket-mode, with one of the following initial conditions:
- Flight operational point, consisting of altitude and Mach no.
- Plenum conditions, initial plenum pressure and total temperature

4.2.2. Implementation Requirements

The implementation requirements describe how the model should be implemented, the inputs and outputs, and if there are requirements on the structuring of the code.

REQ 07 The model shall be implemented as a Python function, with the following interface:
[input, Geometry, Performance, GasProp] = *function*(inp_1, inp_2, ... , inp_n)

With:
Input: Object containing all parameters that have been inputted to the model
Geometry: Object containing all geometric parameters that define the propulsion system
Performance: Object containing all performance parameters of the propulsion system
GasProp: Object containing all the local gas properties at all flow path stations
inp_1, inp_2, ... , inp_n: Input parameters

REQ 08 The model shall be build with a MatLab wrapper to allow it to be called from MatLab

REQ 09 The model shall be created in a modular manner, with sub-models created for the processes occurring, allowing the later addition of at minimum:
- The addition of different fuel and oxidiser types, including liquid hydrocarbon fuels
- The addition of vitiated air effects
- The addition of different phenomena to model

REQ 10 There shall be unit tests created for every function within the model.

4.2.3. Performance Requirements

The performance requirements describe how well the model should perform. For example what physical phenomena it should be able to model, and if the model has a maximum run time.

REQ 11 The model shall model at least the following physical phenomena:
- Parasitic combustion
- Propellent mixing loss due to buffer zone
- Propellant mixing loss due to insufficient mixing
- Heat loss due to unburnt propellants
- Heat loss due to walls
- Total pressure loss due to oblique shock
- Total pressure loss due to injection

REQ 12 The model should be fast running, taking less than 5 seconds per run on a single CPU

5

Simulation Software Development

The processes and phenomenon occurring in an RDE were researched during the literature study, and described in chapter 3. To transform these into a model capable of simulating performance characteristics, a simplified physical model is first made. This is done by using the common thermodynamic approach of defining stations within the engine. In typical models of engines, steady flow is assumed at each station, which is an assumption that cannot be used to represent the unsteady nature of an RDE. This model assumes a hybrid approach, where the outcomes of the unsteady RDE process are represented in quasi-steady thermodynamic states.

Hence, at each station, a quasi-steady flow can be assumed, and as such, flow properties at each station can be defined. In RDE literature, a common station definition for pre-mixed RDE models uses the plenum as station 2, the injector throats as station 3.1, the section just after the injector as station 3.2, the combustion chamber end as station 4, and the full engine throat as station 8. Station 10 is then the nozzle exit, and concludes the model. There are also intermediary stations with no physical location in the combustion chamber: stations 3.3a/b and 3.4. This approach is also used in *Brophy et al.* and is adopted here, with the slight adjustment of using the respective plena as station 2 [29]. The physical station definition for the RDE model can be visualised in Figure 5.1, while the stations without a physical location can be seen in Figure 5.2.

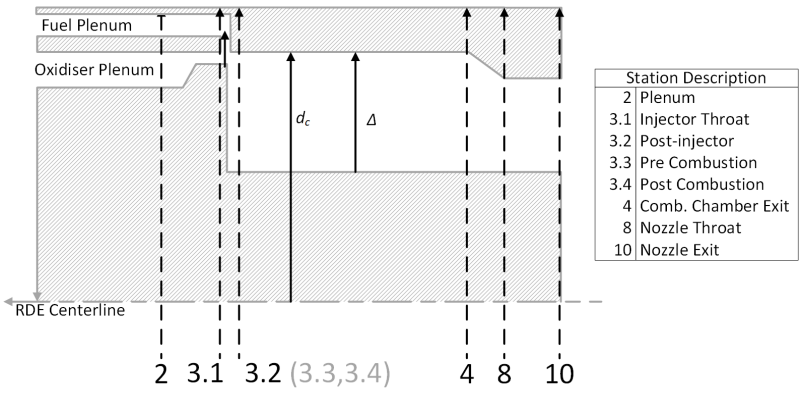

Figure 5.1: Basic diagram of the RDE structure considered for this model, showing the station definition adopted throughout the model. In this figure d_c indicates the chamber outer diameter, while Δ is the chamber channel height.

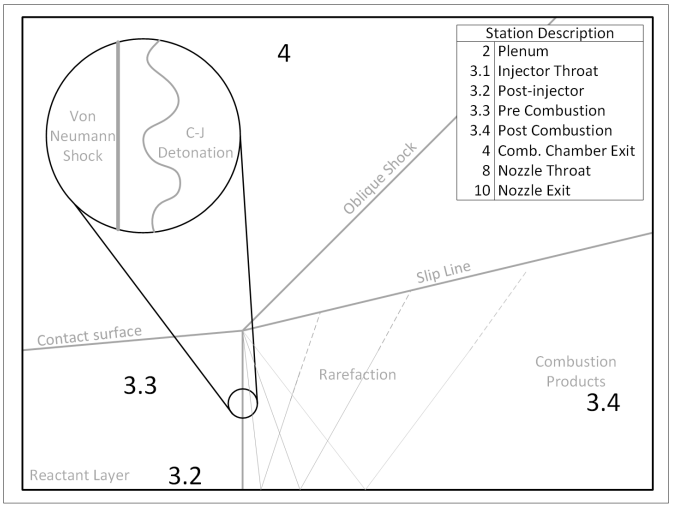

Figure 5.2: Basic diagram of the RDE processes considered within the combustion chamber for this model, showing the station definition adopted throughout the model

This chapter will explain the structure of the model, and the design decisions made to build it in this manner. First, the model main structure is described, including the packages used, the approach taken, and the assumptions made. Then a section for each station as described above will follow. These will describe the approach taken, including the reasoning behind this approach, and the calculations made in the model itself. Lastly, the methodology of calculating the performance parameters, and a number of important checks, are described.

5.1. Software Structure

The RDE performance model first creates a virtual representation of the RDE with the corresponding geometry. This model is further created with a number of sub-models, each representing the physical phenomenon occurring in the RDE itself. These sub-models combine together to add stations to the virtual RDE stored in the model. A basic flow chart of the model structure can be seen in Figure 5.3, where the models associated with the 5 main stations (plenum, post-injector, post combustion, nozzle throat, and nozzle exit) are included, as well as the three main iteration loops of the model.

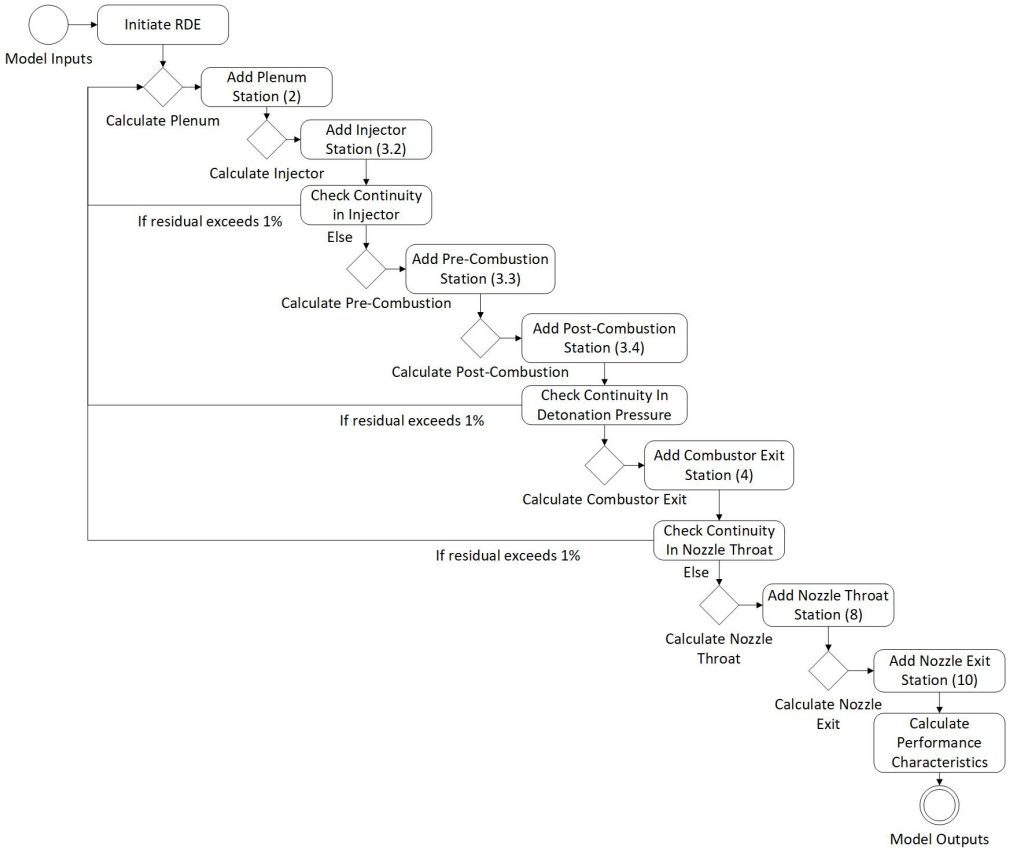

Figure 5.3: Basic flow diagram of the model showing the main structure, the diamonds represent the sub-models, while the blocks are the actions

The first part of the model is the model initiation, here some checks are performed on the inputs, and the structure of the model is built up. There are estimations made for four parameters during this initialisation; the two plenum pressures, and an estimation of the maximal and minimal pressure within the combustion chamber: the detonation and decay pressures.

Next the plenum and the injector stations (stations 2 and 3.2) are calculated with their respective models. With this complete, a continuity check is performed at the injector throat; if the different in mass flow input to the model, and currently flowing through the injector throat does not match, the initial guesses of the plenum pressures are adjusted and the first two models are iterated upon.

Once continuity is ensured in the injector throat, the stations until the completion of the combustion (3.3, 3.4) are calculated. This results in an updated value of the detonation pressure, which is compared against the one from the previous iteration. In case of discrepancies, a second iteration loop is implemented, and the model moves to the plenum again.

Lastly, the combustor averaging station (4) is calculated using it's respective model. After this, a third continuity check is implemented, this time on the nozzle throat. If the average pressure in the combustor does not match the pressure required for choking of the nozzle throat, the initial guess of the decay pressures is adjusted, and the iteration starts again at the plenum model.

If all three continuity checks are passed, the model will calculate the final nozzle properties with the nozzle throat and exit models (stations 8 and 10), and finally the performance parameters are calculated.

To keep a high level of modularity, a sub-model containing various functions is made for each of these stations. This approach allows for the implementation of changes in a specific sub-model, without having to rewrite the full model code. In addition, an approach to the creation of the model using different fidelity levels of detail was implemented. This approach is not further described here, but information on the different fidelity levels and how the coding was approached can be found in Appendix B.

In addition, each station as defined in Figure 5.1 is represented by a sub-model which calculates the respective properties of that station. The full RDE model is built in such a way that an RDE is slowly built up. Each separate sub-model representing a station will add a number of properties to the stored RDE, resulting in an RDE will all relevant properties once the model is complete.

Each sub-model will now be explained in more detail in dedicated sections. Each section will first contain a subsection explaining the various RDE phenomenon that will be modelled here. This explanation is heavily related to the information presented in the literature study in chapter 3. Next, the structure of the model is explained in more detail, with the implementation of the stations as shown above, and an introduction to the iterations necessary to deal with all unknowns. Lastly, the coding approach to creating the model in an efficient and resilient manner is described.

Before discussing the sub-models in detail, an overview of the packages used and assumptions made is given, as well as a short description of a few useful auxiliary functions.

5.1.1. Packages Used

There are two dedicated Python packages that are used to calculate the properties of the gas through the stations, as well as the shock and detonation properties. These are Cantera [67], and the shock and detonation toolbox [68]. The remainder of the packages used in the creation of the model are part of the standard python library.

Cantera

Cantera[1] is a open-source package for primarily python and MatLab, that has the ability to calculate the chemical kinetics, thermodynamics and transport processes of a fluid problem [67]. It will be used in this model as the primary method to keep track, and calculate the properties, of the gas states at various stations.

A gas, with various properties, can be stored in Cantera as a solution entity, and as a subset of this with a particular mass, a quantity entity. When the composition is fixed, two thermodynamic properties can be applied to the gas, and Cantera will calculate the remaining properties matching that state. A composition can also be applied along with these two properties when the composition is not fixed. Quantity entities can also be added together, and the result is a quantity with the combined mass and adiabatically mixed properties.

Unless specified, these process occur under the assumption of frozen flow. When the flows are allowed to react, the gas can be set to go to equilibrium keeping two thermodynamic flow properties constant. Examples of this are keeping the internal energy (U), and specific volume (V), constant for an approximation of a detonation, or keeping the enthalpy (H), and the pressure (P), constant for a deflagration.

Shock and Detonation Toolbox

The shock and detonation toolbox is an open source package for both python and MatLab that interfaces with Cantera [68]. This package is primarily used to calculate the properties of either a shock or a detonation, using a Cantera gas entity as a main input. The output properties are then also applied to a Cantera gas, and the result is a Cantera gas entity that has undergone some form of shock or detonation.

This package will be used within this model to model the ZND structure of the detonation, further explained in section 5.4.

5.1.2. Assumptions Made in the Model

There were a number of assumptions made that were used throughout the model. These can be seen below:

- It was assumed that **isentropic flow relations** could be used from the plenum to injector, and from combustor exit to nozzle exit.
- The total conditions of the gas were assumed to only change within the combustor. This is a consequence of an **assumption of inviscid flow**.

[1] `https://cantera.org/index.html`

- The **calorically perfect gas** assumption has been used from plenum to start of the combustion chamber within the model.
- The gas is assumed to be **thermally perfect** throughout the rest of the model.
- The flow velocity in either plenum is assumed to be negligible, hence the plenum conditions are **assumed to be stagnant**, with the Mach number being zero in both plena
- It is assumed the pressure distribution within the combustion chamber can be **approximated by an exponential function**. This is an assumption derived from literature [17, 65, 69].
- The flow is assumed to be **chocked at the nozzle throat**.
- The model calculates properties based on the time period of a single detonation wave. This implies an assumption has been made of a **single detonation wave** in the combustion chamber.
- There is no more combustion after the identified processes, meaning that the **assumption of frozen flow** is used from the flow mixing onwards (station 3.4).

5.1.3. Model Inputs

The model requires details of the geometry, propellant properties, and model variables to be input. These are displayed in Table 5.1.

This list includes a number of items which are optional. In the case of these, a default value is defined in the model, but it can be overridden by the optional input. In addition, different input variables are selected for the rocket-mode or airbreathing operation of the RDE, as well as for the selection of nozzle type (convergent-divergent or aerospike).

Table 5.1: Table showing the inputs of the RDE model

Geometric Inputs		
	Chamber outer diameter (d_c)	[mm]
	Chamber channel height (Δ)	[mm]
	Chamber length (L)	[mm]
	Fuel injector area (using d_f)	[m^2]
	Oxidiser injector area (using d_o)	[m^2]
	Nozzle throat area (using d^*)	[m^2]
	Nozzle exit area (if converging-diverging nozzle)	[m^2]
	Fuel injector discharge coefficient	[-]
	Oxidiser injector discharge coefficient	[-]
	Nozzle discharge coefficient	[-]
	Inlet area (if airbreathing)	[m^2]
	Mass capture fraction (if airbreathing)	[-]
	Pressure recovery fraction (if airbreathing)	[-]
Propellant Properties		
	Equivalence ratio	[-]
	Total mass flow (if rocket-mode)	[kg/s]
	Fuel type	[-]
	Fuel static temperature (optional)	[K]
	Oxidiser type (if rocket-mode)	[-]
	Oxidiser static temperature (optional, if rocket-mode)	[K]
	Effective viscosity (optional)	[Pa s]
	Turbulent dissipation rate (optional)	[m^2/s^3]
	Kinematic viscosity (optional)	[m^2/s]
	Laminar flame speed (optional)	[m/s]
Other Variables		
	Mach number (if airbreathing)	[-]
	Altitude (if airbreathing)	[m]
	Ambient pressure (if aerospike nozzle)	[Pa]
	χ: detonation heat release	[-]
	α: deflagration flow in detonation	[-]

In addition, the geometric aspects of the basic RDE to be modelled can further be seen in Figure 5.4. The locations of the respective plena, and the orientations of propellant injection are shown here as an example only. In reality this model does not consider these geometries. If needed they can be captured somewhat by the discharge coefficient applied to the injector nozzles.

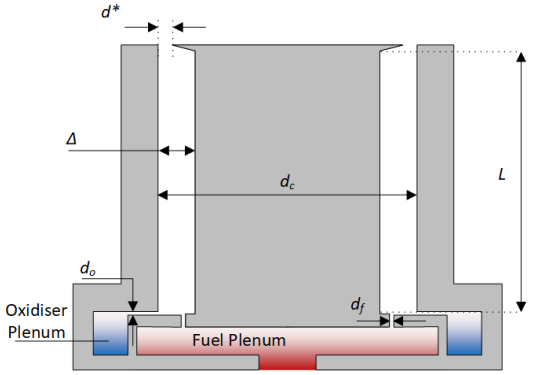

Figure 5.4: Diagram showing all geometric aspects of the RDE Model

5.1.4. Relevant Auxiliary Functions

The sub-models of the model itself, and the performance parameter determination, are described in the following few sections. There are however a number of additional functions that are used within the model initiation, or used in multiple places throughout the model. These functions are described here.

The *Find Gas Properties* function is used at the completion of every sub-model to define all relevant gas properties.

The *Model Initiation* consists of two checks, as well as the set-up to add a station to the RDE model. It first checks whether the RDE is likely to ignite with detonation, based on the detonability limit on the equivalence ratio proposed by *Belles* [70]. It then checks whether the geometry of the engine is likely to be favourable to the stability of the detonation cycle, using methodology from both *Bluemner* and *Bykovskii et al.* [32, 41]. If either of these checks are flagged, a warning is printed to alert the user of potential design issues. Both these functions are elaborated on in this section.

Find Gas Properties

It is a user requirement that each sub-model should result in all gas properties at the relevant station. With two relevant state variables (pressure, temperature, entropy etc.), a representation of the flow total conditions (total pressure, Mach number, etc.), and the gas composition at the station, the remainder of the required state variables can be found.

The gas composition, and static temperature are required inputs for this function. Next to this, any two of the static pressure, total pressure and Mach number must also be input. From here, a combination of isentropic relations and Cantera can be used to find the remaining parameters. The basic steps undertaken in this function can be seen in Figure 5.5.

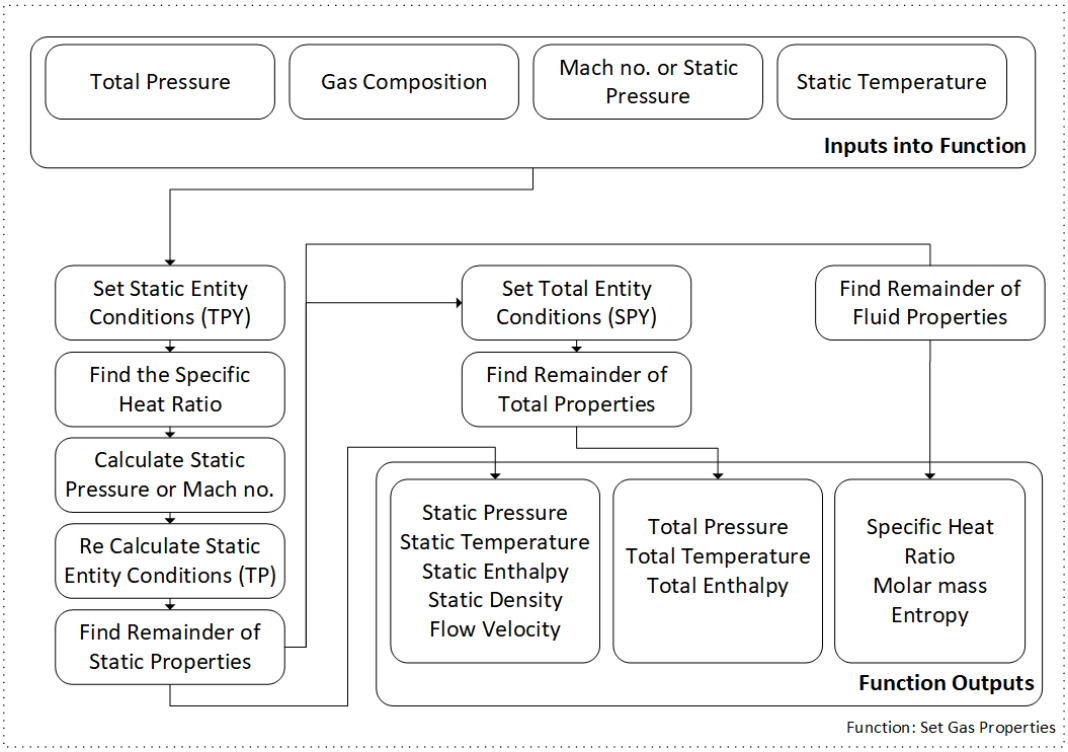

Figure 5.5: Detailed flow diagram of the function used to find all gas properties

The function first uses the static temperature, total pressure and gas composition (indicated by TPY) to initialise a Cantera fluid entity. A simple function is then used to calculate a temporary specific heat ratio, which is necessary to convert between the static pressure and Mach no. If not input, the static pressure is then calculated by Equation 5.1, while similarly the Mach number is calculated by

Equation 5.2. Lastly, the actual specific heat ratio is calculated using the static pressure and static temperature, and this is iterated until values match.

$$P_s = P_t \left(1 + M^2 \left(\frac{\gamma - 1}{2}\right)^{\frac{-\gamma}{\gamma-1}}\right) \tag{5.1}$$

$$M = \sqrt{\frac{2}{\gamma - 1}\left(\left(\frac{P_t}{P_s}^{\frac{\gamma-1}{\gamma}}\right) - 1\right)} \tag{5.2}$$

With these values, the static conditions for the fluid can be applied to the Cantera entity. This is by setting the temperature and pressure to their calculated static values, while keeping the composition constant. Lastly, the remainder of the static conditions can be extracted from the Cantera entity. These values include the static enthalpy, and the static density, while the velocity of the flow can be determined from the Mach number and the stored sound speed. In addition, a number of values which do not differ between static and total conditions can be calculated; namely the molar mass and the entropy.

The entropy, along with the total pressure and the gas composition (using SPY) are then used to initialised and set the conditions of the Cantera entity representing the total flow conditions. Once this has been set, the remaining total temperature and total enthalpy can be extracted in a similar manner as to above.

This yields all the relevant parameters to describe the flow at each station, and it is these parameters which are given as full model output parameters for every station. The full list of the outputs of this function can be found in Table A.23.

Model Initiation

Every time the model is run, there are two checks that are performed to ensure the inputs are within ranges that allow for detonation in the RDE. These checks are the *Check Detonability*, which checks to ensure the equivalence ratio is within correct limits, and *Check Engine Geometry*, which uses empirically derived geometry limits from literature to determine whether the engine is larger enough to accommodate the chosen propellants' detonation cell size.

The *Check Detonability* function is run at the every start of the model, and yields a warning if not passed successfully, and thus the inputs on propellant type and equivalence ratio does not fall within the detonability limits of as calculated by *Belles* [70]. For the propellant combination of H2 and air, the equivalence ratio input is checked against the lower and upper limits of 0.28 and 1.77 respectively, however these are default values and can be adjusted by the user if required.

As mentioned in chapter 2, detonations form a scale-like structure. These shapes within the structure are called detonation cells, and the size of these has a large impact on the size of the geometry that detonations can operate within. If a channel is too small, these detonation cells cannot form, and hence there can be no sustained detonation.

The methodology for the cell size determination is adapted from a shock and detonation toolbox demo program: *demo_ZND_CJ_cells.py* [68]. Two correlation functions were first employed to calculate the detonation cell size; the Gavrikov function by *Gavrikov et al.* [71], and a function by *Ng et al.* [72]. Both were tested for accuracy and were found to have a factor of 100 difference. The cell sizes were compared with those for hydrogen and air from the *Detonation Database* [73], and the values from *Ng et al.* [72] were found to be more reliable.

The second check function implemented in the model initiation uses guidelines from *Bluemner* and *Bykovskii et al.* to determine whether the chamber diameter, length and channel height are favourable for stable detonation operation [32, 41].

The first criteria by *Bluemner* state that the chamber channel heigh must be greater than 0.5 times the detonation cell size to allow for proper detonation within the engine [32]. From *Bykovskii et al.* there are three parameters: first a critical detonation height is calculated as 12 times the detonation cell height.

Then a minimum diameter (Equation 5.3), minimum length (Equation 5.4), and a minimum channel height (Equation 5.5) are calculated. [41]

$$D_{min} = \frac{7 \cdot h_{cr}}{\pi} \tag{5.3}$$

$$L_{min} = 2 \cdot h_{cr} \tag{5.4}$$

$$H_{min} = 0.2 \cdot h_{cr} \tag{5.5}$$

If the input chamber diameter, length, or height is less than the minimum calculated value, a warning is printed to the user. The guideline from *Bluemner* is determined to be leading as it is more recent. For the other criteria, these guidelines are somewhat dated, and have been shown to be incorrect in a number of more recent tests. The implementation of the warning allows the user to make the decision on whether to take this warning into account or not [32, 33, 74].

5.2. Calculating Plenum Properties

The first station defined in Figure 5.1 is the plenum station. This plenum consists of a separate volume for both the fuel and the oxidiser, where the flow is stagnant before the entering the injector. In rocket-mode RDE's, both plena typically are similar in design, and provide the connection between the propellant feed system and the RDE itself. If an RDE is operating in airbreathing mode, the fuel plenum will remain similar, but the oxidiser plenum is attached to the inlet and diffuser.

The user can make the decision to simulate an RDE operating in either mode, but the main assumption made here will remain the same; the Mach number of the flow in the plenum is assumed to be zero, and hence the total and the static conditions are equivalent. Here, the simulation of an RDE in rocket-mode will first be discussed, following by that of an RDE in airbreathing mode.

5.2.1. Rocket-Mode Operation

When operating in rocket-mode, the relevant inputs are the required equivalence ratio, the required total mass flow, the respective supply propellant temperatures as they flow though the propellant feed system.

The total mass flow is separated into the respective fuel and oxidiser mass flows using the equivalence ratio. These inputs are now ready to be used in the next step of the plenum model.

5.2.2. Airbreathing Operation

The inputs for the airbreathing operation are different from the rocket-mode. They include the Mach number of flight, the altitude of flight, the cross-sectional area of the inlet, and two parameters that can be obtained from an inlet model: the Mass Capture Fraction (MCF), and the Pressure Recovery Fraction (PRF).

The altitude is used in a model of the international standard atmosphere to obtain the static pressure, static temperature, and density of the air at the given altitude. The temperature and pressure are transformed to total values using the Mach number and the PRF. The total pressure is not the total pressure in the air plenum, but it is the maximum pressure the air inlet can sustain. If the model determines a higher air plenum pressure is required for RDE operation, the inlet will unstart, and hence a warning is given. This means the user will need to re-design the inlet r change the operating point before running the RDE model again.

The mass flow of air though the inlet can be calculated thought the mass flow equation, using the inlet cross-sectional area, as seen in Equation 5.6.

$$\dot{m_{Air}} = MCF \cdot \frac{A_{inlet} P_t}{\sqrt{T_t}} \cdot \sqrt{\frac{\gamma}{Rg}} \cdot M \cdot \left(1 + \frac{\gamma - 1}{2} M^2\right)^{-\frac{\gamma+1}{2(\gamma-1)}} \tag{5.6}$$

The fuel mass flow, followed by the total mass flow, can both be determined using the mass flow of air and the equivalence ratio. This is all calculated in the *Inlet Model* function, of which the full list of inputs and outputs can be found in Table A.1.

The same parameters are now known as with the rocket-mode version, and the remainder of the RDE model will be calculated in the same manner for both operating modes.

5.2.3. The Iteration Loop

The initial guess for the pressures in both plena are estimated by assuming the respective injector throat is choked. Knowing the geometry, mass flows, total temperature and the properties of the propellant at these conditions, a total pressure can be estimated, as seen in Equation 5.7. This calculation is done by the *Guess Plenum Pressures* function, of which the inputs and outputs can be seen in Table A.3.

$$P_{t_2} = \frac{\dot{m}}{A_3} \cdot \sqrt{\frac{R_g T_{s_2}}{\gamma}} \cdot \left(\frac{\gamma+1}{2}\right)^{\frac{\gamma+1}{2(\gamma-1)}} \tag{5.7}$$

After the initial iteration, this plenum pressure is no longer calculated, but originates as an output of the iteration itself.

5.2.4. Final Plenum Station Properties

With the total pressure and temperature known, and thus due to the stagnation assumption, the static pressure and temperature, the remainder of the flow properties can be calculated using the methodology described in subsection 5.1.4.

The gas properties at the plenum station are then added to the RDE object stored in the model, and an iteration of the plenum model is complete. The attributes of the RDE at completion of the plenum model can be found in Table A.4.

5.3. Calculating Injector Properties

The behaviour of flow through an annulus, in this case an injector, is dependant on the behaviour of the flow on either end of it; here the assumed stagnant flow within one of the plena, and the dynamic processes occurring within the combustion chamber. Because of this direct interaction with these dynamic processes, the flow within the injector can not be considered steady state. However, by considering the flow over a discretised injector, and averaging this, the resulting flow behaviour/characteristics can be represented using a steady state, as will be discussed in this section.

The basic steps take in this injector sub-model of the RDE model are show in Figure 5.6. There are described in mode detail in the remainder of this section.

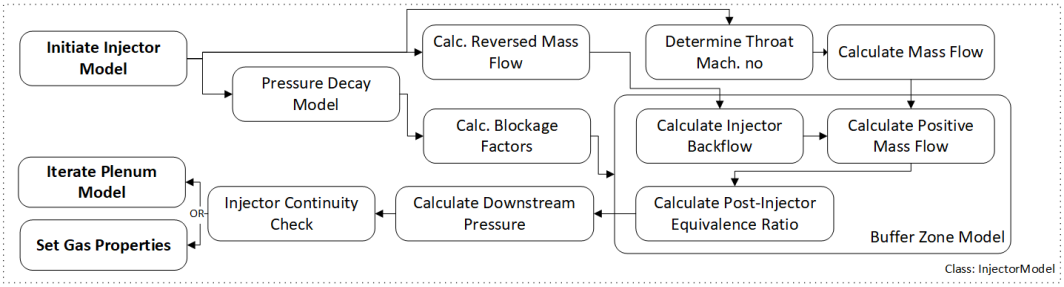

Figure 5.6: Detailed flow diagram of the injector module of the second fidelity level

The respective injector throats are at station 3.1, while station 3.2 is defined as the mixed flow just after entering the combustion chamber; the post-injector station.

5.3.1. The Pressure Decay Curve

The dynamic processes occurring within the combustion chamber can be approximated by an exponential pressure decay curve, pictured in Figure 5.7 [17, 65, 69]. The passage of the detonation wave results in a pressure (and temperature) spike, after which the flow expands (and cools) until the conditions are once again approach those just prior to the detonation wave. This dynamic repeats itself over the course of a single detonation wave period, represented in a normalised fashion by τ. This detonation time period is very short, as the detonation wave often travels with a frequency of over 6000Hz.

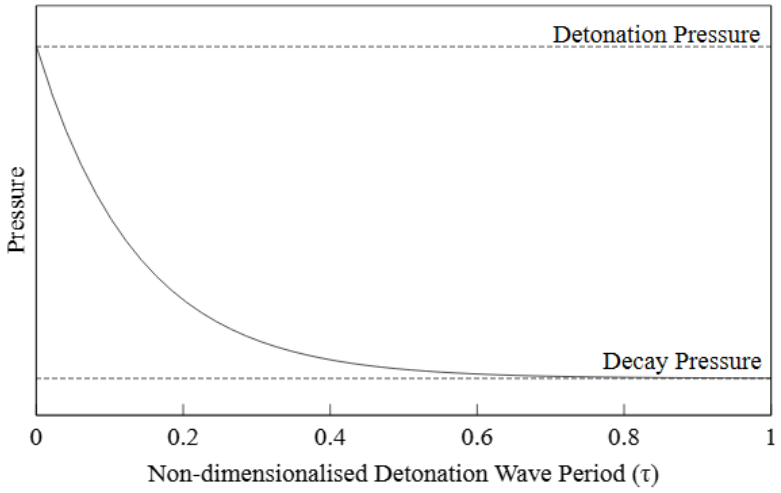

Figure 5.7: The Pressure Decay Curve representing the pressure in the combustion chamber

The pressure decay curve can be represented by Equation 5.8 [69].

$$P(\tau) = P_{decay}\left(1 + \left(\frac{P_{det}}{P_{decay}} - 1\right)e^{-k\tau}\right) \tag{5.8}$$

The pressure decay curve represents the pressure behaviour within the RDE combustion chamber, and hence will be a recurring theme within the model. It requires a number of parameters to construct, namely the pressure immediately before and after the passage of the detonation wave: the decay and detonation pressures, and a pressure decay factor obtained from literature.

These decay and detonation pressures are given initial values for the first iteration round, but these values are adjusted both within the model, and during the nozzle throat continuity iteration. Additionally, the pressure decay factor is calculated from those used in *Kaemming et al.* and *Bedick et al.* [17, 69], and the composition is set to a hydrogen-air mixture.

This pressure decay curve is calculated in the model using the function *Injector Pressure decay Model*, and the inputs and outputs of this function can be seen in Table A.5.

5.3.2. Phases Occurring within the Injector

The pressure fluctuations within the combustion chamber can be quite dramatic, and have a larger effect on the behaviour of the injector.

There are roughly three phases to consider for this injector:

- Injector blockage
- Injector un-blockage
- Injector recovery

The injector is considered blocked when the pressure in the combustion chamber is higher than the pressure in the considered plenum. In this case, there will be hot combustion propellants flowing

backwards from combustion chamber to plenum. This can be indicated by the red region shown in Figure 5.8. This backflow will remain in the plenum (with the assumption of no mixing) until the pressure in the combustion chamber has decreased so it is no longer above the plenum pressure. This point is named the injector unblockage point ($\tau_{unblocked}$), and represents the end of the red region. This fraction of the full detonation period that the injector spends blocked is represented by the blockage factor.

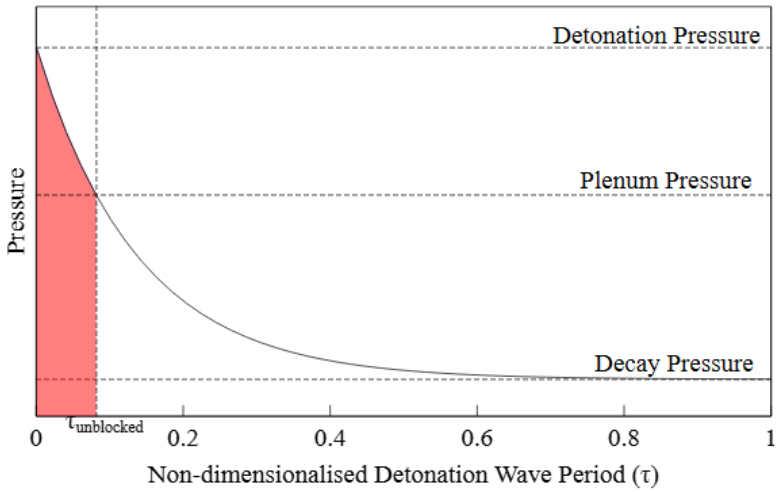

Figure 5.8: The Pressure Decay Curve representing the pressure in the combustion chamber, showing the point of injector unblockage

After the point of injector unblockage, it is assumed that the unmixed, hot combustion products will be the first to be expelled through the injector throat back into the combustion chamber. This process is indicated by the yellow region in Figure 5.9. Once the full amount of backflow has been expelled, the injector is considered to be recovered, and this point is represented by $\tau_{recovery}$.

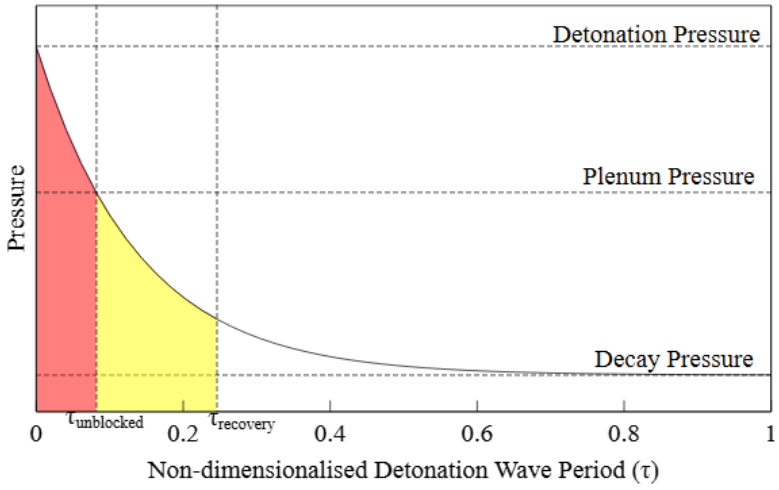

Figure 5.9: The Pressure Decay Curve representing the pressure in the combustion chamber, showing the point of injector recovery

Finally, the considered propellant can be injected from the plenum to the combustion chamber, and this continues until the end of the detonation wave period. This phase can be seen as the green region in Figure 5.10.

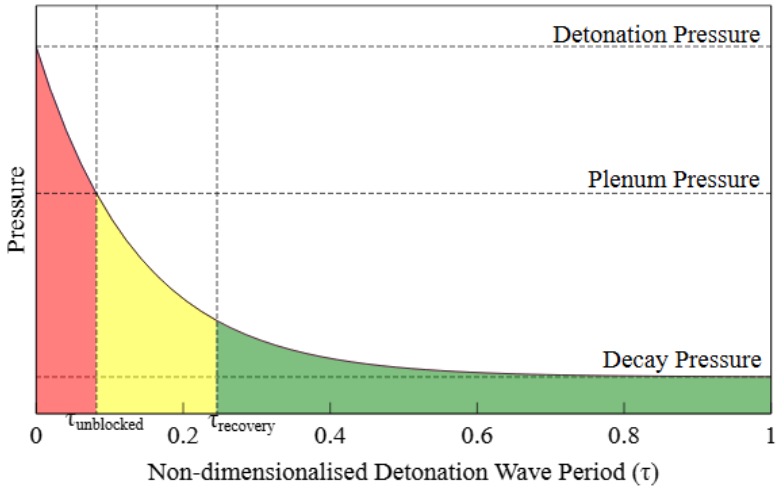

Figure 5.10: The Pressure Decay Curve representing the pressure in the combustion chamber, showing the full three phases of the injector

Each of these phases are modelled within the full injector discretisation, which is discussed below.

5.3.3. Injector Discretisation

As these calculation of the flow through the injector is dependent on the injector back pressure, and this depends on the time-dependant pressure decay curve, which repeats for the passage of every detonation wave, the decision is made to discretise the injector area over a single detonation wave period. Each step in the discretised injector will have a corresponding chamber pressure associated with it. The following steps will then be performed on every slice of injector.

Both injector areas are also adjusted by an user-input discharge coefficient. This discharge coefficient takes the viscosity and dump losses through the throat into account, and can typically be estimated from literature or obtained by testing.

In this injector discretisation, the temporal and spatial variation are considered to be the same. This is possible due to the assumption of a single detonation wave in the chamber. This can be seen with the air of Figure 5.11, where the time-varying pressure within the detonation period, at a single point, is shown on top, while the spatial variation within the combustion chamber is seen below. As can be seen, when a single detonation wave is considered, the temporal variations of pressure at a single location match the spatial pressure variations within the chamber.

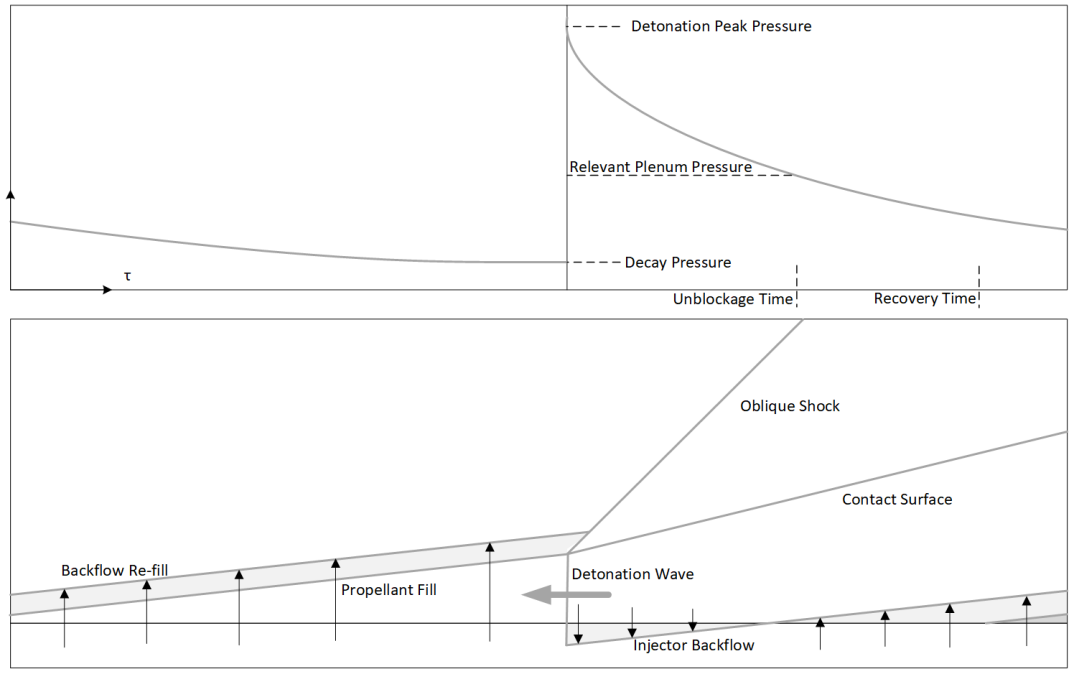

Figure 5.11: Diagram of the injection and combustion process inside the RDE. The temporal pressure variation is shown on top, and the spatial RDE phenomenon are shown on the bottom

The determination of the injector phase (blocked, unblocked or recovered), using the current chamber pressure, is executed first.

Injector blockage

If the injector is blocked, (P_$chamber$ > P_2), the Mach number of the flow flowing from the combustion chamber to the considered plenum is calculated using Equation 5.9. With the usage of this function, the assumption is made that the flow in the chamber is stagnant during the phase of injector blockage, indicating the chamber pressure is a total pressure.

$$M_{reversed} = \sqrt{\frac{2}{\gamma - 1}\left(\left(\frac{P_{chamber}}{P_2}^{\frac{\gamma-1}{\gamma}}\right) - 1\right)} \tag{5.9}$$

This Mach number is then used in the calculation of the corresponding mass flow as shown in Equation 5.10. The combination of these equations is defined in the *Reversed Mass Flow* function, of which the required in- and outputs can be seen in Table A.6.

$$\dot{m}_{reversed} = \frac{A_{3.1}P_{chamber}}{\sqrt{R_g T_{chamber}}} \cdot \sqrt{\gamma} M_{reversed} \cdot \left(1 + M^2_{reversed}\frac{\gamma - 1}{2}\right)^{-\frac{\gamma+1}{2(\gamma-1)}} \tag{5.10}$$

The amount of reversed flow is kept track of for both injectors separately, to allow the recovery time to be calculated later on.

Injector un-blockage

If the injector is unblocked, the hot combustion products must first be expelled from the plenum. The mass flow of these unmixed, hot combustion products from the plenum to the chamber per injector element is calculated in a similar manner as to above. However, in this case it is once again the plenum that is considered to have stagnant flow, and the plenum and chamber conditions in the equations above are exchanged. The amount of backflow remaining in the considered plenum is carefully monitored, and when this drops below zero in an injector element, the injector is considered recovered.

Injector recovery
If the injector is recovered, the fresh flow of propellant into the chamber can be considered. To calculate this, it is first checked whether the flow is sonic, by comparing the critical pressure (calculated by Equation 5.11), to the pressure within the combustion chamber at this point.

$$P_{crit} = P_2 \left(\frac{2}{\gamma + 1} \right)^{\frac{\gamma}{\gamma - 1}} \tag{5.11}$$

If the plenum pressure is higher, the flow is sonic through the injector throat. If not, the Mach number through the injector throat is calculated through Equation 5.12. These calculations are completed in the *Determine Throat Mach* function, of which the in- and outputs can be found in Table A.7.

$$M_{3.1} = \sqrt{\frac{2}{\gamma - 1} \left(\left(\frac{P_2}{P_{chamber}} \right)^{\frac{\gamma - 1}{\gamma}} - 1 \right)} \tag{5.12}$$

Lastly the mass flow of the fresh propellants into the combustion chamber is calculated using Equation 5.13. These calculations are completed in the *Calculate Mass Flow* function, of which the inputs and outputs can be seen in Table A.8.

$$\dot{m}_{3.1} = \frac{A_{3.1} P_2}{\sqrt{R_g T_2}} \cdot \sqrt{\gamma} M_{3.1} \cdot \left(1 + M_{3.1}^2 \frac{\gamma - 1}{2} \right)^{-\frac{\gamma + 1}{2(\gamma - 1)}} \tag{5.13}$$

Overall Implementation
The three injector phases described above are applicable for both plena. However, as will be described in the following section about the buffer zone, it is very likely that one of the plena (typically fuel) has a higher plenum pressure than the other. The model makes use of this fact to avoid iterating over the injector twice. If the fuel plenum has a higher pressure, it is logical that the fuel injector will unblock and recover first. Hence, the mode will then first check to see whether the fuel injector is unblocked. It will then check for both fuel recovery and oxidiser un-blockage. Once the oxidiser injector is also unblocked, it will check for recovery of both injectors.

The logic describing this calculation used in the model itself can be seen in Figure 5.12. This logic is repeated for the case of a higher oxidiser plenum pressure.

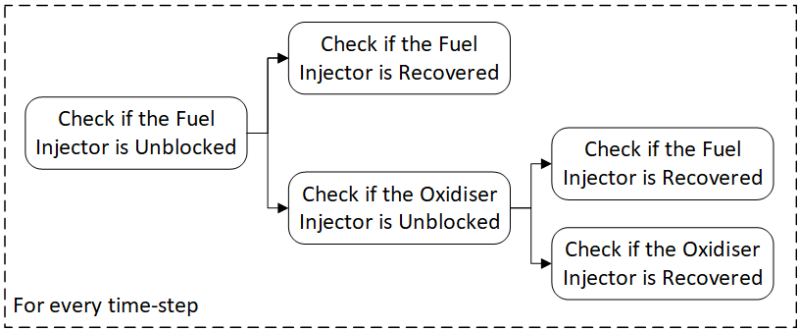

Figure 5.12: Detailed flow diagram of the steps undertaken in the injector discretisation

5.3.4. Formation of the Buffer Zone

The plenum pressures of the fuel or the oxidiser are often not equal in an RDE. It is typically the case that the fuel plenum has a higher pressure, especially in the case of a H2-Air RDE. If there in an inequality in plenum pressures, it leads to different injector recovery times for the separate injectors.

This leads to a phenomena called the buffer zone; a formation of a fuel or oxidiser rich region within the propellant fill zone of an RDE. This is visualised in Figure 5.13, where the fuel plenum is a higher pressure, and hence the fuel injector recovers first.

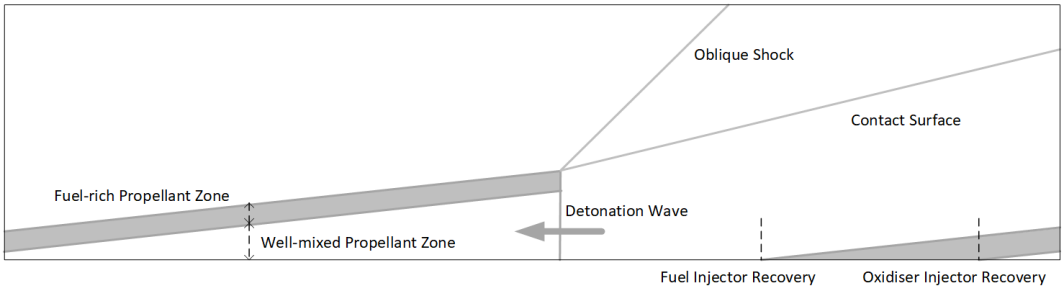

Figure 5.13: Diagram of the buffer zone formed with different injector recovery times. The case shown is where the fuel plenum pressure is higher than the oxidiser plenum pressure

The phenomena called the buffer zone was documented by *Chacon and Gamba* [75] in their study of parasitic combustion in an optically acessed RDE.

Due to the combination of this localised extreme equivalence ratio, and the short detonation wave period not allowing for much mixing, the propellant trapped in this buffer zone cannot be utilised by the RDE, and often exits the RDE as unburnt propellant. It can be said a portion of the mass flow is 'lost' for combustion. The amount of which can be calculated by Equation 5.14, described here in the format for a 'loss' of fuel.

$$\dot{m}_{lost} = \int_{\tau_{ox_{rec}}}^{\tau_{f_{rec}}} \dot{m}_f d\tau \tag{5.14}$$

Here $\tau_{f_{rec}}$ refers to the recovery time of the fuel injector, while $\tau_{ox_{rec}}$ refers to the recovery time of the oxidiser injector.

The total mass flow considered for combustion is the combination of these individual mass flows, with the buffer zone mass flow portion removed from it.

The function that calculates the above mentioned injector discretisation and the formation of the buffer zone in the *Buffer Zone* function, and the inputs and outputs to this function can be found in Table A.9.

5.3.5. Injector Flow Averaging

With the discretisation of the injector complete, the mass flow for the fuel and oxidiser respectively can be found as the summation of the mass flow through each injector element. These are the flows going through the respective injector throats, and will be used in the injector continuity check later.

The mass flow of propellant lost to the buffer zone will alter the equivalence ratio of the propellant mixture that is considered for combustion. The relevant factor is Equation 5.15, and the method is based off that from *Barnouin et al.* [65]. This equation is once again written with the assumption that the buffer zone mass flow portion is fuel.

$$\phi_{comb} = \psi\phi_g = \frac{\int_1^{\tau_{ox_{rec}}} \dot{m}_f d\tau}{\int_1^{\tau_{f_{rec}}} \dot{m}_f d\tau} \tag{5.15}$$

ϕ_{comb} refers to the equivalence ratio that is used for the combustion of the propellants in the further sections, while ϕ_g is the global input equivalence ratio.

One of the requirements for model functioning is to define all state variables at each of the defined stations; plenum, injector, combustor, and the two nozzle stations. To do this however, the time-varying combustion chamber pressure described by the pressure decay curve must be translated into a

representative single pressure value to represent the combined static pressure post injection. Here a similar approach to that of *Bedick et al.* is utilised, where the time-averaged pressure just after injection is the average of the pressure decay curve after injector unblockage, called the downstream pressure. This downstream pressure is calculated separately for each injector, and then a mass averaged value is determined. The downstream pressure can be visualised in Figure 5.14, where the grey region is the region considered for this average pressure.

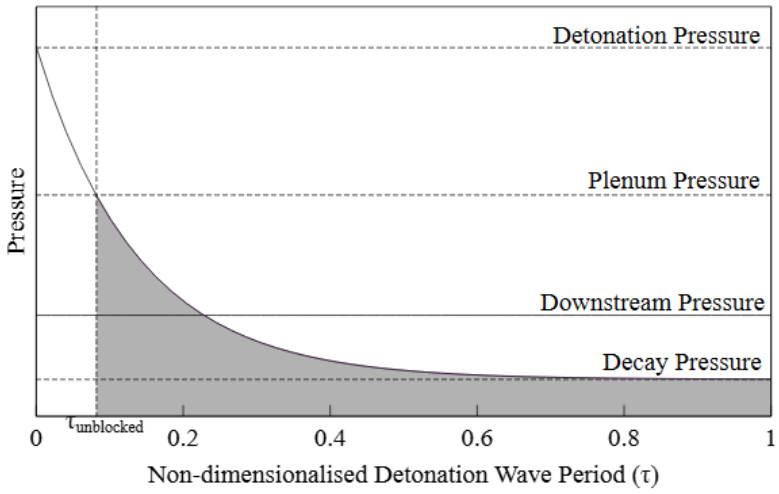

Figure 5.14: The Pressure Decay Curve representing the pressure in the combustion chamber, showing the downstream pressure

The combined static pressure after injection is then simply the mass-averaged value of both the fuel and oxidiser static pressures. The calculation of this pressure, named the downstream pressure, is performed in the *Calculate Downstream Pressure* function, described in Table A.10. Additionally, as the assumption has been made for isentropic flow though the injectors, the total temperature and pressure just after the injector are known for each propellant type. These are simply also mass-averaged to yield an averaged total temperature and pressure at the injector station.

5.3.6. Injector Continuity Check

Due to the initially assumed value of the plenum pressures, and the flow reversal within the injector, the mass flow that results from this injector discretisation described above, is not necessarily the mass flow that is input by the user. Hence, there is an injector mass flow continuity check implemented, which calculates the relative difference between this calculated mass flow, and the initial input. This check is performed for the fuel and oxidiser injector separately.

If the difference between mass flows is more than 1%, an adjustment is made on the initial plenum pressure guess, according to Equation 5.16, and the model is run again, starting from the calculation of the plenum properties.

$$P_{t_2} = P_{t_2} + \left(\frac{P_{t_2} \dot{m}_{diff}}{\dot{m}_{input}} \right) \tag{5.16}$$

If the value is within 1%, the model continues to the combustor calculation. The injector continuity check is performed using the *Injector Continuity Check* function, of which the outputs can be seen in Table A.11.

5.3.7. Final Injector Station Properties

Lastly, with the total temperature and pressure known, as well as the representative static pressure, the remainder of the flow properties at the injector station, (station 3), can be calculated using the *Find Gas Properties* function, as described in subsection 5.1.4.

These properties can then be added to the RDE object being built up by the model. The new attributes, with respect to the previous station, and the full list of methods used within the injector model can be found in Table A.12.

5.4. Calculating Combustor Properties

The basic steps take in the combustion sub-model of the RDE model can be seen in Figure 5.15. These are explained in more detail in the remainder of the section. The combustion chamber itself is split int four distinct stations (3.3a, 3.3b, 3.4, and 4), each with their gas properties output to the user, which can also be seen in the figure.

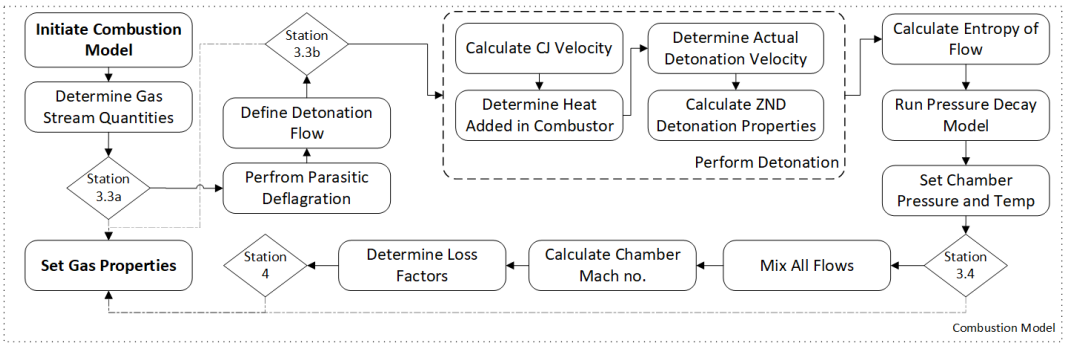

Figure 5.15: Detailed flow diagram of the combustor module of the second fidelity level

There are multiple combustion processes occurring within a single detonation cycle in the combustion chamber, each of these with their own modelling method. Hence, the flow must first be split into the respective streams of propellant, as is described below.

Stations 3.3a and 3.3b define the states of the gas that is split into the relevant flow streams.Station 3.4 is the post-combustion station, where all combustion processes have occurred. Finally, station 4 is defined at the end of the combustion chamber. If the combustion chamber area is constant, and there are no additional processes occurring after combustion, the states at station 3.4 and station 4 are identical.

5.4.1. Definition of Flow Paths

There are a number of different processes occurring within the RDE combustion chamber, resulting in a number of flow paths with different properties and minimal interaction. These flows are:

- Flow lost in the buffer zone (blue)
- Flow undergoing detonation (purple)
- Parasitic deflagration (red)
- Non-combusting flow (brown)

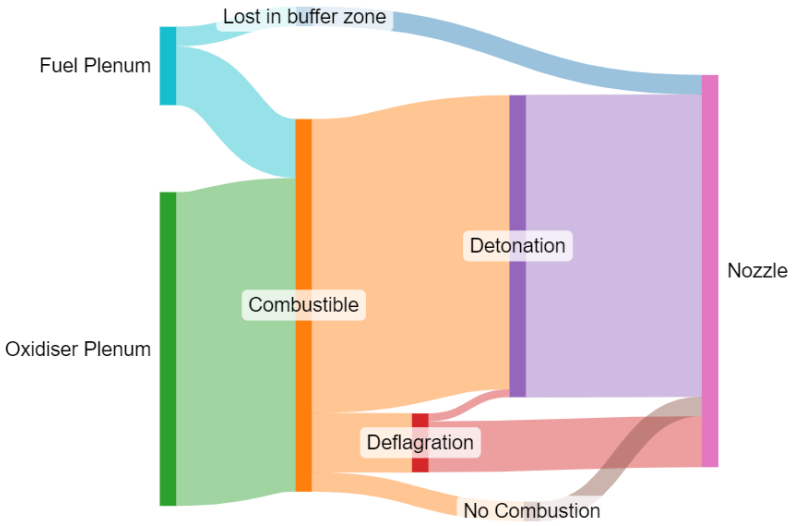

Figure 5.16: Diagram of the different streams of propellant and mixed gas occurring in the RDE

The first of these flows was defined during the injector model, and is the buffer zone portion of mass flow. This is indicated by the darker blue stream at the top of Figure 5.16, and the calculation of which is done by *Define Gas Buffer Zone function*, as seen in Table A.15.

The remaining combustible mass flow (indicated by orange in Figure 5.16) can be split into three streams.

As mentioned in chapter 3, most RDE's operate with a combination of detonative and deflagrative combustion. Parasitic deflagration occurs due to the presence of hot combustion products coming into contact with the fresh propellants, in the time between the passages of the detonation wave. This portion of the flow in indicated in red in Figure 5.16. The amount of parasitic deflagration is defined by ω, and is calculated using the concept of a Partially Stirred Reactor (PaSR), which is explained further in the relevant section below.

The model is built in such a way that the user may define an additional small portion of the flow within the combustion chamber that can be considered to not react at all. When implemented, this is indicated by the brown flow in Figure 5.16, however this portion is normally set to zero. This stream is defined as the *bypass* stream, and if needed can be set by the user.

Lastly, there is the portion of the flow that undergoes detonation. This portion contains the bulk of the combustible mass flow, and is indicated by purple in Figure 5.16. While the largest part of the detonation flow is fresh propellants, a small portion of the deflagrated flow is also included in this. This amount is determined by the input parameter α, and can be set by the user.

The separation of these streams is done using the *Separate Mass Flows* function, of which the inputs and outputs can be seen in Table A.14. With these flow streams separated, the first station within the combustion chamber, station 3.3a, is calculated.

5.4.2. Calculation of the PaSR

Most combustion simulations utilise the assumption of perfectly mixed propellants, as a well-stirred reactor. However, due to the high frequency of the detonation wave, and hence the small time-scale in which the parasitic deflagration operates, this approach is not realistic for use within an RDE. Here, an approach is needed where the reaction and the mixing are simultaneously calculated.

A Partially Stirred Reactor (PaSR) model implements a mixing and reaction process occurring in parallel, and by comparing the turbulent mixing time scale to the turbulent chemical time scale, the portion of the flow that is fully mixed and able to react in a deflagration can be determined [76]. In this way, the

amount of propellants combusting by deflagration before the detonation wave arrives can be estimated by the amount of propellants that have reacted in the PaSR in the time of the detonation period.

The model implements a simplified version of a PaSR model, typically used in CFD calculations, and explained in detail by *Akerblom* [76]. In this methodology, an estimation of the turbulent mixing time scale is compared to an estimation of the turbulent chemical time scale. The non-reacting volume fraction, ω, is related to the ratio of these two as seen in Equation 5.17, where τ_m is the turbulent mixing time scale, and τ_c is the turbulent chemical time scale[2].

$$\omega = \frac{\tau_c}{\tau_c + \tau_m} \tag{5.17}$$

For the turbulent mixing time scale, the relevant parameters are the effective viscosity of the mixture (v_{eff}) and the turbulent dissipation rate of the mixture (ϵ). This can be seen in Equation 5.18. The effective viscosity is determined based on the effective viscosities of the propellant constituents, while the turbulent dissipation rate is estimated based off the work by *Wang et. al.* [77].

$$\tau_m = \frac{v_{eff}}{\epsilon} \tag{5.18}$$

The turbulent chemical time scale depends on the kinematic viscosity of the mixture (v) and the flame speed of the mixture (s_u). This formula can be seen in Equation 5.19. The laminar flame speed is found in *Glassman* [78], while the kinematic viscosity is determined using Cantera.

$$\tau_c = \frac{v}{s_u^2} \tag{5.19}$$

As ω is the non-reacting volume fraction of the gas, $1 - \omega$ is the amount of gas that will undergo the parasitic deflagration reaction. This definition is the same as in the work by *Barnouin*, where ω is the portion of the gas that detonates, and $1 - \omega$ is the portion undergoing parasitic deflagration [65].

The calculation of the PaSR parameters is all completed within the *PaSR* function within the code. The inputs and outputs to the function can be found in Table A.13. Additionally, the default values for the RDE parameters described above are obtained from literature for the combination of H2 and air, and are already implemented in the model. However these are all optional inputs to the model, and can be overridden by the user.

With the parameter ω known, the final flows streams can be defined, leading to the completion of station 3.3b.

5.4.3. Parasitic Combustion

With the determination of the amount of flow deflagrating within the RDE, the deflagration itself can now be performed. As the parasitic deflagration occurs along the line where fresh propellants meet the hot combustion products, as can be seen along the red line in Figure 5.17, this occurs throughout the detonation wave period. Hence, the initial conditions used for this are the conditions that were previously calculated as the average post-injector flow conditions.

[2]Note: The choice of τ as the parameter here is abiding to conventional notation, and this parameter is not related to the normalised detonation wave period, also indicated by τ.

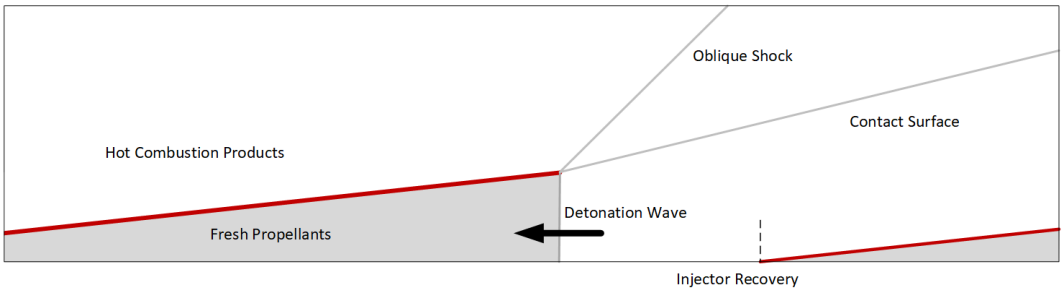

Figure 5.17: Diagram of the processes occurring within an RDE, with the region of parasitic combustion shown along the red line

The combustion itself is simply done with the Cantera equilibrate function: letting the gas entity react until equilibrium conditions have been reached, while holding the static enthalpy and static pressure constant. The static temperature and the gas composition resulting from this combustion is particularly important, as these will be used later when recombining all flows again.

5.4.4. Detonation Combustion

The flows considered for the detonation calculation originate from two separate flows; the smaller has undergone parasitic deflagration, while the larger portion of the flow comes directly from the injectors.

Unlike the parasitic deflagration, the detonation only occurs once per period, and hence requires a single flow condition point from the pressure decay curve. This point occurs where the pressure is equal to the decay pressure, as the decay pressure was defined as the pressure immediately before the passage of the detonation wave. The static temperature used here is the temperature that corresponds to an isentropic expansion of the average flow conditions at the injector to this decay pressure.

In the detonation calculation, the ideal CJ velocity corresponding to the given gas conditions is calculated using the shock and detonation toolbox. However, this velocity is likely not representative of the real detonation process occurring in the RDE. As discussed in chapter 3, it has been shown many times that the detonation velocity measured in tests is not that of an ideal CJ detonation, and that hence a loss factor must be considered. This loss may occur due to the three-dimensional, unconstrained nature of the detonation, or due to improper mixing in the propellants.

An approach to implement this loss is suggested by *Barnouin et al.*, where a factor is added to the heat addition during the detonation [65]. This implementation has also been used here; a factor χ representing the difference of heat added by the detonation, when compared to the ideal detonation, can be input to the model by the user. To apply this factor, the CJ velocity calculated earlier must be translated into the heat addition to the system due to this ideal detonation, and is described in Equation 5.20 [8].

$$Q_{CJ} = \frac{c_0^2 \cdot M_{CJ}^2}{2(\gamma^2 - 1)} \tag{5.20}$$

The speed of sound required to translate this deal detonation velocity to Mach number, and later back, is a result of the detonation calculations of the shock and detonation toolbox.

The model input value χ representing the heat lost compared to an ideal detonation can now be implemented. This factor is used in the reverse of the above equation to get the actual Mach number of the detonation within the RDE, as can be seen in Equation 5.21.

$$M_{act} = \sqrt{2\left(\gamma^2 - 1\right)\frac{Q_{CJ} \cdot \chi}{c_0^2}} \tag{5.21}$$

With the actual detonation velocity determined, the shock and detonation toolbox can be used to calculate the properties of the ZND detonation. This results in knowing the localised static temperature,

static pressure, entropy and gas composition of the flow at the CJ plane. This pressure resulting from the detonation is then defined as the detonation pressure for the next iteration of the pressure decay curve, as can be seen in red in Figure 5.18. These detonation calculations are done in the *Perform Detonation* function, of which the outputs can be seen in Table A.16.

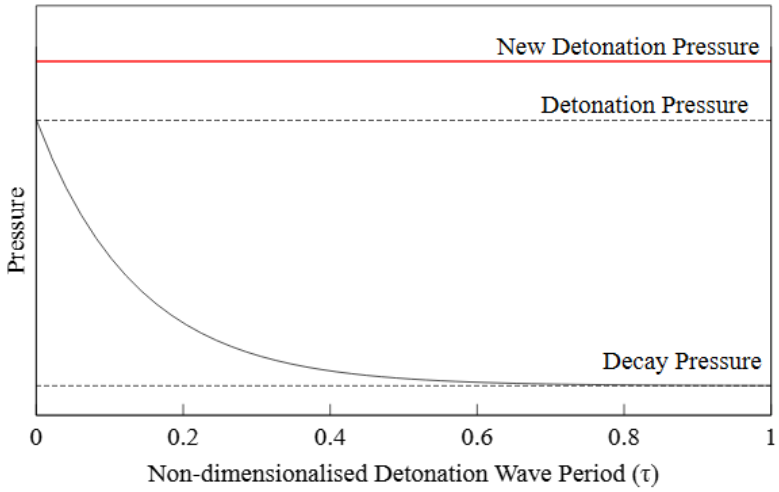

Figure 5.18: The Pressure Decay Curve representing the pressure in the combustion chamber, showing the new detonation pressure

However, as a new detonation pressure has just been defined, this pressure decay curve is no longer representative of the properties calculated in the injector model. The old curve is shown in black in Figure 5.19, while the new curve is shown in red. In addition, representing the changed properties of the injector, the new region of injector unblockage is highlighted in red. These new injector properties are the reason for the iteration at this stage of the RDE model calculations, as descried in the following section.

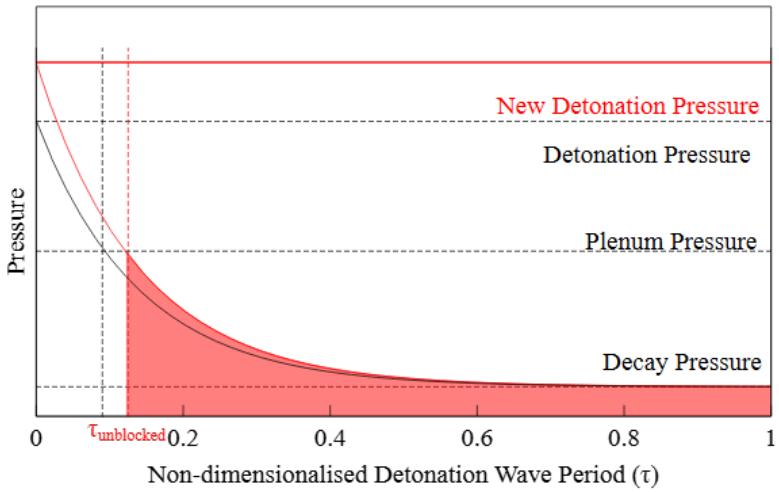

Figure 5.19: The old and new Pressure Decay Curves representing the pressure in the combustion chamber

If the iteration is not necessary, (small difference in detonation pressures), the representative static pressure after combustion is defined. Using this, and knowing that with the current assumptions on RDE phenomena, the entropy of the flow will not change from after the detonation wave onwards, these two properties can be used to calculate the static temperature of the flow that passed though the

detonation wave. This calculation of the average pressure is done in the *Pressure Decay Model*, of which the inputs and outputs can be seen in Table A.17.

While the detonation properties are now known, these are again very localised, and hence representative of only a small portion of the detonation wave period. Hence, after the detonation process, a representative static pressure can be defined. In this case the representative average pressure post combustion is defined as the average pressure of the full pressure decay curve. With the combusted properties of each of the flow paths known, the post-combustion station, station 3.4, is fully defined.

5.4.5. Detonation Pressure Continuity Check

The detonation calculations as described in the previous section give rise to a new value of the detonation pressure. This can be compared to the detonation pressure value of the previous iteration (or the initial guess). If this difference is greater than 1% of the value of the previous detonation pressure, the model will iterate and continue again at the plenum station. The new detonation pressure replaces the initial guess, and the iteration is repeated.

When the difference is less than 1%, the model will continue with the mixing of the flows and the remainder of the calculations required. These calculations are done in the *Check Detonation Pressure* function, of which the inputs and outputs can be seen in Table A.18.

5.4.6. Mixing of the Flow Paths

The now four sets of flows defined throughout the injector and combustion models (buffer zone, non-combusting, deflagration and detonation), can now be mixed together again after combustion (station 3.4). The gas compositions of these four flows are combined in a mass-averaged process. This is done in this manner as the mixture of equilibrium and non-equilibrium gas compositions is important to recognise. It is important to note here that the assumption of frozen flow is used. While each of the separate flow streams are individually in equilibrium, the mixed flow may not be. To prevent further combustion effects from being simulated, the composition is frozen in the mixing process.

The pressure of these separate flows is a little more difficult to define however, as these vary significantly throughout the period of a detonation wave, and simply mass-averaging the pressures results in a large underestimation of the pressure in the combustor. Hence, as the detonation is the dominant process in the RDE combustor, the representative static pressure of the detonation flow, as calculated above, is also representative of the static pressure after combustion for all combined flows.

As this assumption is made that this average decay pressure is valid for each of the flows, most of the gas properties of these flows are no longer valid. Either an expansion or compression to the required pressure must be completed. It is assumed that the entropy of these flows does not change with this expansion or compression, and hence the entropy is used at the second state variable for each of the flows. The entropy of each flow can then be mass averaged, and combined to a single representative flow. Using this, the pressure and the composition defined above, the remainder of the flow properties can once again be determined.

This mixing of all flow paths present in the combustor is performed in the *Mass Average Flows* function, of which the in- an outputs can be seen in Table A.19.

5.4.7. Determination of the Mach Number

With the static temperature, static pressure and the gas composition of the gas known, either the total pressure, or the Mach number must be known to fully define the gas properties after combustion. The Mach number is calculated using an equation derived from the mass flow equation which can be seen in Equation 5.22.

$$M_c = \frac{\dot{m}\sqrt{\frac{TR_g}{\gamma}}}{P \cdot A_c} \tag{5.22}$$

Now the flow properties directly after the combustion processes are known. If there are no additional loss factors in the remainder of the combustion chamber, and the chamber area is constant, the current

station 3.4 properties are identical to the properties at station 4.

5.4.8. Potential for Additional Losses

While there are currently no additional losses implemented after the combustion is completed, there are at least two factors identified during the literature study that may still have an impact on the performance of the RDE. These are the heat loss to the walls, and the total pressure loss due to the presence of a oblique shock and detonation interaction, among others.

This structure is implemented into the code to enable the painless addition of these factors at a later stage. The structure is represented by the *Loss factors after Combustion* function, of which the current inputs and outputs are shown in Table A.20.

5.4.9. Nozzle Throat Continuity Check

The final continuity check of the RDE model is the nozzle throat continuity check. Before this check can be performed however, the total pressure at the end of the combustor must be calculated. This is done with the isentropic flow relation, as seen in Equation 5.23.

$$P_{t_4} = P_4 \cdot \left(1 + M_4^2 \left(\frac{\gamma - 1}{2}\right)\right)^{\frac{\gamma}{\gamma - 1}} \tag{5.23}$$

The nozzle throat continuity check is performed to ensure the mass flow that corresponds to the conditions calculated for the combustor exit is the same as the total mass flow input by the user. This is done by calculating the total chamber pressure that would exist if the nozzle is choked with the mass flow through the injectors, as calculated in Equation 5.24, and comparing this to the total chamber pressure current calculated.

$$P_{req} = \frac{\dot{m}}{A^*}\sqrt{\left(\frac{R_g T_t}{\gamma}\right) \cdot \left(\frac{\gamma + 1}{2}\right)^{\frac{\gamma+1}{2(\gamma-1)}}} \tag{5.24}$$

If these two pressure values differ by more than 1%, a new estimation for the detonation pressure is determined using a Newton-Rhapson iteration scheme. A corresponding new estimation of the decay pressure is then also made by utilising the ratio between the old and new detonation pressure guesses. With these new detonation and decay pressures, the model starts again at the start of the plenum model.

If the pressure difference is less than 1%, the model will go on to calculate the remainder of the gas properties at station 4.

5.4.10. Final Combustor Station Properties

With the static pressure and temperature known, as well as the Mach number at the end of the combustion chamber, the remainder of the flow properties can be calculated using the methodology described in subsection 5.1.4.

The gas properties at the combustor station can be added to the RDE object stored in the model, and an iteration of the combustion model is complete. The attributes of the RDE at completion of the combustion model can be found in Table A.21.

5.5. Calculating Nozzle Properties

The two models calculating the properties at the nozzle throat (station 8), and the nozzle exit (station 10), are the final sub-models of this RDE model. Apart from the necessary assumption of a thermally perfect gas due to the high temperatures in the flow, these calculations are not very different to the nozzle calculations of a traditional rocket engine.

There are two models to cover the full nozzle; the first, the nozzle throat model which runs from station 4 at the combustion chamber end to station 8 at the nozzle throat. The second, the nozzle exit model, runs from the nozzle throat to station 10 at the nozzle exit. Both models are relatively simple, and rely purely on isentropic flow properties and relations.

5.5.1. Nozzle Throat Model

A simple flow diagram of the nozzle throat model can be seen in Figure 5.20.

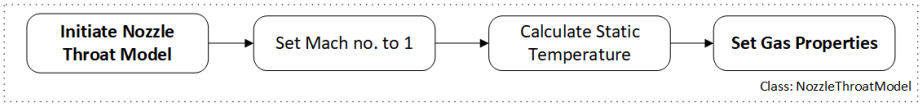

Figure 5.20: Detailed flow diagram of the nozzle throat module of the second fidelity level

Throughout this model, the frozen flow assumption. Hence, either the Mach number, or one static property must be found to obtain the remainder of the flow properties. In this nozzle throat model, the assumption of nozzle choke is made, and the throat Mach number is set to one. This is then used to find the static temperature of the flow. After this, the remainder of the nozzle throat station properties can be found using the same *Find Gas Properties* function as found in subsection 5.1.4.

The gas properties of the nozzle throat can then be added to the RDE object stored in the model. Aside from the addition of the gas properties, neither of the nozzle models contribute any additional attributes to the RDE object, hence there is no table created to show these.

5.5.2. Nozzle Exit Model

This model calculates the properties of the flow right at the exit of the nozzle. There are two possibilities for nozzle type, either a converging-diverging nozzle may be selected, or an aerospike. A flow diagram highlighting the paths of both versions of the model can be seen in Figure 5.21.

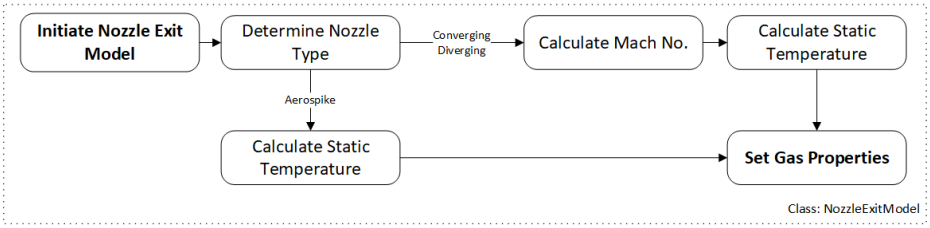

Figure 5.21: Detailed flow diagram of the nozzle exit module of the second fidelity level

This model allows for the user to make a choice between the two different nozzle types; If a nozzle exit area is given as model input, the model will assume a converging-diverging nozzle and calculate accordingly. If there is no exit area given, the model will assume the nozzle is an aerospike type nozzle, and expand the gas to the given ambient pressure (defaults to 1 bar).

As the area ratio for the converging-diverging nozzle is fixed, the Mach-area relation can be used to calculate the Mach number at the nozzle exit. However, as the flow can no longer be considered a calorically perfect gas, the differential form of the Mach-area relation will be used, which allows for thermally perfect effects [79]. This methods integrates the equation shown in Equation 5.25 over the full length of the nozzle, and allows for modelling of the flow expansion process as it does so.

$$\frac{dA}{A} = \frac{1 - M^2}{\rho V^2} dP \tag{5.25}$$

Iterating this equation over the length from nozzle throat to exit allows the pressure at the nozzle exit to be determined. From here the exit Mach number can be calculated. These calculations are performed in the *Find Nozzle Exit Mach* function, the inputs and outputs of which are shown in Table A.22.

Once the exit Mach number is known, the static temperature can be calculated through the isentropic relations, as seen in Equation 5.26.

$$T_{10} = T_{t_{10}} \cdot \left(1 + M_{10} \frac{\gamma - 1}{2}\right)^{-1} \tag{5.26}$$

The calculations for the aerospike nozzle rely on a calculation of the static temperature at the nozzle exit based on the total to static pressure ratio at the nozzle exit, as seen in Equation 5.27.

$$T_{st} = T_t \cdot \left(\frac{P_t}{P_{st}}\right)^{\frac{-(\gamma-1)}{\gamma}} \tag{5.27}$$

Once the static temperature is found, the *Find Gas Properties* function can be used to determine the remainder of the gas properties. Finally, the nozzle exit station gas properties can be added to the RDE object stored in the model.

5.6. Determine Performance Parameters

There are a number of parameters defined as important to characterise the performance of an RDE. As discussed in chapter 3, these are the characteristic velocity, the thrust, the specific impulse, the pressure gain, the combustion efficiency, and the detonation velocity. The detonation velocity is directly calculated in the model itself, and this section explains how the remainder these parameters are calculated once the model is completed.

The characteristic velocity is calculated as shown in Equation 5.28.

$$c^* = \frac{P_{t_4} \cdot A^*}{\dot{m}} \tag{5.28}$$

The thrust is calculated by Equation 5.29.

$$T = \dot{m} \cdot V_e \tag{5.29}$$

The specific impulse (Isp) is defined by Equation 5.30 in the case of rocket-mode operation. When airbreathing operation is used, only the fuel mass flow is considered for this equation.

$$Isp = \frac{T}{\dot{m} \cdot g_0} \tag{5.30}$$

The pressure gain is defined as in chapter 3 and is calculated by Equation 5.31.

$$\Delta P = \left(\frac{P_{t_4}}{P_{t_2}}\right) - 1 \tag{5.31}$$

Lastly, the combustion efficiency is calculated by first defining the ideal characteristic velocity, in Equation 5.32, and then by using Equation 5.34.

$$c^*_{id} = \frac{\sqrt{R_g T_{t_{id}}}}{\Gamma} \tag{5.32}$$

Where Γ is the van de Kerkhoven function, seen in Equation 5.33.

$$\Gamma = \sqrt{\gamma}\left(\frac{2}{\gamma+1}\right)^{\frac{\gamma+1}{2(\gamma-1)}} \tag{5.33}$$

$$\eta = \frac{c^*}{c^*_{id}} \tag{5.34}$$

5.7. Overall Model Creation

This chapter has described the creation of the performance assessment tool for rotating detonation engines. The structure of the software itself was discussed, followed by the main assumptions and auxiliary functions used. This tool is created in Python, with a number of sub-models representing the different stations found within the RDE.

The calculation starts at the plenum where 4 values are guessed, both plenum pressure, the detonation pressure, and the decay pressure. After the calculation of the injector, including the injector discretisation and the buffer zone, the first iteration loop is made, to replace the guessed plenum pressures with more accurate values. The model then calculates the different flow paths in the combustion,. as well as the combustion itself before running the second iteration on the detonation pressure. Finally the remainder of the model is calculated, and the final iteration at the nozzle throat is performed to update the decay pressure.

The model then calculates the nozzle properties and finally the performance parameters identified in chapter 3 to complete a run of the model.

6

TNO Test Campaign

It was mentioned earlier that this thesis is performed at TNO, in parallel with their running RDE project. The RDE data from this campaign, gathered both as part of this thesis and the larger TNO project, is used here for the validation of the RDE model created. In the TNO project, the gathered data will mainly be used to gain a greater understanding of RDE's and how they operate.

The test set-up for performing the RDE tests and gathering the data was created in 2023, partially as the internship project that led to this thesis [80]. The test themselves were carried out as a joint effort between the TNO RDE team and this thesis, and the planning and operating of these took about a month of the overall thesis time.

This section of the thesis describes the test goals of the campaign performed in 2024, the set-up used to gather this validation data, and a few results of this campaign are also shared.

6.1. Test Goals

This test campaign was undertaken with two reasons, firstly to gather enough data to fully validate the model created in this thesis. This requires data to be collected in a wide range of geometry variations and operating conditions. Secondly, to map out the boundaries of where the current TNO RDE operates, and to map the performance within these boundaries.

As the generation of sufficient validation data will also fall within these operational boundaries and hence follow automatically from the second purpose, the goals of the test described here are for the mapping of the RDE performance over the operational conditions of the TNO RDE.

6.2. Test Set-up

The TNO RDE is of a modular design, based closely on that of the TU Berlin [32, 81–83], which is in turn based on the design initially proposed by *Shank et al* [84]. This test setup is also described in the work of *Roos et al.* [74], and this section is heavily based on that description. A cross-section of the engine can be seen in Figure 6.1, where the portions of the engine filled by fuel are indicated in orange, while those with oxidiser are indicated in blue.

The fuel chosen for this test campaign is gaseous hydrogen (H2), while the oxidiser is air. The engine is ignited using a specially engineered pre-detonator device, which runs off a combination of gaseous hydrogen and gaseous oxygen (O2). This pre detonator is implemented in a similar manner as described in chapter 3.

The modularity in the engine design allows for variations of internal engine components; utilised here are variations in fuel and oxidiser injector area, as well as nozzle throat area. Should it be required, this design allows for further alteration of many features, including the chamber channel height, the chamber length, and adding a divergence to the channel itself. The variations in geometry that have been used in this test campaign are listen in Table 6.1. The oxidiser injector area is set by changing a

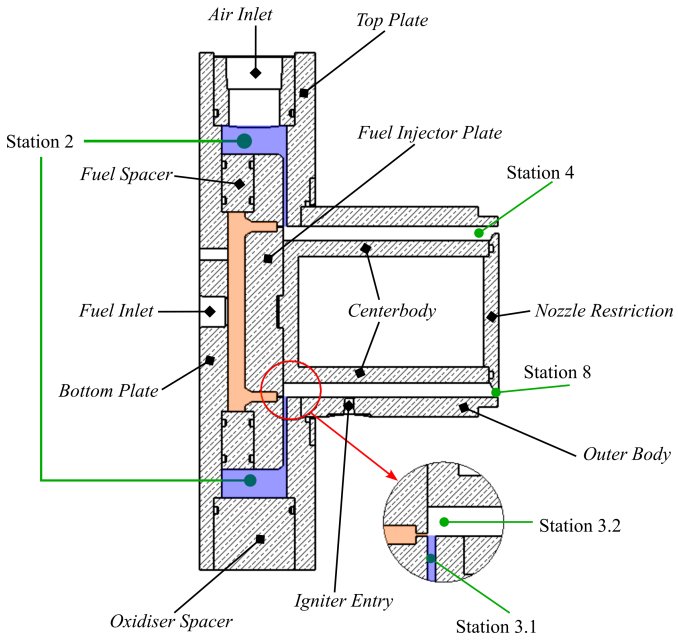

Figure 6.1: Cross-section of the TNO RDE. Image produced by TNO [74]

spacing height, while the fuel injector consists of 100 holes with the diameters given. Lastly the nozzle area is set by applying a restriction on the chamber area.

Table 6.1: The variations in geometry possible with the TNO RDE

Geometrical element	Configurations	Units
Oxidiser injector spacings	1, 1.6 , 2, 2.2, 2.8, 3	[mm]
Fuel injector	5, 7	[mm]
Nozzle restriction	0, 12.5, 25, 37.5, 50	[%]

The oxidiser is supplied to the engine through a single line diverging, through the use of an air manifold, into 5 flexible hoses attached to the oxidiser plenum. The fuel enters the fuel plenum through a singular pipe. Attached between this pipe and the engine is the fast-acting main valve for the hydrogen supply. In both supply lines, a stagnation chamber and orifice are placed to ensure accurate mass flow control, of the system. This set-up can be seen in Figure 6.2, where the portions relevant to the fuel and oxidiser supply to the engine are highlighted.

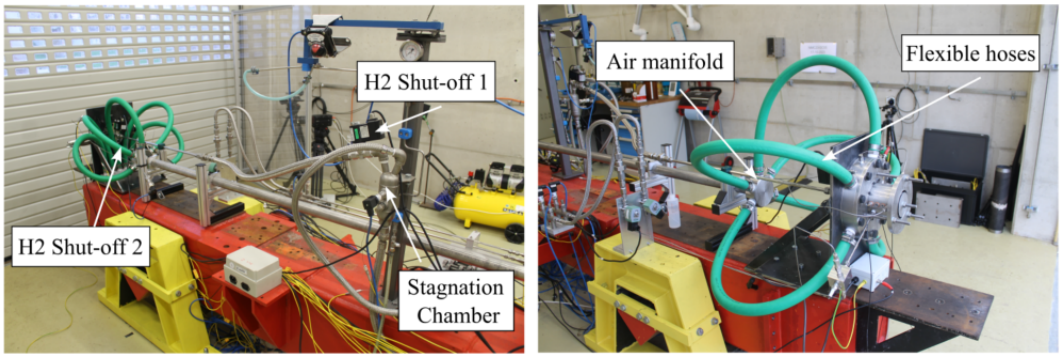

Figure 6.2: The fuel and oxidiser supply to the TNO RDE, based on [74].

The pre-detonator is attached directly to the chamber wall, with lines connecting to the supplies of the relevant fuel and oxidiser. The relevant aspects of the pre-detonator ignition system can be seen in Figure 6.3.

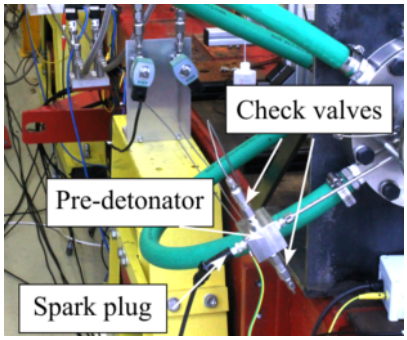

Figure 6.3: The pre-detonator ignition system of the TNO RDE, based on [74].

The test facility supplies the required oxidiser at a maximum pressure of 60 bar, and maximum mass flow of 8.5 kg/s. The fuel supply has a maximum pressure of 80 bar, and a maximum mass flow of 160 g/s. However, the engine geometries and gas feed system impose constraints on the maximal mass flows and pressures. Hence, a testing envelope of total mass flows between 0.3 and 1.7 kg/s and of equivalence ratios between 0.7 and 1.0 was implemented.

The instrumentation of the system consists of two pressure sensors on each plenum; one measuring at 6kHz on the standard DAQ system, and the other at 100 kHz on an oscilloscope. The high frequency sensor measures the possible fluctuation of plenum pressure due to the detonation wave, while the low frequency sensor measures the average plenum pressure. Additionally, both a piezo-electric and a piezo-resistive pressure sensor are attached at the end of the combustion chamber on a long stand-off tube. These act as Capillary Tube Attenuated Pressure (CTAP) measurement devices to measure the average static pressure at the end of the combustion chamber [33].

Finally, up to three high frequency pressure sensors are placed at the entrance of the combustion chamber, where the detonation wave passes. These sensors acquire at a sufficiently high frequency to measure the peaks and troughs of the detonation wave pressure spikes, and hence allow wave-mode analysis to be done on the RDE tests. These sensors can be seen in Figure 6.4, where the three types of instrumentation are indicated[1].

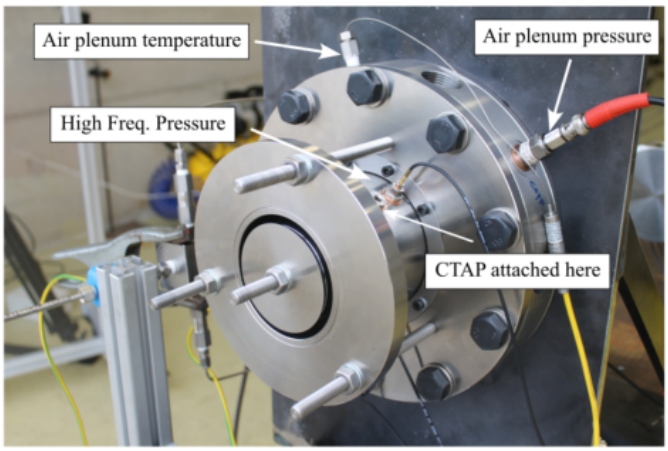

Figure 6.4: The testing instrumentation system of the TNO RDE

The type of instrumentation used in the test campaign can also be seen in Table 6.2, which also indicates the parameters that are directly measured by this instrumentation.

[1]Note that not all correct sensor types are attached in this image, however the locations indicated are accurate.

Table 6.2: The instrumentation used on the RDE test set-up at TNO.

Instrumentation type	Amount	Parameters Measured
Plenum pressure sensor	1 Fuel, 1 Oxidiser	Plenum pressure at 6 kHz
Plenum high-frequency pressure sensor	1 Fuel, 1 Oxidiser	Plenum pressure at 100 kHz
Plenum thermocouple	1 Fuel, 1 Oxidiser	Plenum temperature
CTAP Piezo-electric	1	Average static chamber pressure
CTAP Piezo-resistive	1	Average static chamber pressure
Chamber Pressure sensor	Up to 3	High frequency chamber pressure at 500 kHz

In addition to these sensors, there was a high speed camera present during the test campaign. However this was present for detailed analysis of detonation wave modes. Hence, this analysis is outside the scope of this thesis, and the data is not used for model validation.

After a test is complete, a number of checks are performed before it is deemed a success. This involves ensuring the mass flow of both the fuel and oxidiser, as well as the equivalence ratio, are within the 5% of set value. An example of the equivalence ratio and total mass flow of such a test can be seen in Figure 6.6 and Figure 6.5 respectively. This data is from a test with a total mass flow of 0.3kg/s, and an equivalence ratio of 1.

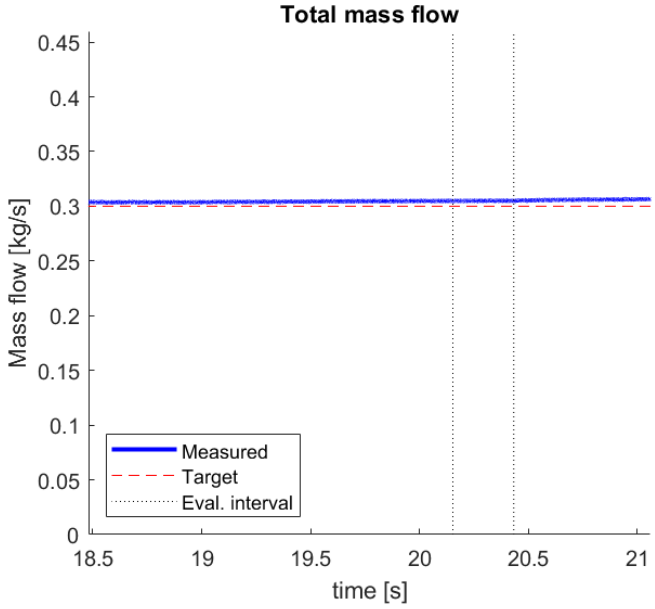

Figure 6.5: The total mass flow measured against the set-point for an RDE test

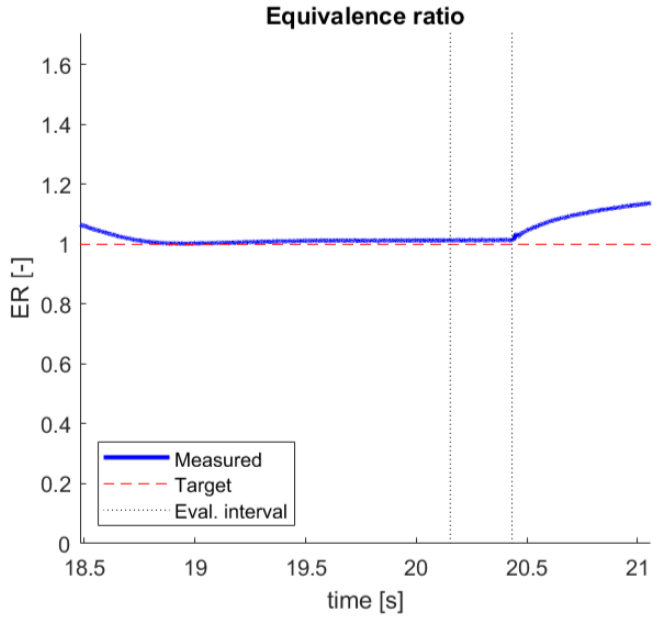

Figure 6.6: The equivalence ratio measured against the set-point for an RDE test

Additionally, it is checked whether the relevant instrumentation worked correctly during a test. If either of these criteria were not met, a test was to be repeated until a successful test was obtained.

6.3. Test Results

The data gathered from this test campaign will be used for the validation of the RDE model developed during this thesis. It would be ideal if the validation could be performed for the gas properties at each of the stations defined in the model, as well as the RDE performance parameters as defined in chapter 3. However, the scope of the validation is limited by usable data obtained from the test results.

The relevant measured parameters are the plenum pressures, the plenum temperatures, and the static chamber pressure. These properties are measured both during the firing of the RDE, as well as in the cold flow phase preceding the test.

An example of the test results obtained from a single RDE test are shown below, with the data already downsampeled. This test has a mass flow of 0.3 kg/s and an equivalence ratio of 1. The unfiltered and filtered records of the combustion pressure can be seen in Figure 6.7, and Figure 6.8 respectively. The ignition occurs at approximately 19.9 seconds, and the full second before this is the cold flow phase of the test.

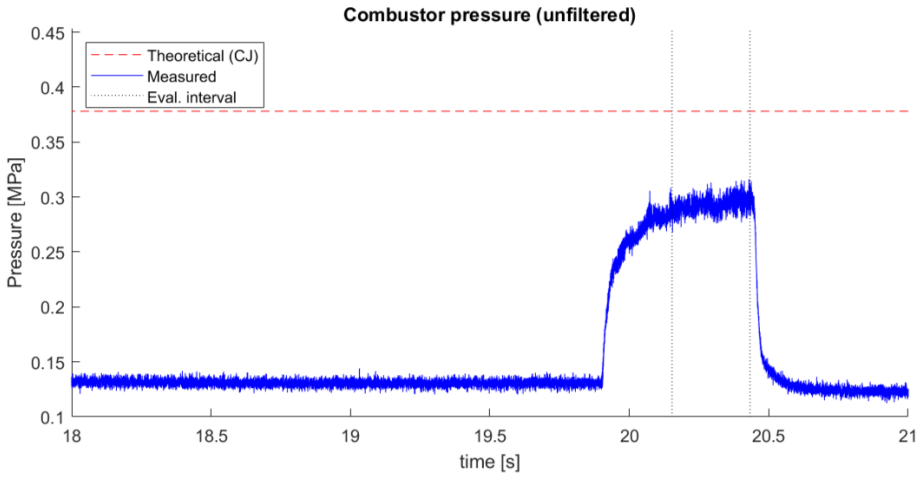

Figure 6.7: The unfiltered chamber pressure records as measured by a CTAP sensor, with the Eval. interval as the time interval selected by the user.

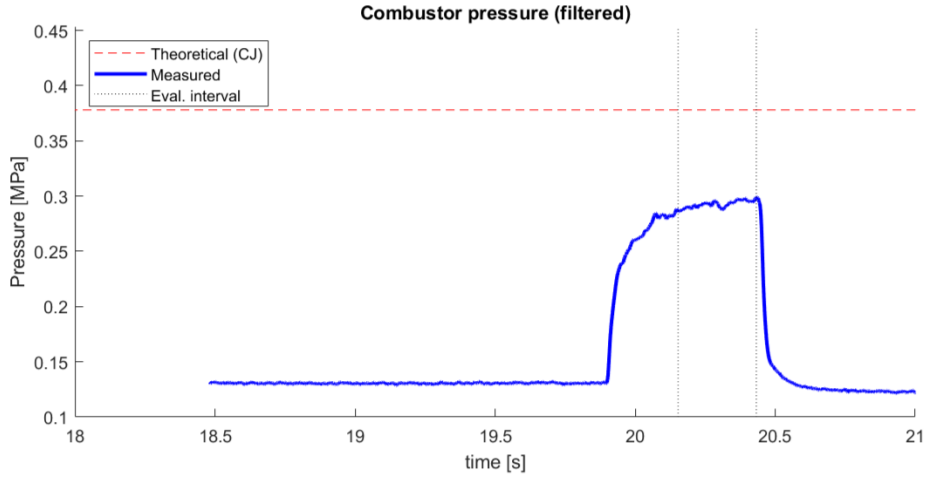

Figure 6.8: The filtered chamber pressure records as measured by a CTAP sensor, with the Eval. interval as the time interval selected by the user.

In addition, the unfiltered and filtered comparison between the air plenum pressure and the combustion pressure can be seen in Figure 6.9, and Figure 6.10 respectively.

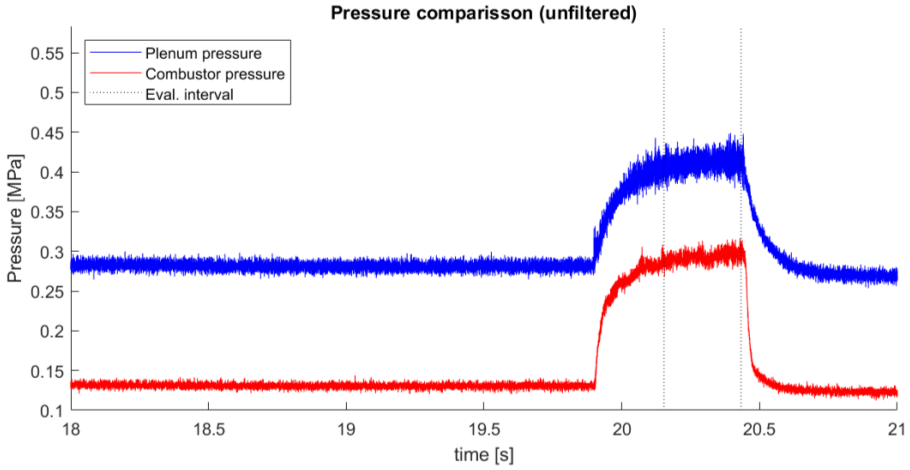

Figure 6.9: The unfiltered air plenum pressure and chamber pressure records, with the Eval. interval as the time interval selected by the user. The theoretical (CJ) indicates the pressure that would be reached with an ideal (CJ) detonation.

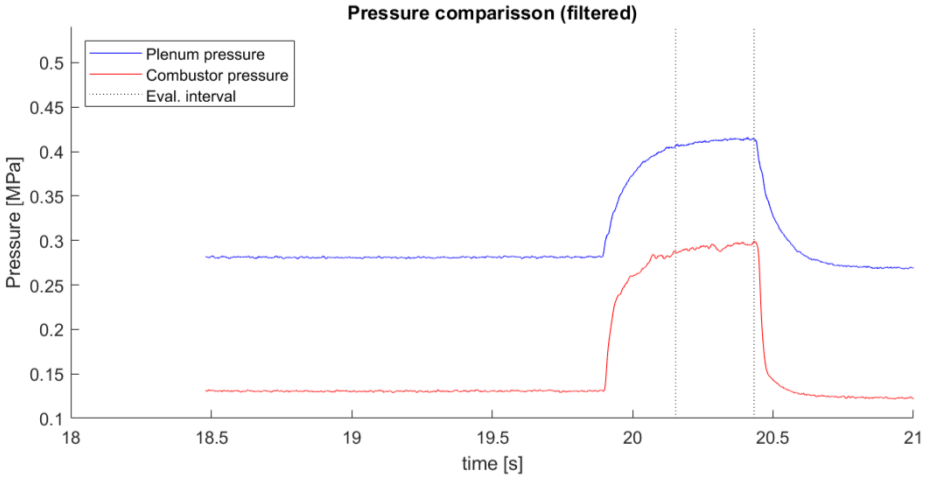

Figure 6.10: The filtered air plenum pressure and chamber pressure records, with the Eval. interval as the time interval selected by the user The theoretical (CJ) indicates the pressure that would be reached with an ideal (CJ) detonation..

There are additional parameters that can be extracted from the test data. For this derivation, use is made of an in-house tool which calculates the total chamber pressure, the total and static combustion temperatures, the pressure gain, the characteristic velocity, and the combustion efficiency.

While the data from the high speed camera is not useable to gather data, it does provide some interesting images. The ignition phase gives the largest contrast, and an example ignition of the RDE can be seen in Figure 6.11, where the total sequence of 12 frames is approximately 100 μs. The ignition starts from the pre detonator, at the bottom right of each frame.

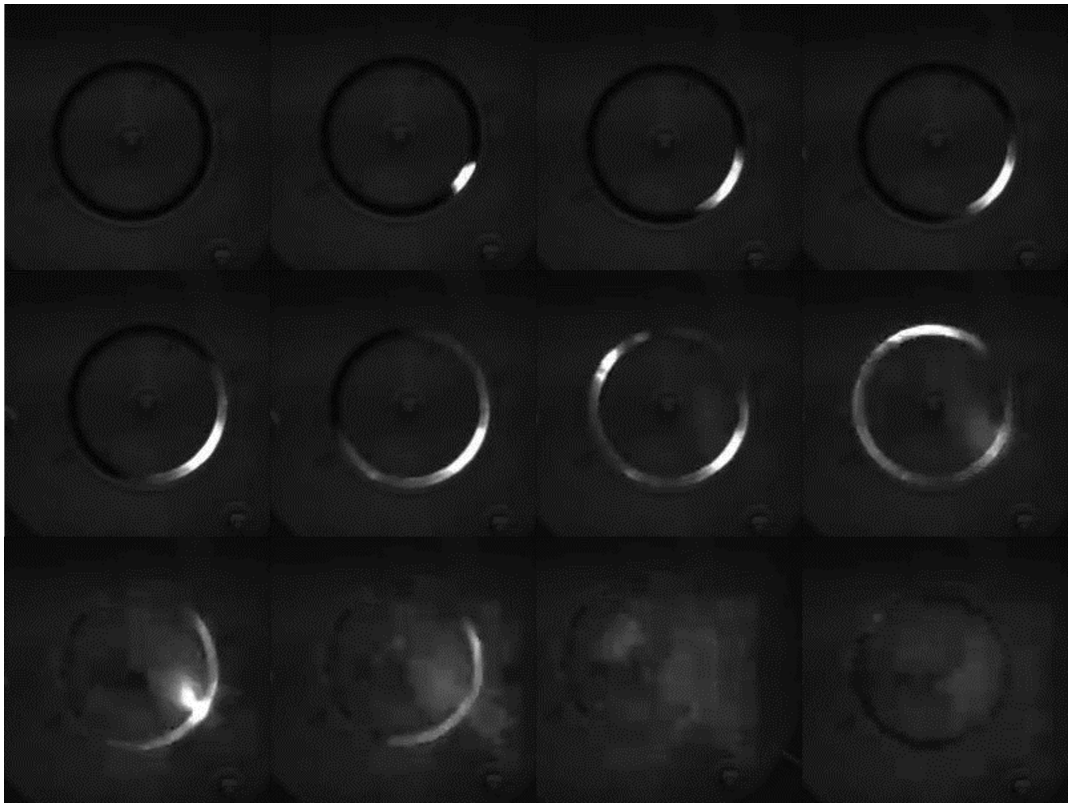

Figure 6.11: The ignition of the RDE, with frames 80μs apart.

6.4. Selection of Test Data

There were 118 hot fires completed during the RDE test campaign. However, as is typical with test campaigns, a few tests were required to get the sensor configuration initialised correctly, and there were a number of faulty sensors during the course of the test campaign. Hence, a number of tests do not accurately represent the reality of what may have been occurring in the RDE, and are thus disregarded for the future validation of the RDE Model.

The first set of tests were removed as these were performed without proper data from the high frequency pressure sensors on the chamber, which occurred due to oscilloscope issues. In addition, a number of other tests were found to be outside of the operating point which was initially defined for each test, however after further analysis it was decided these would be suitable to still use for validation. Lastly, a set of tests was removed from the possible dataset as the pressure sensors attached to the CTAP's were yielding unusual results.

This results in a set of 82 test of which the data can be used for validation of the model.

6.5. Test Campaign Conclusions

This chapter has presented the test campaign run at at TNO as part of this thesis, the test set-up and instrumentation is described, and compared to be very similar as used in *Roos et al.* [74].

An example of the test results from this campaign is shown, and it is explained that this is reworked to find the reevant performance parameters for validation later on. Finally, a selection of test data is made, resulting in 82 sets of data usable for the validation of the RDE model.

7

Software Verification and Validation

A large part of the creation of a model or program is ensuring it both works as intended, and accurately represents the reality that is being modelled. The first part of this is the software verification, while the second part refers to software validation. This chapter will describe the verification and validation techniques undertaken for the RDE model.

There are two verification steps, the first is the software verification; ensuring all small components of the model function as intended. The second is the requirement verification which verifies that the model is created as was intended by the stakeholders.

There are three main validation steps, the first of which is performing a comparison between the model results and reality in the form of test results. This section is done in two steps, first an intermediate validation with the completion of the first fidelity level, and secondly a full validation against the test results presented in chapter 6. Next, a sensitivity analysis of a number of input parameters to the model is performed in order to quantify the effect an error in these parameters may have on the full RDE model.

7.1. Software Verification

This software verification is the process of ensuring all building blocks to the model work as intended. The first aspect is creating verification tests for every separate function in the model.

Next a number of small scale sensitivity analyses are performed on functions and parameters within the model, namely the PaSR and the pressure decay curve.

7.1.1. Verification Tests

Software verification is applied to the RDE model using primarily unit tests of every function used within the model. These tests are set-up in a separate file, and should also be used with every code change to verify the model still works as intended. To aid in this, a new function has been created, which generates a default RDE with inputs from a TNO test case. A verification test is made for every individual function in the model, and these are described in Table 7.1.

Table 7.1: Table showing the verification tests for every function used in the model

Model Initiation Function	Test Purpose	Test description

test find gas properties	This tests whether aspects of find gas properties function as intended	A cantera entity is made, and a GasProp dictionary is generated based on this entity. If the values are calculated with isentropic relations in the function, flow properties in this entity are checked against the GasProp dictionary. If they are generated using cantera, the GasProp dictionary is checked against manual isentropic relations.
test supersonic isentropic conversions	This test checks whether there is a mistake in one of the supersonic insentropic conversion functions at supersonic conditions	A number of standard gas properties (temperature, pressure, enthalpy, density) are transformed from static to total conditions using the functions that contain the isentropic relations for this model, and then back to static using the functions for total to static. The resulting static conditions are checked against the input static conditions, they should be identical.
test subsonic isentropic conversions	This function checks whether there is a mistake in one of the supersonic isentropic conversion functions at subsonic conditions	Functions in the same way as the test described above
test mach and gamma	This test checks whether the functions to calculate the Mach number and the specific heat ratio are correct	Creates a Cantera entity with standard conditions, checks to ensure the specific heat ratio is 1.4 for air. Then defines a total to static pressure ratio corresponding to super- and subsonic conditions. Uses this to calculate the Mach no., and checks this against manually calculated and verified values.

Plenum Model		
Function	**Test Purpose**	**Test description**
test plenum pressure guess	Ensure the plenum pressure and mass flow in this equation is calculated correctly	The function is used with a particular mass flow as input. The resulting plenum pressure is then used in a different, manual, mass flow calculation to get the mass flow corresponding to that pressure. These mass flows are then checked to be identical.
test cantera plenum	Ensure the Cantera gas states in the plenum are correct	The plenum model is run with the values assigned in the default instance function. A Cantera gas entity is made using the entropy, pressure, and composition resulting from this plenum model. A check is then performed to make sure the enthalpy from this Cantera entity and the default RDE instance are identical. The same test is made for both the oxidiser and fuel plena.

Injector Model		
Function	**Test Purpose**	**Test description**
test pressure decay	Ensure the pressure decay function uses the correct values	Creates the pressure decay curve with given values. Checks to makes sure the first (peak) value is the in-putted detonation pressure, and the last (lowest) value is the in-putted decay pressure)

test blockage factor	Ensure the blockage factor calculation works as intended	Tests a case where the blockage should be zero (not blocked) and one (fully blocked) respectively. Checks this is also the case
test mass flow	Ensure the mass flow though the injector is correctly calculated	Compares the mass flow from the function with a manually calculated, verified mass flow value
test reversed mass flow	Ensure the injector back flow is correctly calculated	Using the same input, compares the mass flow from the reversed mass flow function with the mass flow resulting from the Mach no. and mass flow functions verified earlier. The values should be identical
test buffer zone	Ensure the equivalence ratio adjustment and mass flow lost is in correct format	Runs three sets of the buffer zone function; where the plenum pressures are equal, fuel is higher pressure, and oxidiser is higher pressure. Checks to make sure the equivalence ratio does not change with the first, and that there is no mass flow lost. For the second, it checks to ensure the new equivalence ratio is less than 1, and the lost mass flow is fuel. And for the final round, checks to make sure the new equivalence ratio is greater than 1, and the mass flow lost is oxidiser.
test downstream pressure	Ensure the downstream pressure calculations have the correct trend	Runs the downstream pressure function three times, with two variations of blockage ratios and pressure decay curves. Checks to make sure the higher detonation pressure yields a higher downstream pressure, and higher blockage ratios yield a lower downstream pressure.

Combustion Model		
Function	**Test Purpose**	**Test description**
test PaSR	Ensure the PaSR calculation yields correct trend	Tests the PaSR model at two different temperatures and pressures. Ensures a higher degree of deflagration occurs at higher temperature and pressure
test perform detonation	Ensure the factor χ functions as intended	Runs the detonation function with two different χ as input. Should give a lower temperature and pressure for the lower χ. Additionally checks the resulting detonation velocity when $\chi = 1$ against a perfect CJ calculation.
test pressure decay model	Ensures the pressure decay model functions as expected.	First tests to see whether an increase in detonation pressure yields the expected increase in decay pressure. Then checks to makes sure the average pressure calculated is the same as would be calculated by the pressure decay model in the injector model.
test calculate Mach number	Checks the calculated Mach number is the same as would be calculated using the Mach-area relation	Calculates both Mach numbers and raises an error if they are not the same

Nozzle Models		
Function	**Test Purpose**	**Test description**

test calculate Mach number	Ensures the imperfect Mach no. relation works as intended	Tests the imperfect Mach no. with a gas that is perfect. Checks to make sure the same conditions are calculate as with the standard Mach-area relation.
test static temp no Mach	Ensures the correct static temperature is calculated.	tests the function against a combination of previously verified functions. Ensures the static temperature resulting from both are equal.

7.1.2. Component Sensitivity Analyses

There are a few parts of the model that require inputs for well-documented physical attributes, such as the flame speed of the propellant combination, or less well known factors from literature. As these are values that have been directly obtained from literature and input to the model, an important step of the model verification is ensuring the correct values are used, and further ensuring variation in these inputs does not cause too large a variation in the results of the RDE.

This section describes the sensitivity analyses performed on the inputs to the partially stirred reactor, all of which have been obtained from well documented parameters. A second sensitivity analysis is performed on the inputs to the pressure decay curve, obtained from RDE-specific literature.

Partially Stirred Reactor Sensitivity Analysis

The PaSR is an aspect of the model which includes a number of variables obtained from literature. This includes the effective viscosity of the propellants ν_{eff}, the turbulent dissipation rate of the mixture ϵ, the kinematic viscosity of the mixture ν, and the flame speed of the mixture s_u. It is important to quantify how far an error in one of these inputs will propagate towards difference performance parameters in the RDE model. Hence, two sets of sensitivity analysis are carried out; the first is to see how sensitive the value of ω is, which defines the portion of flow to go through the detonation instead of the deflagration. The second is to quantify the effect of changes in ω on the performance characteristics of the RDE.

The graphs displaying the results of the first set of sensitivity analysis can be found in Appendix E, section E.1. Using these, it was found that a 10% difference in either the turbulent dissipation rate, or in the kinematic viscosity leads to a 1.1% difference in ω. Additionally, a 10% difference in the laminar flame speed leads to a an approximate 2.1% difference in ω, in this case the analysis is not linear. Lastly, changes in the effective viscosity do not affect the parameter ω, as this factor cancels out in the equations.

The results of the second sensitivity analysis, the effect of changes in the parameter ω on the parameters of the RDE, can be seen in Table 7.2. The parameters chosen for this analysis are the same as those parameters that can be easily obtained from the test data, as described in chapter 6, and as such can be directly compared to the results of the validation round performed in section 7.4.

Table 7.2: The results of the second sensitivity analysis, showing the impact a 10% change in ω has on the relevant RDE parameter.

Parameter	Change in parameter [%]
Oxidiser Plenum Pressure	3.1
Fuel Plenum Pressure	3.5
Total Combustion Temperature	-2.1
Total Combustion Pressure	-0.9
Pressure Gain	3.2
Combustion Efficiency	-1.5
Characteristic Velocity	-0.9

It can be seen that all changes in the parameter are relatively low (below 4%), and the parameter ω has the largest impact on the fuel and oxidiser plenum pressure, as well as the pressure gain. This is due to the fact that an increase in ω means there is an increase in the amount of propellant detonating, leading to higher back pressure and thus a higher plenum pressure.

A full table showing the effect of the three inputs in the PaSR on the aforementioned RDE parameters can be seen in Table E.1 in Appendix E. A 10% change in any of the three inputs in the PaSR results in a maximum of 0.74% change in the RDE parameters considered.

Pressure Decay Sensitivity Analysis

In a similar manner as to above, the value of k used in the pressure decay curve generation is obtained through comparisons to literature. As this value is not nominally changed in the code, a sensitivity analysis has been done to determine the impact variation in this parameter has on the RDE performance.

The full graphs of this sensitivity analysis can be found in Appendix E, section E.2. While doing the analysis, it became apparent that the model does not converge when the parameter k dropped below 6, approximately a reduction of 20%. Additionally, the largest deviations in the performance parameters became apparent when the parameter k went above 9.5, an increase of approximately 30%. It must be noted that the sensitivity analysis is hence bound by the points $k = 6$ and $k = 9.5$, and the value of k should not fall outside these bounds.

Additionally, the parameter k has the largest influence on the plenum pressures, and hence the pressure gain. This is especially apparent near the chosen value of $k = 7.2$, and becomes less apparent in the ranges $k = 8$ to $k = 9.5$.

The impact of a 10% change in the parameter k on each of the performance parameters can be seen in Table 7.3.

Table 7.3: The results of the second sensitivity analysis, showing the impact a 10% change in the parameter k has on the relevant RDE parameter.

Parameter	Change in parameter [%]
Oxidiser Plenum Pressure	0.04
Fuel Plenum Pressure	-0.32
Total Combustion Temperature	-0.83
Total Combustion Pressure	-0.63
Pressure Gain	0.50
Combustion Efficiency	-0.60
Characteristic Velocity	-0.63

As can be seen here, the RDE model are not very sensitive to changes in these input parameters, specifically so for the pressure decay parameter k.

7.2. Requirement Verification

In addition to the verification of the building blocks within the model, it is also necessary to verify that the model functions as intended. This will be verified though the use of a requirement verification process, to ensure every requirement has been met.

This requirement verification process is documented in Table 7.4. For some requirements, a further explanation is needed, and this is given in the section below.

Table 7.4: Table showing the verification of the requirements for the model.
Requirements can be fully achieved (Y), partially achieved (P), or not achieved (N)

Functional Requirements		
Requirement	**Met?**	**Verification**
REQ01	Y	An example output print of the model can be seen in Appendix D. It can clearly be seen that the 6 defined parameters of engine performance are calculated and given as an output to the function. Additionally for each station (stations 2, 3, 4, 8, 10), the required set of local gas properties is also provided.
REQ02	Y	The station definition used in the model is given in Figure 5.1. This follows the definition used by *Brophy et al.* [29].

REQ03	P	The model currently supports all conditions described apart from the alternative propellants. There is no limit to the chamber pressure that can be calculated, and there is a test implemented to ensure the model can identify what the detonability limits are for the equivalence ratio. However, currently the only propellants the model works with are H2 as fuel, and air as oxidiser, however Appendix C described how the addition of new propellant types should be implemented into the model. Additionally, preliminary work has been done on adding methane as an additional fuel to the model.
REQ04	Y	The model calculates the properties of the gas at every station described by Figure 5.1, but does not allow for radial variation within the RDE. This makes the model a 1D tool. Additionally, the model functions in a similar manner to the thermodynamic tools described in chapter 3, and hence can be classed as a thermodynamic cycle analysis tool.
REQ05	Y	This check is implemented according to the guidelines given by *Bykovskii et al.* [41]. A warning is given to the user when the geometry falls outside the limits
REQ06	Y	The two sets of initial conditions are implemented to allow for both the rocket-mode and airbreathing operation of the RDE.
Implementation Requirements		
Requirement	**Met?**	**Verification**
REQ007	Y	An example of the usage of the model, and the implementation in python is shown in Appendix D. The implementation format is clearly as stated in the requirements.
REQ08	Y	A MatLab script has been completed in which the model can be called. All input and output variables are defined as MatLab variables.
REQ09	Y	The Model is structured in such a manner to allow for the easy addition of further models or functions within models. The addition of a new model is a simple addition of a few lines within the main code, and the creation of a new class in a similar manner to the models already in use. Additionally, extra functions can be added to any of the exiting models, and implemented within the *find gas properties* function.
REQ10	Y	As described in the section above, every unique function has been tested and these test can be run on a git workspace or similar.
Performance Requirements		
Requirement	**Met?**	**Verification**
REQ11	P	The impact of each of each of the described physical phenomena have been included within the model. A full description of how each phenomena is included in the model is given below.
REQ12	P	The model takes approximately between 3 and 10 [s] to run.

Modelling of Physical Phenomena: REQ11

Requirement 11 describes the physical phenomena that should be modelled by this RDE model. These phenomena are highlighted here, and it is explained where each of these are implemented in the model.

The parasitic combustion is modelled with the deflagration occurring in the combustion chamber, the amount of which being determined by the PaSR. Propellent mixing losses due to the buffer zone are modelled by the buffer zone in the injector model. Propellant mixing loss due to insufficient mixing are modelled by the combination of the buffer zone and PaSR, in both the injector and combustor models.

Heat loss due to unburnt propellants is implemented through the ability to let a portion of propellant go unburnt throughout the full RDE. The total pressure loss in injection is reflected in the injection losses.

Finally, the implementation of the oblique shock is not yet complete, and as discussed in Appendix B, the trade-off was made between the implementation of this and a more detailed validation of the model.

7.3. Sensitivity Analysis of Input Parameters

There are a number of parameters that remain as an input to the model at this stage. They may, in the future, be calculated by additional functions within the model itself, but at the moment these need to be input by the user. These input parameters are:

- χ: the heat loss in detonation when compared to ideal
- α: the amount of deflagration products passing though the detonation wave
- the discharge coefficient of the main nozzle

While the discharge coefficients of the oxidiser and fuel injector nozzles are also input parameters, it is assumed that the value of these is known from the injector design, and hence these are not considered input parameters in the same manner as those above.

A reasonable value estimation has been found from literature for each of the parameters, but the impact of changes in these parameters on the outcomes of the model must also be assessed. Hence, this sensitivity analysis takes a range of values for each of the three inputs, and runs the model over this range. The two previous sensitivity analyses were done using a single test point. However, in this case it was determined that using a number of test points would ensure a more through sensitivity analysis. In addition, using points that will also be used in the validation would allow for further insight on the sensitivity analysis. Hence, test cases have been randomly sampled from those that will be used for validation, and the results are compared to the model outcomes for the sensitivity analysis.

The residual in the validation parameters for variation in the first input parameter, χ, can be seen in Figure 7.1. Here a clear trend can be seen that the residual becomes more positive when the factor χ is closer to 1. It can be seen that the trendline of the residuals is at zero when the value of χ is approximately 0.95.

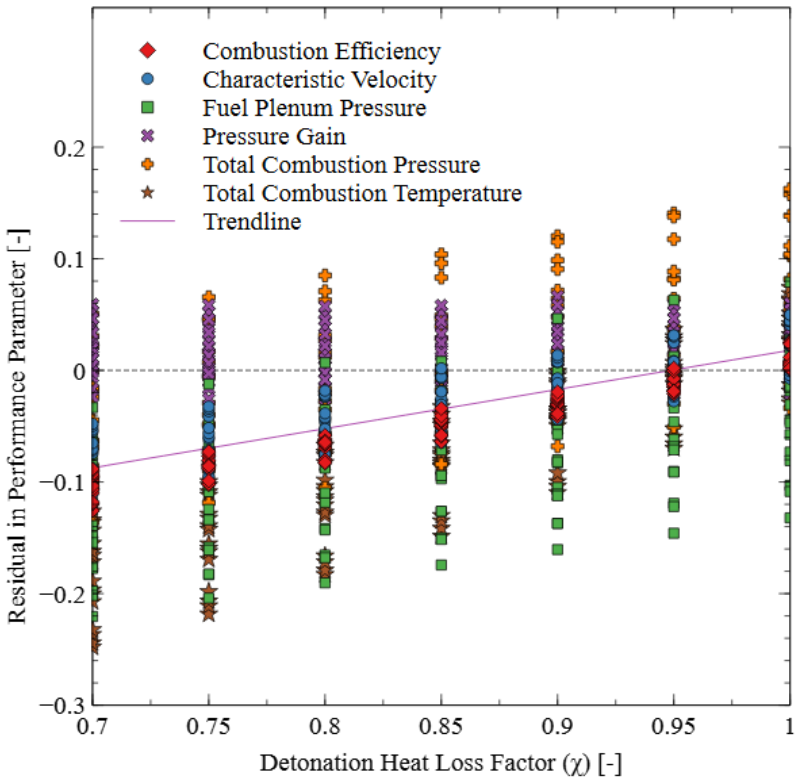

Figure 7.1: The sensitivity analysis results showing the residual in the validation parameters against the heat release factor in the detonation, χ

Additionally, it can be noted that the model results vary by approximately 5% for a 0.15 change in χ.

The residual in the validation parameters for a change in α can be seen in Figure 7.2. While initially a larger scale sensitivity analysis was run from $\alpha = 0$ to $\alpha = 1$, it was noticed that the residual was closest to zero with the α bounds shown here.

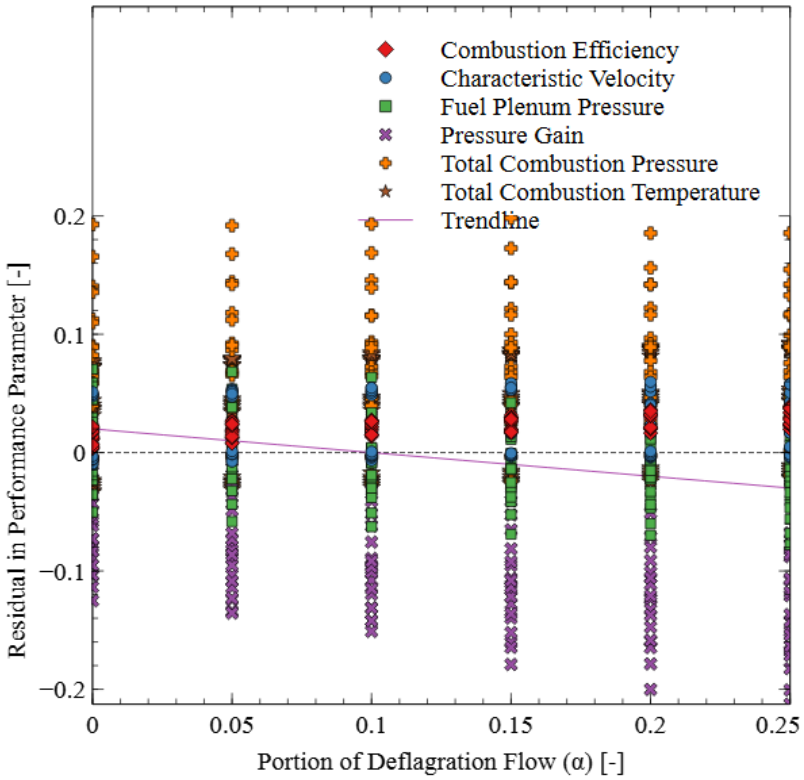

Figure 7.2: The sensitivity analysis results showing the residual in the validation parameters against the portion of deflagrated flow to pass through the detonation

The trendline indicates the optimum value of α is approximately 0.1, meaning that 10% of the parasitic deflagration flow also passes through the detonation wave. Additionally, there is only about a 3% difference in residual when the value of α is changed by this ideal value.

Lastly, the residual in validation parameters for variation in the nozzle discharge coefficient can be seen in Figure 7.3. In this case the trendline is a second order polynomial. Similarly to the parameter α above, a more coarse sensitivity analysis was performed first, before narrowing the range to values between 0.84 and 0.94.

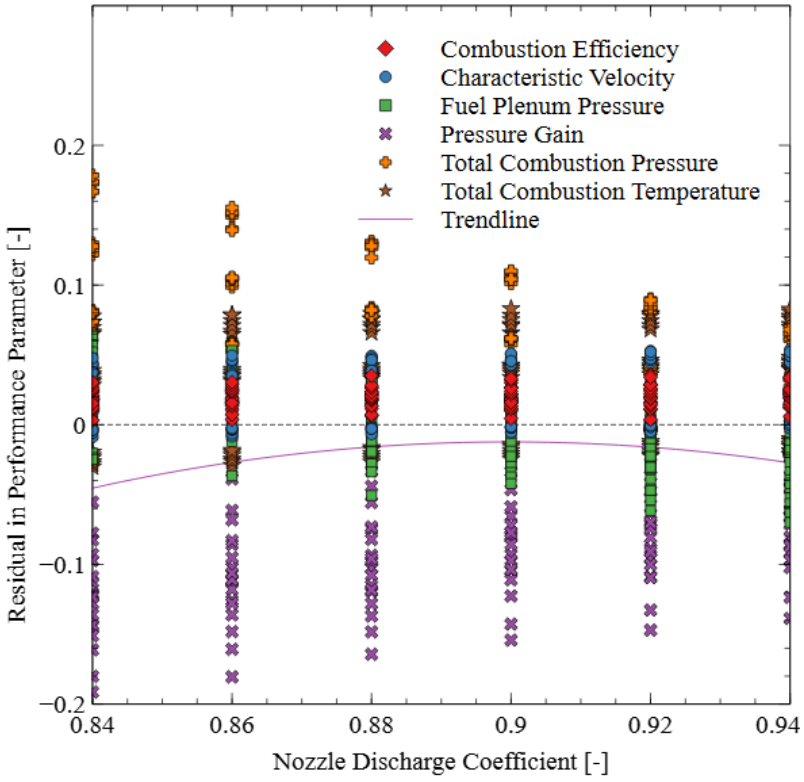

Figure 7.3: The sensitivity analysis results showing the residual in the validation parameters against the discharge coefficient of the nozzle throat

For the nozzle discharge coefficient, the optimal value (with the residual closest to zero) lies approximately at 0.9, however the spread of the residuals for different performance parameters is lower when the discharge coefficient is at 0.92 or 0.94. Additionally, the change in residual within this range is at most 3%. However with the seemingly parabolic nature of this trend, it can be expected that this residual increases more the further from the optimum.

While the parameters χ and α seem to be relatively robust against the input values due to linear nature of the trendline, the nozzle discharge coefficient needs to be determined more accurately. However, this nozzle discharge coefficient will also largely depend on the geometry of the nozzle in the actual RDE, and hence this effect on the validation parameters may be a direct result of the RDE used in the TNO test campaign.

7.4. Experimental Data Validation Results

Validation of the model is the process of ensuring it accurately represents reality, and can be trusted as a resource on the performance of RDE's. While the previous verification performed was to ensure the building blocks of the model are correct, this validation round is to ensure the validity of the model and that it accurately represents reality.

This validation of the final version of the code for the purpose of this thesis, was completed using the full dataset generated by the test campaign. This full dataset consisted of 82 tests where the data was complete, and deemed to be error free, as described in chapter 6. The propellants used here are hydrogen and air, and the model is used in rocket-mode with an aerospike nozzle.

The goal of this validation round is to show the residuals between the model outcomes and the test data generated by the test campaign are small enough so that the model may be trusted by the academic community. The accuracy of similar models was discussed in chapter 3, and was found to be between 2-30% for those papers that performed a validation.

The parameters chosen for this validation are a combination of the parameters measured directly, and those derived from the experimental data, and can be seen in Table 7.5.

Table 7.5: The RDE parameters selected to be used for validation.

Parameter	Measurement type
Oxidiser Plenum Pressure	Direct measurement
Fuel Plenum Pressure	Direct measurement
Total Combustion Temperature	From initial data analysis
Total Combustion Pressure	From initial data analysis
Pressure Gain	From initial data analysis
Combustion Efficiency	From initial data analysis
Characteristic Velocity	From initial data analysis

The additional parameters not directly measured are chosen as they are output by the initial data analysis tool described in chapter 6, and are good indicators of the flow properties and performance of the engine. The remainder of the performance parameters as defined in chapter 3, the Isp, thrust, and the detonation velocity are not calculated by this data analysis tool, and as such cannot be used here. The parameters measured directly are expected to be slightly more reliable than those with a calculation step in between. However, the data analysis tool is expected to be dependable and valid, and the outcomes are deemed to be comparable to the remainder of the test data.

Figures 7.4, 7.5, and 7.6 show a selection of the validation results, where the test results are plotted against the model output for the given validation parameter. A perfect fit is indicated by a trendline with a slope of 1. As can be seen, the plenum pressures show a slight deviation from the perfect fit, with the model tending to overestimate the oxidiser plenum pressure slightly, and underestimating the fuel plenum pressure slightly.

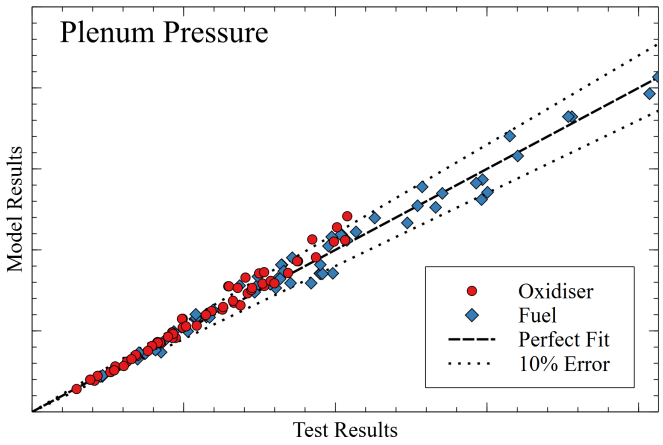

Figure 7.4: The validation results showing the respective plenum pressures resulting from test results compared to the model output for the selected runs

Similar can be said for the combustion pressure, shown in Figure 7.5, where the total and the static combustion pressures each show a near-perfect fit, both at the higher and lower end of the pressure range.

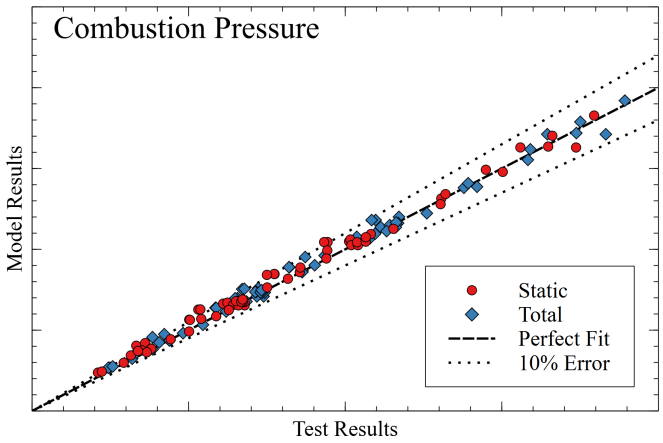

Figure 7.5: The validation results showing the chamber pressure resulting from test results compared to the model output for the selected runs

In Figure 7.6, the pressure gain seems to have a larger spread, and on the whole the model has a slight tendency to underestimate the pressure gain of the engine. This pressure gain is a combination of the plenum and combustor pressures as shown above, and hence the pressure will have a larger error.

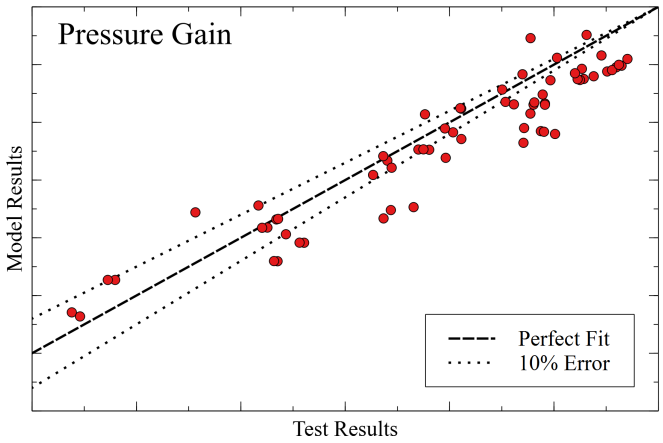

Figure 7.6: The validation results showing the pressure gain resulting from test results compared to the model output for the selected runs

However, the error in the pressure gain as seen in Figure 7.6 is is the relative error, and the values of the pressure gain are relatively small. An absolute pressure gain difference of 0.02 on a measured value of -0.04 will already give a relative error of 50%. Hence, for this parameter is is better to view the error as an absolute error. These error bars can be seen in Figure 7.7, where the error is the absolute error. This will also be used in further analysis.

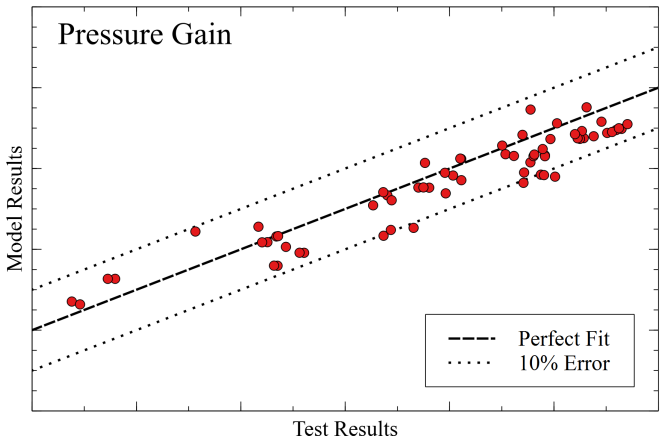

Figure 7.7: The validation results showing the pressure gain resulting from test results compared to the model output for the selected runs

As can be seen, all points lie within a 10% error margin using the absolute error. Lastly, the test results against the model outcomes for the static and total combustion temperatures can be seen in Figure 7.8.

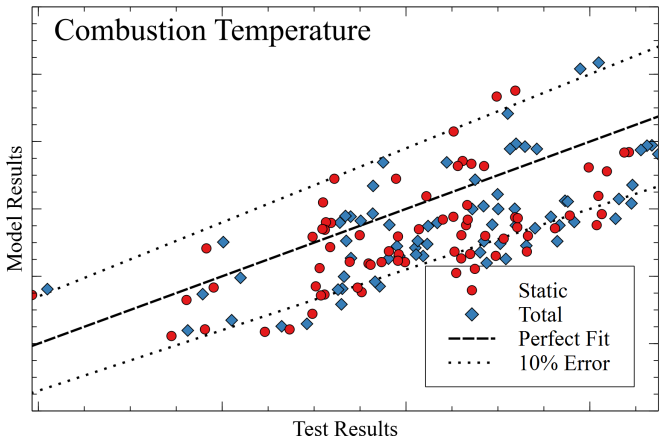

Figure 7.8: The validation results showing the respective total and static combustion temperatures resulting from test results compared to the model output for the selected runs

When compared to the pressure shown previously, there is a significant difference in the spread of the data points. While the majority still fall within the 10% error margin, the combustion temperature seems to be underestimated. This may be because of the fact that the pressures were directly measured as part of the experiment, while the temperature data was derived from a number of experimental data parameters.

Similar graphs for the remainder of the validation parameters can be found in Appendix F.

Figure 7.9 shows the distribution of the residuals of the validation parameters. The graph echoes the trend as shown above in Figure 7.4 with respect to the plenum pressures; a slight overestimation is seen in the oxidiser plenum pressure, and a slight underestimation in the fuel plenum pressure.

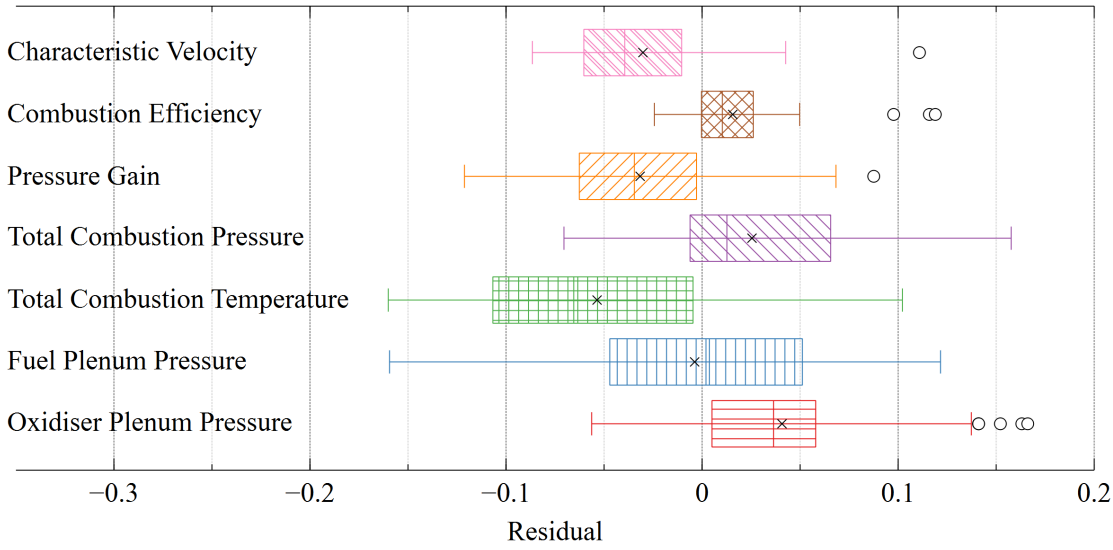

Figure 7.9: The validation results showing the distribution of the residuals between the model outputs and test results

Additionally, it can be seen that the total combustion temperature has the largest mean residual of approximately 6%. In comparison, the fuel plenum pressure is the most accurate with a mean residual less than 1%. Additionally, the remainder of the performance parameters have a mean residual of less than 5%, which is an excellent accuracy for this type of tool.

Additionally, all extremes of the residuals are well within the 20% error margin for the combustion temperature, and most are within 10% for the remainder of the parameters.

While it was assumed the test data obtained from the non-directly measured parameters is fully accurate, the variance in specifically the combustion temperature as compared to the remainder of the variables might indicate this is not fully the case. The derivation of the combustion temperature from the test data requires the knowledge of the gas composition, and more specifically of the gas constant, which is not required in the derivation of the other parameters. The gas constant used in this derivation assumes full detonation of the flow, and as such may differ from the actual gas constant found in the engine.

This validation shows what parameters of the model are more reliably trusted than others. As can be seen the pressures (both plenum and chamber) are fairly accurate with respect to the test data. This indicates that the pressures at the remainder of the stations are most likely also quite accurate. This means that the performance parameters based on such aspects, such as the pressure gain, thrust and specific impulse can be trusted. In comparison, the accuracy of the combustion temperatures here in the model seems slightly lower, and the reliability of this conclusion is not fully determined. Hence, the accuracy of the combustion efficiency may be slightly lower, and this result should be treated with more care.

7.5. Verification and Validation Conclusions

This chapter has described the verification and validation undertaken on this model to ensure the model adheres to client wishes and accurately represents reality. The software verification is first discussed, where the verification unit tests for every function of the model are shown and explained. Each of these verification tests are successful. In addition, two small sensitivity analyses are carried out on the propellant and model parameters, to ensure a deviation does not cause significant changes to the output of the model.

The verification of the requirements is next, where it is discussed which requirements are met. If any requirements have not been met, this has been discussed with the client, and the explanation has been provided.

A larger scale sensitivity analysis has al;so been performed on the full model, regarding the model

inputs that are selected by the user. These inputs are the parameters α, χ, and the discharge coefficient of the nozzle. Here it was found that changing these inputs does have a slight impact on the model outputs. However, the outputs differ by at most 5% if these inputs stay within the reasonable ranges identified.

Lastly, the model was validated using the experimental data collected in the test campaign. Here it was found that the largest difference between the test data and model output lies in the combustion temperature, with a mean residual of 6%. Additionally, the average mean residual is approximately 4%. There are no outliers with a residual larger than 20% for any of the performance parameters analysed, and the vast majority of these residuals lie within the 10%. This is compared to the accuracy of models in literature and found to be of good quality.

8

RDE Performance Assessment

Up until this point, this thesis has been focussed on creating a verified and validated model for a hydrogen and air based Rotating Detonation Engine. A large part of the research objective of this thesis however is to use this performance model to assess the impact of various geometries and operating conditions on the identified performance characteristics of an RDE. In this chapter, the model will be used to assess the RDE performance for a large range of input parameters.

The direct relationships between the input parameters and the performance of the RDE will first be shown. In addition to this, the performance is compared for combinations of input parameters, such as the area ratio between the oxidiser inlet and the nozzle, throat, or the mass flux through various locations in the RDE. From here it can be determined which input parameters have an important impact on the performance. Finally, the relationship between performance parameters can also be investigated.

These performance characteristics were identified in chapter 3, and the various geometries and operating conditions that can be varied were determined in the creation of the performance assessment model itself, described in chapter 5. The full list of both of these can be found in Table 8.1.

Table 8.1: The performance parameters, geometry inputs, operating conditions, and combinations of these used in the RDE performance assessment

Performance Parameters	
Name	**Unit**
Thrust	[N]
Isp	[s]
Pressure gain	[-]
Combustion efficiency	[-]
Detonation velocity	[m/s]
Geometry Inputs	
Name	**Unit**
Oxidiser injector area	[m^2]
Fuel injector area	[m^2]
Nozzle throat area	[m^2]
Chamber outer diameter	[mm]
Chamber channel height	[mm]
Operating Conditions	
Name	**Unit**
Equivalence ratio	[-]
Total mass flow	[kg/s]
Combined Parameters	
Name	**Unit**
A_2/A_8 (Injector to throat area ratio)	[-]
J_4 (Chamber mass flux)	[kg/m^2s]
J_8 (Nozzle throat mass flux)	[kg/m^2s]

The independent parameters used in the further analysis were selected based on their relevance and importance as identified in the literature. These parameters are dependent on a combination of the geometries and operating conditions shown in Table 8.1, and their effects on the performance parameters have been investigated.

Firstly, the results of the model run for differences in area ratio between the oxidiser injector area, and the nozzle throat area ($A_{3.1}/A_8$) are discussed. Then the impact of the parameter defined as the power density by *Bach et al.* is investigated. This parameter is a combination of the chamber cross-sectional area, the mass flow of the oxidiser, and the equivalence ratio [81]. Lastly, the direct impact of the equivalence ratio are investigated.

Adjustments in the remainder of the geometric inputs did not show a significant relationship with the performance parameters in comparison to the results shown here.

For each of the cases run, the model input parameters χ, α, and the relevant discharge coefficients remain constant. In addition, it must be noted that while the combination of hydrogen and air as propellants may be indicative of an airbreathing application, the topic of this thesis is to investigate the performance parameters of RDE's for use in launcher or space-based applications, and hence the model was run in rocket-mode for this performance assessment. This may lead to difference to the values in literature of specifically the specific impulse of the RDE, where the total mass flow is considered.

8.1. Area Ratio

A key geometric parameter of the RDE is the ratio between the oxidiser injector area and the nozzle throat area, ($A_{3.1}/A_8$). This is especially relevant with propellant combinations such as hydrogen air, where the fuel injector is by necessity much smaller than the oxidiser injector. Both the oxidiser injector area and the nozzle throat area are individually important parameters, as they define the choking of

the injector and full engine. However, when combined, the area ratio is a dimensionless and scalable parameter which can be used to compare performance for all RDE sizes. This parameter has also been said to capture the largest geometrical impacts of the RDE [65, 81].

The area ratio parameter has the most significant impact on the pressure gain of the RDE, which is shown in Figure 8.1.

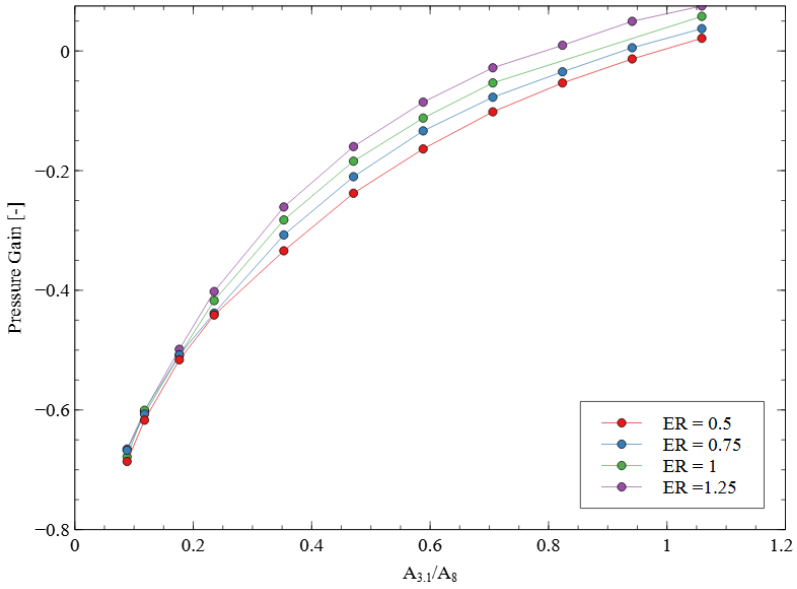

Figure 8.1: The relationship between the area ratio, ($A_{3.1}/A_8$), and pressure gain of the RDE, with lines for different equivalence ratios.

As can be seen, the larger area ratio indicates the larger pressure gain achieved by the RDE. This is a phenomena also seen in literature, summarised neatly by *Bach et al.* [17, 29, 81]. As mentioned in chapter 3, a larger oxidiser injector area results in less injection losses. In addition, the smaller nozzle throat area will cause the average chamber pressure to increase. This combination of parameters drive the pressure gain up with increasing area ratio, resulting in the trend shown above.

There are downsides to a large area ratio however; a larger oxidiser injector area will cause more coupling between the plenum and combustion chamber. In addition, aside from further increasing this coupling, the increased chamber pressure will also give rise to longitudinal pulsed detonations. Longitudinal pulsed detonation are instabilities within the combustion chamber of the RDE, which are believed to reduce the performance [41]. More recent work has shown that these may not be entirely loss effects, and in the right conditions, can lead to the spinning pulsed detonation mode [85].

Similarly to all thermodynamic models of RDE's discussed in this thesis, the model does not yet incorporate these loss effects due to plenum-chamber coupling, nor those due to potential longitudinal pulsed detonations.

Aside from the pressure gain, the relationship between this area ratio and the combustion efficiency can be seen in Figure 8.2.

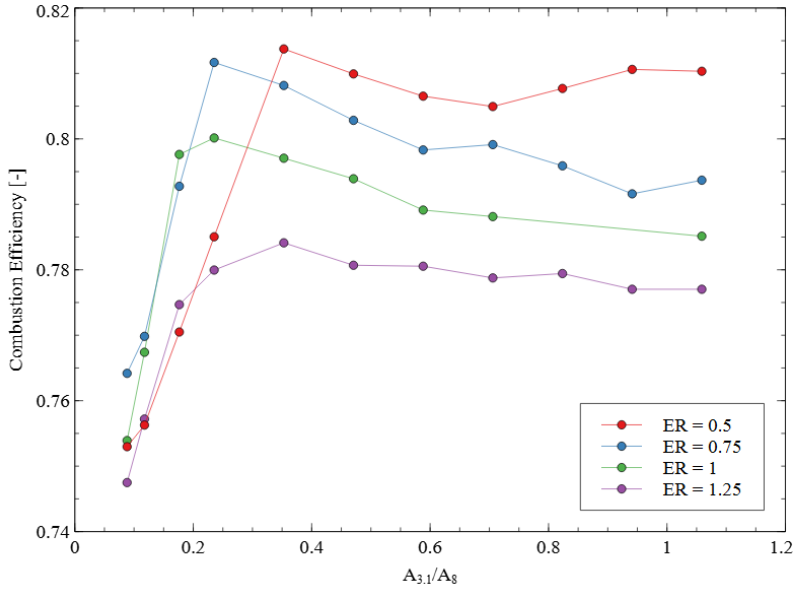

Figure 8.2: The relationship between the area ratio, ($A_{3.1}/A_8$), and combustion efficiency of the RDE, with lines for different equivalence ratios.

Although no direct trend can be seen with regards to the full range of area ratios, it is interesting to note the sharp drop-off in combustion efficiency with the area ratios approximately less than 0.2.

In contrast to the above two, the relationships between the area ratio and the detonation velocity, specific impulse, and thrust show a decrease in performance with an increase of area ratio. This can be seen most clearly in the detonation velocity, shown in Figure 8.3, but the additional two graphs can be seen in Figures G.1 and G.2 in Appendix G.

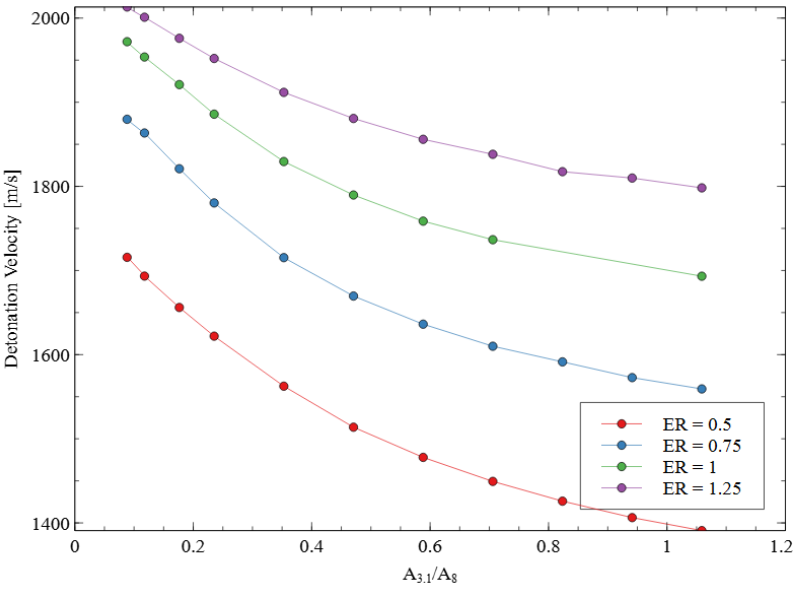

Figure 8.3: The relationship between the area ratio, ($A_{3.1}/A_8$), and detonation velocity of the RDE, with lines for different equivalence ratios.

The trend in the detonation velocity can potentially be linked to the periodic fluctuations occurring within the combustion chamber due to the passage of the detonation wave. When the oxidiser injector is small, the amount of injector backflow is also less, and hence the injection into the combustion chamber

is more stable, potentially leading to a higher detonation velocity. Additionally, there is more time for mixing within the combustion chamber, which can potentially lead to a higher detonation efficiency.

It is interesting to note that the one performance parameter, the pressure gain, increases with the increasing area ratio, while the detonation velocity, specific impulse, and thrust decrease with this same parameter. Additionally, the sharp drop-off in combustion efficiency occurs at the peak of the performance in detonation velocity, specific impulse, and thrust. This indicates that, similar to many engineering problems, the design process of an RDE is not linear, and a balance must be found between the various performance parameters to optimise on.

The main advantage of RDE's over deflagration are the possible efficiency increases with pressure gain combustion. Hence, when optimising an RDE, the logical assumption would be to optimise the pressure gain. As presented above, this can be done by increasing the injector to nozzle air ratio ($A_{3.1}/A_8$), with the caveat of a few known, not modelled, drawbacks. However this results in an RDE with relatively low thrust and specific impulse. Hence, to further optimise this RDE design, the remainder of the design variables should be explored and adjusted to improve the performance of these parameters.

8.2. Power Density

The power density of an RDE is a design parameter that was coined by *Bach et al.* [81]. It is an expansion of the concept of the mass flux (mass flow though a given cross-sectional area), with the addition of the effect of the equivalence ratio. This design parameter instead represents the nominal surface power density ($\Psi_{3.2}$) of the same cross-sectional area, in this case the chamber area, and the formula can be seen in Equation 8.1.

$$\Psi_{3.2} = \frac{er \cdot LHV_{fuel} \cdot \dot{m}_{ox}}{OFR_{stoich} \cdot A_{3.2}} \tag{8.1}$$

Where the LHV_{fuel} is the lower heating value of the fuel, $119.96\ MW/kg$ for hydrogen, and OFR_{stoich} is the stoichiometric oxidiser to fuel ratio, 34.3 in the case of hydrogen and air.

The relationships between the power density and the specific impulse of the RDE can be seen in Figure 8.4.

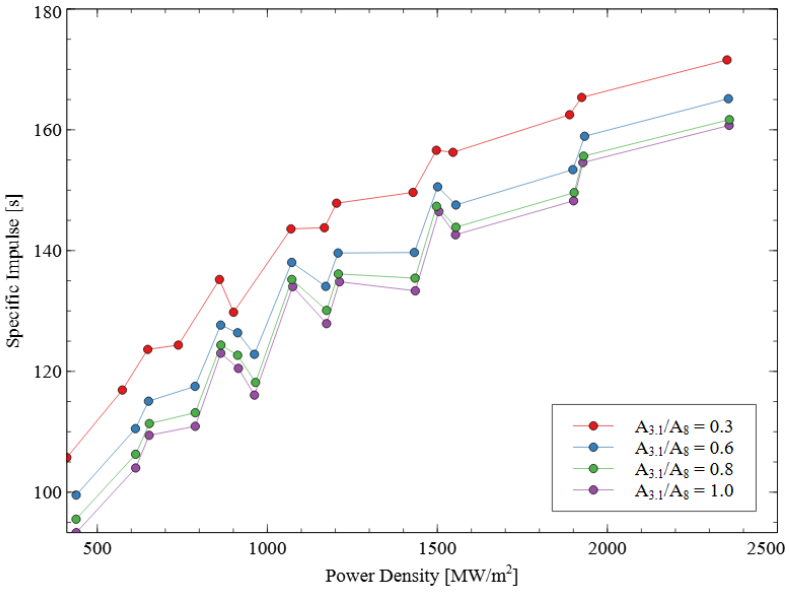

Figure 8.4: The relationship between the power density, and specific impulse of the RDE, with lines for different area ratios, ($A_{3.1}/A_8$).

As can be seen in the graph, the specific impulse tends to increase when the power density of the RDE

increases, and hence the RDE has a higher combination of mass flow and equivalence ratio. Similar trends, through with greater spread, can be seen in the thrust shown here in Figure 8.5, and the detonation velocity shown in Figure G.4.

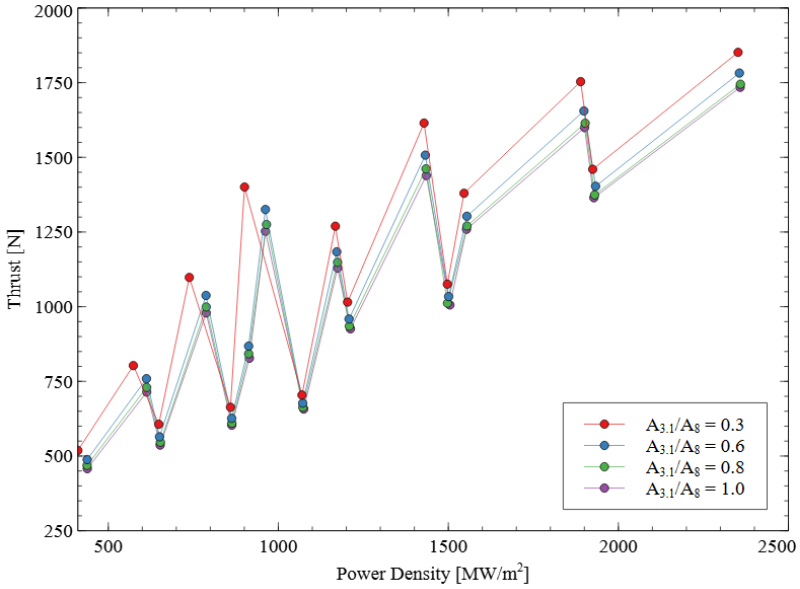

Figure 8.5: The relationship between the power density, and thrust of the RDE, with lines for different area ratios, ($A_{3.1}/A_8$).

The greater spread in the graphs of the thrust and the detonation velocity are due to the larger impact of one of the variables in the power density equation. More specifically, the oxidiser mass flow has a larger impact than the equivalence ratio on the thrust, while the opposite is true for the detonation velocity. While this does cause some more spread within the graphs, the general positive trend shown still holds.

These trends are as expected for an RDE. As the generation of thrust is characterised by the change in momentum of the exhaust gasses, a higher mass flow, has a correspondingly higher momentum transfer. In addition, the specific impulse is directly related to the effective exhaust velocity, which is increased for higher mass flows and equivalence ratios.

Interestingly, the opposite trend can be seen in the combustion efficiency of the engine, as shown in Figure 8.6. In this case, the area ratios have been specifically chosen to be above the drop-off point for combustion efficiency, as identified above.

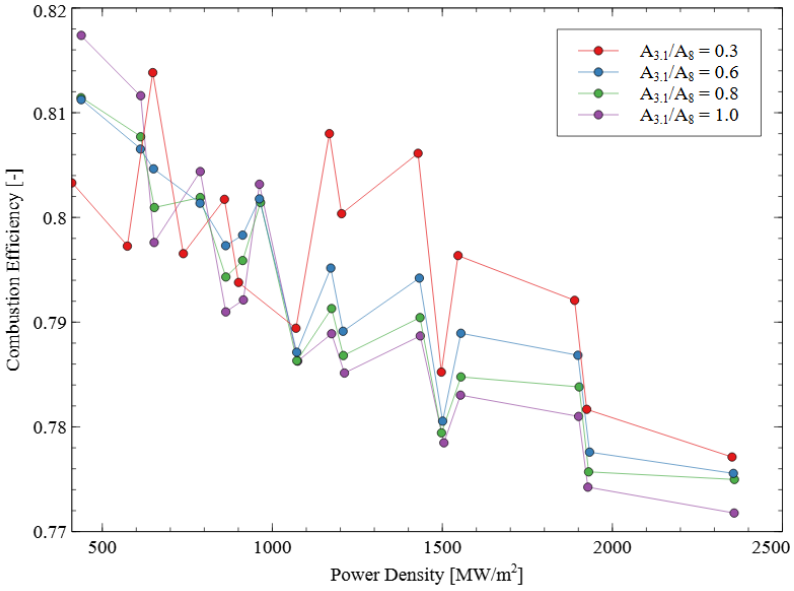

Figure 8.6: The relationship between the power density, and combustion efficiency of the RDE, with lines for different area ratios, $(A_{3.1}/A_8)$.

Here an increase in the power density of the RDE leads to a decrease in the combustion efficiency. In addition, there is a negligible trend shown with the pressure gain, as can be seen in Figure G.3.

This provides an interesting design challenge to the design engineer, as it was shown above that increasing the area ratio $(A_{3.1}/A_8)$ increases the pressure gain and combustion efficiency, but decreases the remainder of the performance parameters. Here an opposite trend is shown, where increasing the power density decreases the combustion efficiency (and has no effect on the pressure gain), but increases the remainder of the performance parameters.

However, it does seem like the positive impact of the area ratio $(A_{3.1}/A_8)$ is greater than the negative effects of the power density, and vice versa. Hence, it seems the design engineer will be able to strike a balance between these two important design parameters, and create an optimised RDE design.

8.3. Equivalence Ratio

Although the effect of the equivalence ratio is indirectly captured in the power density, there are a number of interesting direct trends to observe. The relationship between the combustion efficiency and the equivalence ratio is shown in Figure 8.7.

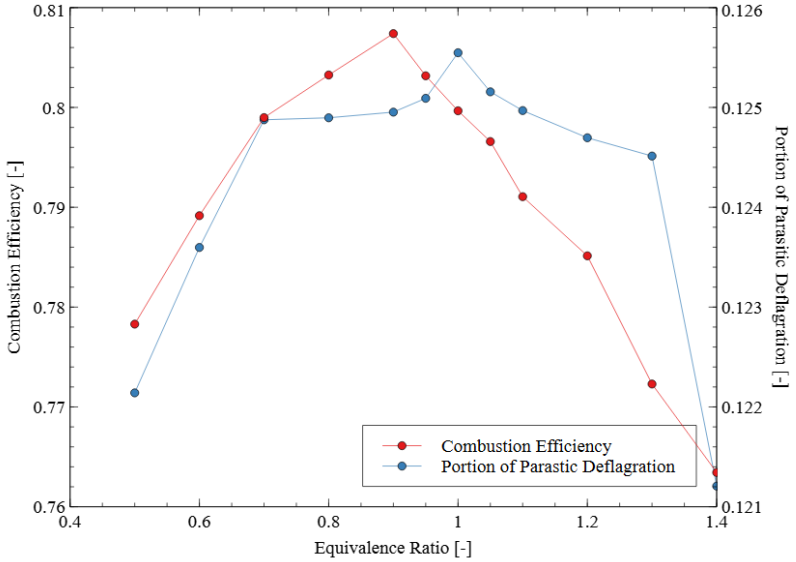

Figure 8.7: The relationship between the equivalence ratio and combustion efficiency of the RDE on one axis, with equivalence ratio and portion of parasitic deflagration on the other.

It is interesting to note here that the peak combustion efficiency is not at the expected stoichiometric conditions, but is shifted to have the peak approximately when the equivalence ratio is 0.9. The most likely reason for this is the presence of deflagration within the combustion chamber, which is expected to lower the combustion efficiency. As can be seen by the second axis on Figure 8.7, the largest portion of parasitic deflagration when the equivalence ratio is 1, thereby reducing the combustion efficiency at this point.

8.4. Performance Assessment Conclusions

This chapter has discussed the usage of the thermo-chemical analysis model created during this thesis. The model has been run for a range of geometries and operating conditions, and the impact of these on the performance of the RDE has been analysed.

Overall an increase of the area ratio between oxidiser injector throat and nozzle throat leads to a higher performance in terms of pressure gain, but a lower performance for specific impulse, thrust and detonation velocity. There is additionally a sharp drop-off seen in the combustion efficiency with the lower values of this area ratio.

When looking at the power density of the RDE, a measure of mainly the equivalence ratio and mass flow, an opposite trend appears. The specific impulse, thrust and detonation velocity all increase with increasing power density, while the combustion efficiency decreases for these same values. There is no significant trend for the pressure gain.

Lastly, the impact of equivalence ratio on specifically the combustion efficiency has been discussed, and the shift in expected peak at $er = 1$ to $er = 0.9$ has been explained.

9

Conclusion

This concluding chapter brings together the key aspects of this thesis. A summation of the results and their link to the research objectives and questions is presented, and it is shown these are answered by the research performed. The significance of these findings to the identified knowledge gap is discussed.

In addition, the some limitations of this research, and especially of the analysis model of the RDE, are discussed, and recommendations for continuation of this work are given. This chapter aims to call attention to the principal aspects of the thesis, and highlight its contributions to the field.

9.1. Research Conclusions

The goal of this thesis is to develop a thermo-chemical analysis model of an RDE, and to use this to investigate the impact of different operating conditions on RDE performance characteristics. This research aimed to fill a knowledge gap in existing literature by developing a model that both models a number of loss factors within an RDE, as well as requires very little inputs from testing or literature.

This research objective was achieved through the use of three main research questions, describing the creation of the model, the validation of the model, and the usage of the model to analyse the effect on the performance parameters.

The current state-of-the-art of RDE modelling was found to be either CFD-type models, or thermodynamic models detailing a single aspect of certain the processes within the RDE, and requiring inputs for the remainder. In these models, the required inputs are often difficult to obtain without testing and CFD analysis.

The key phenomena within the RDE were identified as mixing on both the macro- and micro-scale, represented in the created RDE model by the buffer zone and the partially stirred reactor aspects. The incomplete reaction of propellants with the multiple modes of combustion is represented by the parasitic combustion, and the 'losses' of propellant to both the detonation wave and in the buffer zone. Inefficiencies when compared to the ideal CJ detonation were implemented through the use of the heat loss parameter, χ.

In addition to these key phenomena, the model contains a number of interesting aspects. Firstly, two usage modes are implemented; the RDE can either be used in air breathing or rocket-mode. There are a number of stations defined, seen in Figure 5.1, at which all the flow properties are known.

Key performance metrics of an RDE were identified as the total pressure ratio between oxidiser plenum and chamber (the pressure gain), the specific impulse, thrust and combustion efficiency, as well as the detonation velocity of the engine. These are given as output to the model, in addition to the flow properties calculated at every station.

With this, the first research question, *How can a thermo-chemical analysis model be formulated to accurately represent the detonation wave physics in an RDE?* is answered, and the model is created.

A RDE test campaign was conducted at TNO to gather data for the validation of the model. The tested RDE was modular, with the ability to change a number of important geometric parameters; the fuel and oxidiser injector areas, and the nozzle throat area. With these RDE tests, the plenum temperatures and pressures, and the chamber static pressure during both the hotfire and coldflow were measured.

These validation parameters, further defined in chapter 7, were used to compare against the performance of the model. The largest mean deviation in parameters was found to be the total combustion temperature with 6%, with most being below a 5% mean deviation. The maximum variation was at most 17% error in temperature, ad the amjority of points lie within the 10%. A sensitivity analysis on the main input parameters of the RDE model was carried out in parallel to this validation, documenting how robust the model is to changes in these inputs. Reasonable variations in these model inputs caused at maximum a 5% difference in one of the performance parameters.

This answers the second research question, *What is the accuracy of the thermo-chemical analysis model with respect to experimental data?*

Lastly, the model was used to quantify the impacts of the various engine geometries and operating conditions of the performance of the RDE. It was found that the ratio between the injector and nozzle areas ($A_{3.1}/A_8$) has a significant positive relationship with the pressure gain and a less significant positive relationship with the combustion efficiency, while showing a negative relationship with the other parameters.

Adjusting the power density of the engine (a measure of the mass flow and equivalence ratio), showed the opposite trend, a negative relationship for the combustion efficiency, and positive for the detonation velocity, specific impulse and thrust.

With these results, the last research question is answered; *What are the impacts of variations in geometry and operating conditions on the performance characteristics of RDEs?* Additionally, it is shown that the design process of an RDE, even on the macro-scale, is not linear, and a balance must be found between different inputs and performance parameters. During the performance assessment it was also found that a number of phenomenon not included in the model may have a significant impact on the performance of the RDE at higher area ratios ($A_{3.1}/A_8$).

9.2. Recommendations for Further Work

There are a number of limitations to the current state of the model, which would be expanded upon and improved in the future. Many of these recommendation were not implemented because it was unclear whether they would become necessary for the project, and their execution would have required a significant amount of time. In addition, a number of the recommendations named here are for further elaborate research on this same research topic.

The first recommendation is the expansion of the available propellant types. This model has been built only for the combination of hydrogen and air as propellants, but if a different combination of is wished, these should be added to the model. The instructions on how to do this can be seen in Appendix C. It is also important to note that this model is currently only validated for the combination of hydrogen and air, and users adding additional propellant types must either further validate the model, or use at their own discretion. It must be noted here that preliminary work on the addition of methane as a fuel has been done, but this is less easily verified, and cannot be validated without a full test campaign.

In addition to the implementation of different fuel types, all propellants are currently assumed to be in a gaseous state. If the addition of a liquid fuel is required, an additional function should be built to describe the vaporisation of the liquid before detonation.

Secondly, in the creation of this model, the assumption of a single detonation wave was made. However, the validation of the model was done using test data in which multiple detonation waves were seen. So far little research has been done into the impact of different detonation wave numbers at the same operating point, and as such it would be an interesting research topic to investigate the impact of this single wave assumption on the validity and accuracy of the model.

Lastly, as discussed in chapter 8, there are still a number of phenomena that may potentially have significant impacts on the behaviour of the flow within the combustion chamber of the RDE. Such flow

phenomena could include the oblique shock present after the detonation wave, the impact plenum-chamber coupling on the detonation, heat transfer within the engine, and the impact of the longitudinal pulsed detonation. In addition, commensal combustion is a phenomena that could be implemented by allowing further reaction of the gasses after the mixing of the different flow streams. While research on detailed flow within the chamber is currently state-of-the-art, further investigation on these phenomena, and their impact on RDE performance would be of significant interest, and the addition of more flow phenomena to the current model could yield valuable insights.

While not a model improvement, there is a further recommendation that should be given. This thesis has created and validated a thermodynamic model of an RDE, and has used this to discern some trends within RDE design. However, this investigation and subsequent discussion can be very much expanded upon. This model is only one of the steps in furthering the knowledge of RDE's within the community, and should also be used not only for the design of RDE's in the future, but also in their analysis.

Although there is clear potential for improvements on this model, the RDE model created in this thesis provides a significant step in the direction of designing, operating, and flying this new type of engine.

Bibliography

[1] M. Berthelot, "Sur la vitesse de propagation des phénomènes explosifs dans les gaz," *CR Acad. Sci., Paris*, vol. 94, pp. 822–823, 1882.

[2] M. Berthelot and P. Vieille, "L'onde explosive," *Ann. Chim. Phys. Ser*, vol. 5, no. 28, pp. 289–332, 1883.

[3] D. L. Chapman, "Vi. on the rate of explosion in gases," *The London, Edinburgh, and Dublin Philosophical Magazine and Journal of Science*, vol. 47, no. 284, pp. 90–104, 1899.

[4] E. Jouguet, "On the propagation of chemical reactions in gases," *J. Math. Pures Appl*, vol. 1, no. 2, pp. 347–425, 1905.

[5] É. Jouguet, *Mécanique des explosifs: étude de dynamique chimique*. Paris: Octave Doin, 1916.

[6] J. Rayleigh, *The Theory of Sound, Volume ll*. Dover Publications, 1945.

[7] H. Hugoniot, "Propagation du mouvement dans les corps," *J. Ec. Polyt. Paris*, vol. 57, pp. 1–125, 1889.

[8] J. H. Lee, *The detonation phenomenon*. Cambridge University Press, 2008.

[9] Y. B. Zeldovich, "On the theory of detonation propagation in gaseous systems," *Zh. Eksp. Teor. Fiz*, vol. 10, no. 5, pp. 542–568, 1940.

[10] J. von Neumann, "Theory of detonation waves," *John von Neumann, collected works*, vol. 6, pp. 203–218, 1942.

[11] W. Doring, "Detonation waves," *Ann. Phys. 5e Folge*, vol. 43, pp. 421–436, 1943.

[12] G. Brayton, "Improvements in gas-engines," *US Patent A*, vol. 125166, p. 2, 1872.

[13] W. H. Heiser and D. T. Pratt, "Thermodynamic cycle analysis of pulse detonation engines," *Journal of propulsion and power*, vol. 18, no. 1, pp. 68–76, 2002.

[14] R. Vutthivithayarak, E. Braun, and F. Lu, "On thermodynamic cycles for detonation engines," in *28th International Symposium on Shock Waves: Vol 2*, Springer, 2012, pp. 287–292.

[15] J. R. Burr and E. Paulson, "Thermodynamic performance results for rotating detonation rocket engine with distributed heat addition using cantera," in *AIAA Propulsion and Energy 2021 Forum*, 2021, p. 3682.

[16] E. J. Paulson, R. Kimura, W. A. Hargus, and V. Sankaran, "Ideal thermodynamic performance results for rotating detonation rocket engine thrust chambers using cea," in *AIAA SciTech 2020 Forum*, 2020, p. 0193.

[17] T. Kaemming, M. L. Fotia, J. Hoke, and F. Schauer, "Thermodynamic modeling of a rotating detonation engine through a reduced-order approach," *Journal of Propulsion and Power*, vol. 33, no. 5, pp. 1170–1178, 2017.

[18] I. V. Walters, A. Lemcherfi, R. M. Gejji, S. D. Heister, and C. D. Slabaugh, "Performance characterization of a natural gas–air rotating detonation engine," *Journal of Propulsion and Power*, vol. 37, no. 2, pp. 292–304, 2021.

[19] D. Davidenko, Y. Eude, I. Gokalp, and F. Falempin, "Theoretical and numerical studies on continuous detonation wave engines," in *17th AIAA international space planes and hypersonic systems and technologies conference*, 2011, p. 2334.

[20] D. P. Stechmann, S. D. Heister, and A. J. Harroun, "Rotating detonation engine performance model for rocket applications," *Journal of Spacecraft and Rockets*, vol. 56, no. 3, pp. 887–898, 2019.

[21] D. Schwer and K. Kailasanath, "Numerical study of the effects of engine size n rotating detonation engines," in *49th AIAA aerospace sciences meeting including the new horizons forum and aerospace exposition*, 2011, p. 581.

[22] D. Schwer and K. Kailasanath, "Numerical investigation of rotating detonation engines," in *46th AIAA/ASME/SAE/ASEE joint propulsion conference & exhibit*, 2010, p. 6880.

[23] P. Wolański, "Detonative propulsion," *Proceedings of the combustion Institute*, vol. 34, no. 1, pp. 125–158, 2013.

[24] S. She-Ming Lau-Chapdelaine, M. I. Radulescu, and Z. Hong, "Quasi-two-dimensional simulation of a rotating detonation engine combustor and injector," *Journal of Propulsion and Power*, vol. 40, no. 1, pp. 42–49, 2024.

[25] R. Zhou and J.-P. Wang, "Numerical investigation of flow particle paths and thermodynamic performance of continuously rotating detonation engines," *Combustion and Flame*, vol. 159, no. 12, pp. 3632–3645, 2012.

[26] D. Schwer and K. Kailasanath, "Numerical investigation of the physics of rotating-detonation-engines," *Proceedings of the combustion institute*, vol. 33, no. 2, pp. 2195–2202, 2011.

[27] B. R. Bigler, J. R. Burr, J. W. Bennewitz, S. Danczyk, and W. A. Hargus, "Performance effects of mode transitions in a rotating detonation rocket engine," in *AIAA propulsion and energy 2020 forum*, 2020, p. 3852.

[28] T. A. Kaemming and D. E. Paxson, "Determining the pressure gain of pressure gain combustion," in *2018 Joint propulsion conference*, 2018, p. 4567.

[29] C. M. Brophy, J. Codoni, J. A. Teneyck, and S. Ewing, "Experimental performance characterization of an rde using equivalent available pressure," in *AIAA Propulsion and Energy 2019 Forum*, 2019, p. 4212.

[30] H. Zheng, L. Qi, N. Zhao, Z. Li, and X. Liu, "A thermodynamic analysis of the pressure gain of continuously rotating detonation combustor for gas turbine," *Applied sciences*, vol. 8, no. 4, p. 535, 2018.

[31] J. Sosa, K. A. Ahmed, R. Fievisohn, J. Hoke, T. Ombrello, and F. Schauer, "Supersonic driven detonation dynamics for rotating detonation engines," *International Journal of Hydrogen Energy*, vol. 44, no. 14, pp. 7596–7606, 2019.

[32] R. Blümner, *Operating mode dynamics in rotating detonation combustors*. Technische Universitaet Berlin (Germany), 2020.

[33] C. M. Brophy and A. Thoeny, "Geometry impact on the operability and delivered pressure gain characteristics of a rotating detonation combustor," in *AIAA SCITECH 2024 Forum*, 2024, p. 2609.

[34] I. J. Shaw *et al.*, "A theoretical review of rotating detonation engines," in *Direct Numerical Simulations*, S. Rao, Ed., Rijeka: IntechOpen, 2019, ch. 7. DOI: 10.5772/intechopen.90470. [Online]. Available: https://doi.org/10.5772/intechopen.90470.

[35] E. M. Braun, F. K. Lu, D. R. Wilson, and J. A. Camberos, "Airbreathing rotating detonation wave engine cycle analysis," *Aerospace Science and Technology*, vol. 27, no. 1, pp. 201–208, 2013.

[36] S. Nakagami *et al.*, "Experimental visualization of the structure of rotating detonation waves in a disk-shaped combustor," *Journal of Propulsion and Power*, vol. 33, no. 1, pp. 80–88, 2017.

[37] B. A. Rankin, D. R. Richardson, A. W. Caswell, A. G. Naples, J. L. Hoke, and F. R. Schauer, "Chemiluminescence imaging of an optically accessible non-premixed rotating detonation engine," *Combustion and Flame*, vol. 176, pp. 12–22, 2017.

[38] N. T. Fiorino, N. J. Snow, F. R. Schauer, M. D. Polanka, S. Alexander Schumaker, and B. C. Sell, "Improving detonability in a small-scale rotating detonation engine using partial premixing," *Journal of Propulsion and Power*, vol. 39, no. 2, pp. 232–241, 2023.

[39] Z. M. Ayers, V. Athmanathan, T. R. Meyer, and D. E. Paxson, "Variably premixed rotating detonation engine for evaluation of detonation cycle dynamics," *Journal of Propulsion and Power*, vol. 39, no. 3, pp. 351–364, 2023.

[40] J. Suchocki, S.-T. Yu, J. Hoke, A. Naples, F. Schauer, and R. Russo, "Rotating detonation engine operation," in *50th AIAA aerospace sciences meeting including the new horizons forum and aerospace exposition*, 2012, p. 119.

[41] F. A. Bykovskii, S. A. Zhdan, and E. F. Vedernikov, "Continuous spin detonations," *Journal of propulsion and power*, vol. 22, no. 6, pp. 1204–1216, 2006.

[42] A. K. Hayashi *et al.*, "3d numerical study on flow field in disc-rde," in *AIAA Propulsion and Energy 2021 Forum*, 2021, p. 3665.

[43] S. A. Boller, M. D. Polanka, R. Huff, F. Schauer, M. Fotia, and J. Hoke, "Experimental flow visualization in a radial rotating detonation engine," in *AIAA Scitech 2019 Forum*, 2019, p. 1253.

[44] R. T. Huff, S. A. Boller, M. D. Polanka, F. R. Schauer, M. L. Fotia, and J. L. Hoke, "Radial rotating detonation engine driven bleed air turbine," *Journal of Propulsion and Power*, vol. 37, no. 2, pp. 252–260, 2021.

[45] M. Kawalec and P. Wolański, "Development of rocket engine with continuously rotating detonation supplied by liquid propellants," *Proceeding of EUCASS, Lille, France*, vol. 27, 2021.

[46] D. E. Paxson, "Preliminary computational assessment of disk rotating detonation engine configurations," in *AIAA Scitech 2020 Forum*, 2020, p. 2157.

[47] K. Ishii, K. Ohno, H. Kawana, K. Kawasaki, A. Hayashi, and N. Tsuboi, "Operation characteristics of a disk-type rotating detonation engine," *Shock Waves*, vol. 33, no. 3, pp. 267–274, 2023.

[48] C.-H. Wang, Y. Liu, and L.-Z. Qin, "Aerospike nozzle contour design and its performance validation," *Acta Astronautica*, vol. 64, no. 11-12, pp. 1264–1275, 2009.

[49] M. Fotia, F. Schauer, and J. Hoke, "Experimental testing of a rotating detonation engine coupled to nozzles at conditions approaching flight," in *Proceedings of the 25th International Colloquium on the Dynamics of Explosions and Reactive Systems, Leeds, UK*, 2015, p. 15.

[50] K. Ishihara, K. Matsuoka, J. Kasahara, A. Matsuo, and I. Funaki, "Performance evaluation of a rotating detonation engine with conical-shape tail," in *53rd AIAA Aerospace Sciences Meeting*, 2015, p. 0630.

[51] J. R. Codoni, K. Y. Cho, J. L. Hoke, B. A. Rankin, and F. R. Schauer, "Simultaneous mid-ir h2o/co2 emission and oh chemiluminesence measurements within a rde operating with and without backpressure," in *2018 AIAA Aerospace sciences meeting*, 2018, p. 1882.

[52] G. Ge, L. Deng, H. Ma, X. Liu, L. Jin, and C. Zhou, "Effect of blockage ratio on the existence of multiple waves in rotating detonation engine," *Acta Astronautica*, vol. 164, pp. 230–240, 2019.

[53] M. Ross, J. Burr, Y. Desai, A. Batista, and C. Lietz, "Flow acceleration in an rdre with gradual chamber constriction," *Shock Waves*, vol. 33, no. 3, pp. 253–265, 2023.

[54] S. M. Frolov, V. S. Aksenov, V. S. Ivanov, S. N. Medvedev, and I. O. Shamshin, "Flow structure in rotating detonation engine with separate supply of fuel and oxidizer: Experiment and cfd," *Detonation control for propulsion: Pulse detonation and rotating detonation engines*, pp. 39–59, 2018.

[55] W. Fan *et al.*, "Initiation process of non-premixed continuous rotating detonation wave through schlieren visualization," *Combustion and Flame*, vol. 265, p. 113 437, 2024.

[56] K. Goto *et al.*, "Flight demonstration of detonation engine system using sounding rocket s-520-31: Performance of rotating detonation engine," in *AIAA Scitech 2022 Forum*, 2022, p. 0232.

[57] D. Schwer and K. Kailasanath, "Fluid dynamics of rotating detonation engines with hydrogen and hydrocarbon fuels," *Proceedings of the Combustion Institute*, vol. 34, no. 2, pp. 1991–1998, 2013.

[58] R. Guangyao, M. Cheng, Z. Sheng, Y. Zhang, X. Liu, and J. Wang, "Flow field characteristics and particle path tracking of a hollow rotating detonation engine with a laval nozzle," *Physics of Fluids*, vol. 35, no. 5, 2023.

[59] T. Gaillard, D. Davidenko, and F. Dupoirieux, "Numerical simulation of a rotating detonation with a realistic injector designed for separate supply of gaseous hydrogen and oxygen," *Acta Astronautica*, vol. 141, pp. 64–78, 2017.

[60] M. Folusiak, K. Swiderski, A. Kobiera, B. Lukasik, and P. Wolanski, "Three-dimensional numerical simulations of the combustion chamber of the rotating detonation engine," *Journal of KONES. Powertrain and Transport*, vol. 20, no. 1, pp. 83–88, 2013.

[61] R. T. Fievisohn, "Cycle analysis of simple detonative propulsion systems," in *Proceedings of the International Constant Volume and Detonation Combustion Workshop, Berlin, Germany*, 2022, p. 6.

[62] V. Ramanujachari, R. Dutta Roy, and P. Amrutha Preethi, "Design and analysis of rotating detonation wave engine," in *Proceedings of the National Aerospace Propulsion Conference: Select Proceedings of NAPC 2020*, Springer, 2022, pp. 415–430.

[63] C. A. Nordeen, D. Schwer, F. Schauer, J. Hoke, T. Barber, and B. Cetegen, "Thermodynamic model of a rotating detonation engine," *Combustion, Explosion, and Shock Waves*, vol. 50, pp. 568–577, 2014.

[64] J. E. Shepherd and J. Kasahara, "Analytical models for the thrust of a rotating detonation engine," *GALCIT Report FM2017*, vol. 1, 2017.

[65] P. Barnouin, E. Bach, E. J. Gutmark, C. O. Paschereit, and M. Bohon, "Low-order model for detonation velocity suppression in rotating detonation combustors," in *AIAA SCITECH 2023 Forum*, 2023, p. 1291.

[66] S. A. Zhdan, A. M. Mardashev, and V. V. Mitrofanov, "Calculation of the flow of spin detonation in an annular chamber," *Combustion, Explosion and Shock Waves*, vol. 26, pp. 210–214, 1990.

[67] D. G. Goodwin, H. K. Moffat, I. Schoegl, R. L. Speth, and B. W. Weber, *Cantera: An object-oriented software toolkit for chemical kinetics, thermodynamics, and transport processes*, `https://www.cantera.org`, Version 3.0.0, 2023. DOI: `10.5281/zenodo.8137090`.

[68] S. Kao, J. Ziegler, N. Bitter, B. Schmidt, J. Lawson, and J. E. Shepherd, *Sdtoolbox: Numerical tools for shock and detonation wave modeling*, `https://shepherd.caltech.edu/EDL/PublicResources/sdt/doc/ShockDetonation/ShockDetonation.pdf`, Revised April 18 2023, 2023.

[69] C. Bedick, D. H. Ferguson, and P. Strakey, "Validation and application of a reduced-order rotating detonation engine inlet and fill zone model," in *AIAA Scitech 2021 Forum*, 2021, p. 0193.

[70] F. Belles, "Detonability and chemical kinetics: Prediction of limits of detonability of hydrogen," in *Symposium (International) on Combustion*, Elsevier, vol. 7, 1958, pp. 745–751.

[71] A. Gavrikov, A. Efimenko, and S. Dorofeev, "A model for detonation cell size prediction from chemical kinetics," *Combustion and flame*, vol. 120, no. 1-2, pp. 19–33, 2000.

[72] H. D. Ng, Y. Ju, and J. H. Lee, "Assessment of detonation hazards in high-pressure hydrogen storage from chemical sensitivity analysis," *International Journal of Hydrogen Energy*, vol. 32, no. 1, pp. 93–99, 2007.

[73] M. Kaneshige and J. E. Shepherd, "Detonation database," 1997.

[74] T. Roos, W. Wieling, M. Lengkeek, and M. Olde, "Design and commissioning of tno's modular rotating detonation engine (rde) test facility," in *HiSST: 3rd International Conference on High-Speed Vehicle Science Technology*, 2024.

[75] F. Chacon and M. Gamba, "Study of parasitic combustion in an optically accessible continuous wave rotating detonation engine," in *AIAA scitech 2019 forum*, 2019, p. 0473.

[76] A. Akerblom, "Turbulence-chemistry interaction in openfoam and how to implement a dynamic-pasr model for les of turbulent combustion," in *In Proceedings of CFD with OpenSource Software,*, Edited by Nilsson. H., http://dx.doi.org/10.17196/OS, 2022, 2022.

[77] G. Wang *et al.*, "Estimation of the dissipation rate of turbulent kinetic energy: A review," *Chemical Engineering Science*, vol. 229, p. 116 133, 2021.

[78] I. Glassman, R. A. Yetter, and N. G. Glumac, *Combustion*. Academic press, 2014.

[79] A. H. Shapiro, "The dynamics and thermodynamics of compressible fluid flow," *New York: Ronald Press*, 1953.

[80] M. Lengkeek, "Operation of a rotating detonation engine," *TU Delft Internship Report*, 2023.

[81] E. Bach, C. O. Paschereit, P. Stathopoulos, and M. Bohon, "Advancement of empirical model for stagnation pressure gain in rdcs," in *AIAA Scitech 2022 Forum*, 2022, p. 0834.

[82] E. Bach, C. O. Paschereit, P. Stathopoulos, and M. Bohon, "Rdc operation and performance with varying air injector pressure loss," in *AIAA Scitech 2020 Forum*, 2020, p. 0199.

[83] E. Bach, P. Stathopoulos, C. O. Paschereit, and M. D. Bohon, "Performance analysis of a rotating detonation combustor based on stagnation pressure measurements," *Combustion and Flame*, vol. 217, pp. 21–36, 2020.

[84] J. C. Shank, "Development and testing of a rotating detonation engine run on hydrogen and air," 2012.

[85] D. Shen *et al.*, "Spinning pulsed detonation in rotating detonation engine," *Aerospace Science and Technology*, vol. 126, p. 107 661, 2022.

A

Functions Used Within the Model

This appendix contains the input and output tables of the function and classes used within the model. The class used for every sub-model is followed by the functions used within each of the sub-models. Additionally, the remainder of the functions used within the model initiation, throughout the model, or as a final few steps can be found in the auxiliary functions, section A.5.

A.1. Plenum Calculations

The *Inlet Model* function calculates the mass flow and total conditions of the air plenum if the RDE is used in airbreathing mode. The mass flow is calculated using Equation 5.6.

Table A.1: Table showing the inputs and outputs of the *Inlet Model* function

Inputs	
	input_list (list): List containing: *mach (float):* The Mach number of flight [-] *altitude (float):* The altitude of flight [m] *inlet_area (float):* The cross-sectional area of the inlet [m^2] *mcf (float):* The mass capture fraction of the inlet [-] *prf (float):* The pressure recovery fraction of the inlet [-]
Outputs	
	tot_temp (float): The total temperature of the air in the inlet [K] *mass_flow (float):* The mass flow of air in the inlet [kg/m^3] *tot_pressure (float):* The maximal total pressure the inlet can supply [Pa]

The *Initialise Gas Objects* function creates the Cantera entities to be used throughout the iteration.

Table A.2: Table showing the inputs and outputs of the *Guess Plenum Pressures* function

Inputs	
	fuel (str): The name of the fuel *oxidiser (str):* The name of the oxidiser *mech (str):* The Cantera solution mechanism used
Outputs	
	fu (str): The composition of the fuel *ox (str):* The composition of the oxidiser *fuel_gas (composite.Quantity):* The Cantera gas entity representing the fuel *ox_gas (composite.Quantity):* The Cantera gas entity representing the oxidiser

The plenum pressures in the initial iteration round are estimated by the *Guess Plenum Pressures* function, using Equation 5.7 to calculate the pressures.

Table A.3: Table showing the inputs and outputs of the *Determine Plenum Pressures* function

Inputs
R (float): Universal gas constant [J/mol K] *gas (composite.Quantity):* Cantera quantity of gas with all relevant properties *area (float):* The relevant injector area [m^2] *mass_flow (float):* The mass flow for the respective propellant type [kg/s] *static_temp (float):* The initial temperature for the respective propellant type [K]
Outputs
plenum_pressure (float): The plenum pressure value calculated with Equation 5.7 [Pa]

The full list of attributes of the RDE after the completion of the plenum model, as well as all methods used by this model can be seen in the table below.

Table A.4: Table showing the RDE attributes after the plenum model

Attributes
rde (RDE_Actor): the stored RDE to model, containing the variables: *A_chamber (float):* chamber cross-sectional area [m^2] *alpha (float):* Portion of combusted products to mix again with detonation gasses [-] *ambient_pressure (float):* Pressure outside of the engine, defaults to 1 bar [bar] *cell_size (float):* The estimated size of the detonation cells in the engine [m] *chamber_channel_height (float):* The distance between the chamber inner and outer walls [m] *chamber_length (float):* The length of the combustion chamber [m] *chamber_outer_diameter (float):* The diameter of the chamber outer walls [m] *er (float):* The equivalence ratio as input [-] *exit_area (float):* The nozzle exit area, if None; the model expands to ambient [m^2] *file_name (str):* The ID given to the run *fuel (str):* The name of the fuel used *fuel_injector_area (float):* The cross-sectional area of the fuel injector [m^2] *fuel_mass_flow (float):* The current fuel mass flow [kg/s] *fuel_static_temperature (float):* The initial temperature of the fuel [K] *initial_fuel_mass_flow (float):* The inputted mass flow of the fuel [kg/s] *initial_ox_mass_flow (float):* The inputted mass flow of the oxidiser [kg/s] *mass_flow (float):* the inputted total mass flow [kg/s] *mech (str):* The chosen reaction mechanism to use in Cantera calculations *ox_injector_area (float):* The cross-sectional area of the oxidiser injector [m^2] *ox_mass_flow (float):* The current oxidiser mass flow [kg/s] *ox_static_temperature (float):* The initial temperature of the oxidiser [K] *oxidiser (str):* The name of the oxidiser used *throat_area (float):* The cross-sectional area of the nozzle throat [m^2] *xi (float):* The portion of heat kept during the detonation [-]

A.2. Injector Model

The pressure decay curve which lies central to the determination of the injector behaviour is calculated in the *Injector Pressure Decay Model* function, and an example can be seen in Figure 5.7.

Table A.5: Table showing the inputs and outputs of the *Injector Pressure Decay Model* function

Inputs	
	steps (float): The number of steps in the injector discretisation *decay_pressure (float):* Minimum pressure in the combustion chamber [Pa] *detonation_pressure (float):* Maximum pressure in combustion chamber [Pa] *k (float):*Pressure decay parameter [-]
Outputs	
	pressure_decay (array): The pressure at every point in (non-dimensional) time in the combustion chamber [Pa] *average_combustor_pressure (float):* The average pressure in the combustion chamber, to be used in the nozzle continuity check [Pa]

The *Reversed Mass Flow* function calculates the flow going from the combustion chamber to the considered plenum during the blocked injector phase. This function uses Equation 5.9 to calculate the Mach number, and Equation 5.10 to calculate the mass flow.

Table A.6: Table showing the inputs and outputs of the *Reversed Mass Flow* function

Inputs	
	R (float): Universal gas constant [J/mol K] *gas (composite.Quantity):* Quantity of gas with all relevant properties *plenum_pressure (float):* The pressure in the respective plenum [Pa] *pressure_decay (float):* The pressure in the chamber at the current time [Pa] *area (float):* The effective injector area for the respective injector element [m$\hat{2}$]
Outputs	
	mass_flow (float) The mass flow of combustion products through the injector element [kg/s]

The *Determine Throat Mach* function calculates the Mach number through the injector throat through the methodology defined in subsection 5.3.3, and Equations 5.11 and 5.12.

Table A.7: Table showing the inputs and outputs of the *Determine Throat Mach* function

Inputs	
	gas (composite.Quantity): Quantity of gas with all relevant properties *plenum_pressure (float):* The total pressure in the respective plenum [Pa] *downstream_pressure (float):* The static pressure downstream of the injector nozzle [Pa]
Outputs	
	injector_mach (float): The Mach number of the flow in the injector throat [-]

The *Calculate Mass Flow* function calculates the mass flow through a defined injector throat, from plenum to combustion chamber. This is done using Equation 5.13.

Table A.8: Table showing the inputs and outputs of the *Calculate Mass Flow* function

Inputs
R (float): Universal gas constant [J/mol K]
gas (composite.Quantity): Quantity of gas with all relevant properties
plenum_pressure (float): The pressure in the respective plenum [Pa]
plenum_temp (float): The temperature in the respective plenum [K]
area (float): The effective injector area for the respective injector element [m$\hat{2}$]
Outputs
mass_flow (float): The mass flow though the injector element [kg/s]

The injector discretisation and the determination of the mass flow and equivalence rationthrough the injecxtor is calculated through the *Buffer Zone* function. This function also utilises the two functions above. Additionally, Equations 5.14, and 5.15 are used to calculate the 'lost' mass flow and the new equivalence ratio respectively.

Table A.9: Table showing the inputs and outputs of the *Buffer Zone* function

Inputs
R (float): Universal gas constant [J/mol K]
steps (float): The number of steps in the injector discretisation
fuel_injector_area (float): The area of the fuel injector element [m^2]
ox_injector_area (float): The area of the oxidiser injector element [m^2]
fuel_static_temperature (float): The temperature of the fuel plenum [K]
ox_static_temperature (float): The temperature of the oxidiser plenum [K]
fuel_plenum_pressure (float): The pressure of the fuel plenum [Pa]
ox_plenum_pressure (float): The pressure of the oxidiser plenum [Pa]
fuel_gas (composite.Quantity): Cantera entity of the fuel gas
ox_gas (composite.Quantity): Cantera entity of the oxidiser gas
pressure_decay (array): The pressure at a particular location in the combustor [Pa]
Outputs
ψ *(float):* The change in equivalence ratio after the buffer zone [-]
ox_mass_flow (array): The oxidiser mass flow over the injector element [kg/s]
fuel_mass_flow (array): The fuel mass flow over the injector element kg/s]
mass_flow_lost (tuple): The total mass flow lost, indication of fuel or oxidiser lost

The representative average pressure post injector is called the downstream pressure, and is calculated by the *Calculate Downstream Pressure* function.

Table A.10: Table showing the inputs and outputs of the *Calculate Downstream Pressure* function

Inputs
ox_blockage_ratio (float): Fraction of the oxidiser injector blocked [-]
fuel_blockage_ratio (float): Fraction of the fuel injector blocked [-]
pressure_decay (array): Time-varying pressure in the combustion chamber [Pa]
ox_mass_flow (float): The mass flow through the oxidiser injector [kg/s]
fuel_mass_flow (float): The mass flow through the fuel injector [kg/s]
Outputs
downstream_pressure (float): The average pressure in the combustion chamber just after injection [Pa]

The continuity check to ensure the mass flow though the respective injector throats corresponds to the

input mass flow is performed in the *Injector Continuity Check* function. The new plenum pressure that results from this is calculated using Equation 5.16.

Table A.11: Table showing the outputs of the *Injector Continuity Check* function

Inputs	
	start_time (float): RDE property, the time at which the model started running *mass_flow_lost (tuple):* The total mass flow lost, and an indication of whether this is fuel (1), or oxidiser (2) *fuel_mass_flow (float):* The mass flow of the fuel [kg/s] *ox_mass_flow (float):* The mass flow of the oxidiser [kg/s] *fuel_plenum_pressure (float):* The pressure in the fuel plenum *ox_plenum_pressure (float):* The pressure in the oxidiser plenum *initial_fuel_mass_flow (float):* The mass flow of the fuel as input by user [kg/s] *initial_ox_mass_flow (float):* The mass flow of the oxidiser as input by user [kg/s]
Outputs	
	iteration_ox_mass_flow (Boolean): True if the plenum pressures should continue being iterated on *plenum_pressure (tuple):* Contains the new oxidiser and fuel plenum pressure [Pa]

The full list of RDE attributes that were added to the RDE during the injector model, as well as the methods used during this model can be seen below.

Table A.12: Table showing the additional RDE attributesafter the completion of the injector model

Attributes	
	rde (RDE_Actor): the stored RDE to model, containing the additional variables: *fuel_plenum_pressure (float):* The pressure of the fuel plenum [Pa] *gas (composite.Quantity):* Quantity of gas with all relevant properties, represents the combined flow *k (float):* The pressure decay factor [-] *ox_plenum_pressure (float):* The pressure in the oxidiser plenum [Pa] *plenum_pressure (tuple):* The pressures of both plenums after one iteration [Pa]

A.3. Combustor Model

The portion of the flow that undergoes parasitic deflagration is calculated by the *PaSR* function. This function uitilises the Equations 5.17, 5.18, and 5.19 in this calculation.

Table A.13: Table showing the inputs and outputs of the *PaSR* function

Inputs
gas (composite.Quantity): Quantity of gas with all relevant properties
m1 (float): The mass portion of the fuel [kg]
m2 (float): The mass portion of the oxidiser [kg]
fuel (str): The name of the fuel
oxidiser (str): The name of the oxidiser
v_eff (float): The effective viscosity of the propellant mix (or None) [Pa s]
epsilon (float): The turbulent dissipation rate of the propellant mix (or None)
v (float): The kinematic viscosity of the propellant mix (or None) [Pa kg s/m^3]
s_s *(float):* he laminar flame speed of the propellant (or None) [m/s]
Outputs
1 - omega (float): Reacting volume fraction [-]

The *Separate Mass Flows* function simulates the splitting of the gas into three different steams; deflagration, not-deflagration (but still combustion), and not-combustion.

Table A.14: Table showing the inputs and outputs of the *Seperate Mass Flows* function

Inputs
gas (composite.Quantity): Quantity of gas with all relevant properties
*bypass (float):*The portion of flow not being combusted at all [-]
ω *(float):* The reacting portion of gas, as output of PaSR function [-]
Outputs
gas_def (composite.Quantity): The gas to deflagrate, as stored by Cantera
gas_not_def (composite.Quantity): The gas that will not deflagrate, but will combust, as stored by Cantera
gas_not_combust (composite.Quantity): That gas that will not combust, as stored by Cantera

The gas that was lost in the buffer zone is defined in a separate function, namely the *Define Gas Buffer Zone* function.

Table A.15: Table showing the inputs and outputs of the *Define Gas Buffer Zone* function

Inputs
mech (str): The name of the mechanism used for Cantera
mass_flow_lost (tuple): The total mass flow lost, and an indication of whether this is fuel (1), or oxidiser (2)
fuel (str): The name of the fuel
oxidiser (str): The name of the oxidiser
static_temp (float): The static temperature of the gas at the injector stration (3.2) [K]
static_pressure (float): The static pressure of the gas at the injector stration (3.2) [Pa]
Outputs
gas_buffer zone (composite.Quantity): he gas lost in the buffer zone, as stored by Cantera

The detonation calculations are done in the *Perform Detonation* function, with the use of the shock and detonation toolbox, as well as the two functions to include the heat loss factor χ: Equation 5.20 and Equation 5.21.

Table A.16: Table showing the inputs and outputs of the *perform detonation* function

Inputs
mech (str): The name of the mechanism used for Cantera *gas_det (composite.Quantity):* The gas entity for the detonation flow, as stored by Cantera *decay_pressure (float):* The pressure immediately preceding the detonation wave, minimum of pressure decay curve [Pa] χ *(float):* The portion of heat lost in the detonation *cell_size (float):* Cell size, None if it should be calculated here [m] *comp (dict):* Mass based composition of the gas at the injector station 3.2
Outputs
gas_post_det (composite.Quantity): Cantera quantity of the gas post detonation *detonation_temp (float):* The temperature immediately after the detonation was has passed [K] *detonation_pressure (float):* The pressure immediately after the detonation was has passed [Pa] *post_det_composition (dict):* The mass based composition immediately after the detonation was has passed [K] *entropy_post_det (float):* The entropy immediately after the detonation was has passed [J/kg K] *cj_speed (float):* Ideal detonation velocity [m/s] *cell_size (float):* Cell size of the propellant mixture [m] *detonation_velocity (float):* Actual speed of the detonation [m/s]

The static pressure at the end of the combustor is defined as the average of the pressure decay curve (represented by Equation 5.8). The function *Pressure Decay Model* first calculated an updated decay pressure, before defining this average pressure.

Table A.17: Table showing the inputs and outputs of the *pressure decay model* function

Inputs
steps (float): The number of steps in the injector discretisation [-] *decay_pressure (float):* The pressure immediately preceding the detonation wave, minimum of pressure decay curve [Pa] *detonation_pressure (float):* The detonation pressure resulting from the detonation calculations [Pa] *k (float):* The pressure decay parameter [-]
Outputs
average_pressure (float): The average pressure at the end of the combustion chamber [Pa]

The second continuity check, performed this time on the detonation pressure, is calculated in the *Check Detonation Pressure* function.

Table A.18: Table showing the inputs and outputs of the *check detonation pressure* function

Inputs
old_detonation_pressure (float): The detonation pressure of the previous iteration [Pa]
current_detonation_pressure (float): The detonation pressure calculated this iteration [Pa]
Outputs
iteration_decay_pressure (Boolean): True if the iteration loop should be run again
new_detonation_pressure (float): The detonation pressure for the next iteration

The recombination of all flows into a singular gas entity is performed in the *Mass Average Flows* function.

Table A.19: Table showing the inputs and outputs of the *Mass Average Flows* function

Inputs
flow1 (composite.Quantity): One of the four flows in the engine, stored as a Cantera gas quantity
flow2 (composite.Quantity): One of the four flows in the engine, stored as a Cantera gas quantity
flow3 (composite.Quantity): One of the four flows in the engine, stored as a Cantera gas quantity
flow4 (composite.Quantity): One of the four flows in the engine, stored as a Cantera gas quantity
*average_P (float):*The average pressure of the pressure decay curve [Pa]
Outputs
comb_gas (composite.Quantity): The combined gas, stored as a Cantera gas quantity

The structure for the potential inclusion of the oblique shock or heat loss to the walls is included in the *Loss Factors after Combustion* function.

Table A.20: Table showing the inputs and outputs of the *Loss Factors after Combustion* function

Inputs
st_temp (float): The static temperature of the gas after combustion [K]
tot_pressure (float): The total pressure of the gas after combustion [Pa]
mach (float): The Mach number of the gas after combustion [-]
Outputs
st_temp (float): The static temperature of the gas after inclusion of the loss factors [K]
tot_pressure (float): The total pressure of the gas after inclusion of the loss factors [Pa]
mach (float): The Mach number of the gas after inclusion of the loss factors [-]

The full list of RDE attributes that were added to the RDE during the combustion model, as well as the methods used during this model can be seen below.

Table A.21: Table showing the additional RDE attributes after the completion of the combustion models

Attributes
rde (RDE_Actor): the stored RDE to model, containing the additional variables:

average_combustor_pressure (float): The average pressure at the end of the combustion chamber[Pa]
cj_speed (float): The detonation velocity of a CJ detonation [m/s]
er_def (float): The equivalence ratio for the combustion reactions [-]
omega (float): The factor representing how much propellant undergoes parasitic deflagration [-]
steps (float): The number of steps used in the nozzle discretisation [-]
xi (float): The portion of heat kept during the detonation [-]

A.4. Nozzle Models

The Mach number at the nozzle exit with a converging-diverging nozzle is calculated with the *Calc. Mach Number* function, and utilises Equation 5.25.

Table A.22: Table showing the inputs and outputs of the *Calc. Mach Number* function

Inputs
exit_area (float): The area of the nozzle exit [m$\hat{2}$]
gas (composite.Quantity): Quantity of gas with all relevant properties
throat_area (float): The area of the nozzle throat [m$\hat{2}$]
Outputs
exit_mach (float): The Mach number at the nozzle exit [-]

A.5. Auxiliary Functions

Table A.23: Table showing the outputs of the *find gas properties* function

Inputs
gas (composite.Quantity): Quantity of gas with all relevant properties
st_temp (float): The static temperature of the gas [K]
tot_pressure (float): The total pressure of the gas [Pa] (Optional)
st_pressure (float): The static pressure of the gas [Pa] (Optional)
mach (float): The Mach number of the flow [-] (Optional)
Outputs
gas_prop (dict): contains for both Oxidiser and Fuel (or the mixed gas):
cp (float): The specific heat at constant pressure of the gas [J/kg K]
entropy (float): The entropy of the gas [J/kg K]
flow_velocity (float): The flow velocity of the gas [m/s]
gamma (float): The specific heat ratio of the gas [-]
gas_composiotn (str): String containing the composition of the gas
mach (float): The Mach number of the gas [-]
molar_mass (float): The average molar mass of the gas [g/mol]
st_density (float): The static density of the gas [kg/m$\hat{3}$]
st_enthalpy (float): The static enthalpy of the gas [J/kg]
st_pressure (float): The static pressure of the gas [Pa]
st_temp (float): The static temperature of the gas [K]
tot_enthalpy (float): The total enthalpy of the gas [J/kg]
tot_pressure (float): The total pressure of the gas [Pa]
tot_temp (float): The total temperature of the gas [K]

B

Methodology of the Creation of the Model

In the planning for this thesis, it was decided to start with the basics in terms of modelling. Building a working, if less accurate, model and expanding on this by adding detail and phenomena is more desirable than modelling complex phenomena from the ground up. Hence, the creation of the model used a *fidelity levels* approach, first creating a model with only the basic structure and capabilities, and adding increasing levels of complexities to it. This approach also prevents the model from becoming more complex than necessary, as only the necessary additions will be included.

A description of the physical phenomena that should be implemented in each of the levels can be seen in Figure B.1. Fidelity level one consists of the most simple building blocks: the most simple model possible is an injector, a combustor process and a nozzle. In addition to this, a plenum is required to ensure the inputs can accurately be implemented. Using constant injection and a constant volume combustion process eliminates the need to make it time and spatially variable, thereby reducing the complexity even further, and keeping it a true one-dimensional model. An iteration is needed between the combustion and plenum processes, as well as between the plenum and injector, to ensure the continuity is being met in the full RDE.

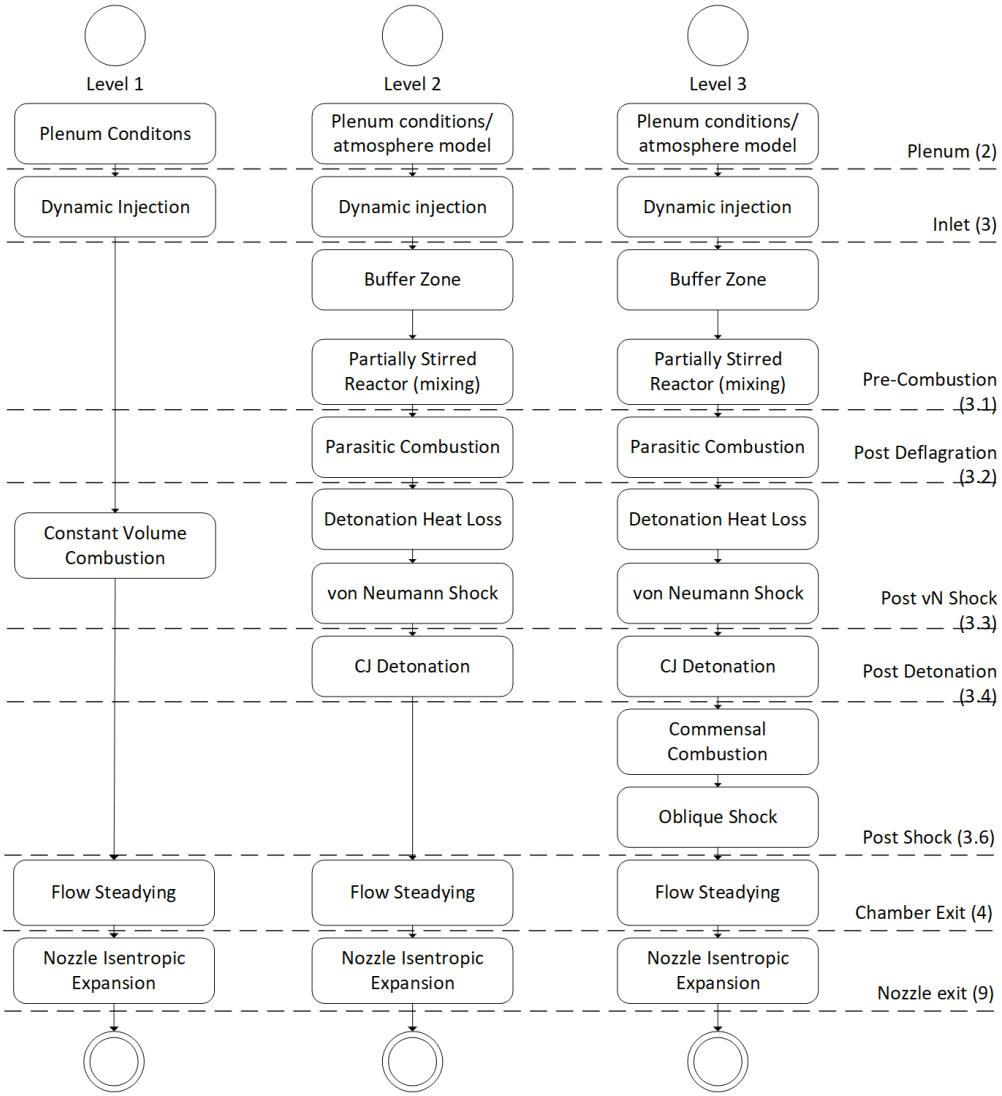

Figure B.1: Diagram of the three main fidelity levels during the creation of the model

The second fidelity level is intended as a step between the fully detailed mixing and combustion simulations. The aspects that can be implemented individually should be implemented, and the model should be functional before continuing to the next fidelity level. This level includes an aspect of mixing (in the PaSR), some loss effects occurring in the chamber (parasitic combustion and oblique shock), and the ZND model of the detonation. The PaSR implementation was deemed necessary for the determination of the amount of parasitic deflagration. This parasitic deflagration is, along with the oblique shock, determined to be the largest order loss effects on the performance of the RDE. Additionally, it was deemed necessary to create a detailed detonation simulation at this stage. Lastly, due to the difference in behaviour of the injector and combustor when compared to the previous level, a new iteration should be added between calculationg the detonation pressure and the plenum properties.

The third fidelity level includes the remainder of the phenomena identified in chapter 3 to have a significant impact on the function of the model, namely the commensal combustion and the effect of the oblique shock in the combustion chamber. While it was the intention to add this fidelity level, it was decided in discussion with TNO that a detailed validation and performance assessment was of larger significance to the use of the model in the future.

B.1. Fidelity Level One

The start of the coding of the model was created by implementing the structure similar to that as described in (figure). An initial guess is made for plenum pressure. The model then calculates the plenum, injector, and combustor properties. A continuity check is then performed to determine whether the pressure at the end of the combustion chamber is consistent with the pressure required for nozzle choke. If yes, the model continues to calculate the nozzle properties, but if this criterion is not met, an adjustment is made to the plenum pressure and the model is run again.

It was rather quickly realised that the current iteration/approach did not work: There was such a large error in the continuity check, that the iteration was unable to converge. After some reasoning it was determined that the problem lies with the coupling of the injector and the combustion chamber. In the current version of the model there is no accounting for the potential backflow to the plenum. In this adjustment process, it was initially thought that assuming time-constant injection was not valid, and that the pressure variations in the injector and chamber has to be spatially integrated. However after some further work it was noticed that the problem lies with the mass flow reduction due to nozzle blockage after the passage of the detonation wave. Removing a portion of both the mass flow and the injector area allows this blockage to be implemented without having to integrate a 2D model. This new approach keeps the simplicity and integrity of the stated 1D approach towards the RDE model.

The combustion and injector modelling was also implemented in more detail; a simple pressure decay model simulates the pressure within the detonation chamber. This decay model ranges from peak detonation pressure, to a given decay pressure, and is used to find the post-injector and average combustion chamber exit pressures. During the implementation of this, it was rather quickly realised that an additional two iteration loops are needed, as an initial guess for both the peak detonation and decay pressure is made.

This first loop determined the decay pressure to ensure the injector properties remain constant, and is completed entirely within a single function of the model. The second is the iteration over the nozzle throat, as described above, and causes the model to run again in (almost) it's entirety if there is no convergence.

However, during the implementation of this new methodology, it was found the model still does not converge. The assumption that mass flow is lost over the injector is physically incorrect, and as such he above will not be realistic. Instead, the plenum pressure is iterated over the injector until the mass flow through the injector, including the blockage factor, is equal to the set point. A following iteration is then done to match the decay pressure with the pressure resulting from the iterated injector, after which the combustion process is modelled. The final iteration is implemented over the assumption of nozzle choke, and the peak detonation pressure is altered if continuity is not yet met here.

B.2. Fidelity Level Two

After the completion of the first fidelity level, the approach for fidelity level 2 was further detailed. During this process, it was noticed that the implementation of the buffer zone is an important part of the mixing process. While it would be possible to implement this in fidelity level 3, this would require significant alterations to the code at that point. Additionally, the implementation of the buffer zone works well together with the implementation of the PaSR, and it was hence decided to pull this forward to fidelity level 2.

To once again make the steps between levels more equal, it was decided to push the calculation of the oblique shock back to fidelity level 3. This calculation is not expected to require a detailed integration with the remainder of the code, and as such can easily be swapped around.

When viewing the combustion chamber as an unwrapped 2D shape, the equivalence ratio varies with respect to two variables within the combustion chamber; the azimuthal location of the injection with respect to the detonation wave, and the axial location of the flow. Both these parameters are related, and vary with time, which makes the separate modelling somewhat difficult. The variation in equivalence ratio with respect to the azimuthal location of the injector can be determined quite simply with the buffer zone model. However, when the introducing the axial variance, multiple PaSRs should be implemented along the azimuthal axis, each modelling the axial variation in flow for that segment.

During the implementation of the PaSR, it was noticed that this method is very computationally intensive. Two different PaSR methods were implemented to compare, one with Cantera keeping track of all gas properties, and a simplified version where only the composition is modified. Using the simplified model, it was noticed that at least 20,000 volume elements are necessary to make the statistical methods within a PaSR valid. Using this, a single run of the most simplified PaSR possible takes about 5 seconds, while the more complex run takes over 20 minutes. Unfortunately, to achieve the spatial variation necessary to model even the simplified RDE would require a number of PaSR's implemented. Hence, an alternative methods is necessary.

This alternative method was found to be a simplified form of PaSR typically used in CFD applications highlighted by *Akerblom* [76] which relies on knowledge of flow and reaction properties as opposed to a computation-heavy statistical approach. This implementation requires a simple calculation and results in a singular value of reacting mixture fraction.

After the implementation of this last PaSR method, the implementation of the detailed detonation calculations started, using the shock and detonation toolbox and Cantera. The shock and detonation toolbox is used in three separate occasions; calculating the ideal CJ velocity for the given gas, determining the properties of the von Neumann shock, an finally determining the properties after the ZND detonation. However, these three calculations combined take between the 8-16 seconds to complete, meaning the requirement for computation time has already been exceeded. Additionally, these combustion calculations take place in the convergence loop for mass flow through the throat, meaning they are completed between 3-8 times in a full model calculation. These calculation speeds depend mainly on the equivalence ratio chosen, as Cantera, like CEA has more difficulty computing equilibrium states when near stoichiometric combustion.

However a solution to this problem was easily found, as different Cantera reaction mechanisms have significantly different computation times. Using the Mevel2018 mechanism resulting in a run time varying from 50 to 300 seconds, while switching to the Mevel2017 mechanism lowered this to a consistent 4 seconds.

With this implementation and switch, the model was complete, and the validation for this level could start. A set of test data from the 2024 TNO RDE test campaign was used as an initial validation set. With the initial validation steps, it was found there were significant differences between the test results and the model output, mostly significantly in the plenum and chamber pressures, and the chamber temperatures. This is an indication there may still yet be errors in the model, which need to be fixed.

After some debugging it was found that the mass flow was not properly traced between the stations. This was fixed by implementing the Cantera solutions as quantities, which have a mass stored within. This removed the need to keep track of the mass flow separately, and eliminated the possibility of losing/gaining some mass along the simulation.

In addition, a few more problems were found that contributed to small errors in the code. These fixes improved the static temperature and static enthalpy values in the nozzle calculations, and the entropy and both temperature values in the combustion calculations. Additionally, a check was implemented to ensure all temperature values at all stations match the entropy and pressure values of the gas. In this way, all properties of both the static and total gas should be consistent.

Lastly, after reviewing the code, it was determined that the manner of iteration over the detonation and decay pressure throughout the model was inefficient, and an artefact of the upgrade from the first to the second fidelity level. A simpler approach was now available, with the variable injector implemented, the necessity for keeping the downstream pressure constant over the model was removed, and the second (small) iteration could be expanded to a larger iteration over the detonation pressure. The nozzle continuity check then became an iteration of mainly the decay pressure, and as such a much cleaner set of iterations for the detonation and decay pressure was created.

This finalised the last few changes made to the code before the preliminary validation round started, and Fidelity level 2 is complete.

C

Adding Additional Propellants

The model is currently only suitable for the use of H2 as fuel, and air as oxidiser. However, there is a high likelihood that different propellant combinations are required in the future. This appendix is created to show the steps required to add a new fuel or oxidiser to the model.

There are five aspects in the code that must be added to with the addition of a new propellant. These sections are described below.

C.1. Reaction Mechanism

Cantera works with reaction mechanisms. These are files that store the possible reactions with a combinations of propellants. Hence, with a new propellant type, a suitable mechanism file must be selected and obtained. The mechanism file used for the H2 and air combination is the *'Mevel2017.yaml'* file. With a new mechanism file selected, the *self.mech* parameter in the *RDE_Builder* class must be adjusted. This is done in the initialisation of the model, and the specific line can be seen below.

```
self.mech = 'Mevel2017.yaml'
```

C.2. Detonability Limits

Whether a propellant is able to detonate or not depends largely on the ratio of the fuel to the oxidiser, the equivalence ratio. If the equivalence ratio falls below, or climbs above certain limits, there is a high chance that the propellant combination will not be able to detonate, and hence the RDE will not function.

For the combination of H2 and air, these limits are 0.287 and 1.77 [70].

These detonability limits are currently hard-coded into the *check detonability* function, described in subsection 5.1.4, and the code describing this can be seen below.

```
        if self.fuel == 'H2' and self.oxidiser == 'Air':
            if self.er <= 0.28 or self.er>=1.77:
                self.detonability = False
                raise Warning("Propellant combination input does not fall within"
                              "detonability limits")
            else:
                 self.detonability = True
        else:
            raise Warning("Incorrect propellant combination selected")
```

If a new propellant combination is added, the detonability limits must be determined and can be added into this function.

C.3. Setting Gas Properties

When working with Cantera, the gas entities should be given an initial composition, which depends on the propellants used in the RDE. There is a check implemented in the plenum model which sets the

composition of the fuel and oxidiser seperately based on the propellant types. This must also be added to when a new fuel or oxidiser is used.

The code for this check can be seen below.

```
        # Check fuel/oxidiser types
        if self._rde.oxidiser == "Air":
            self._rde.ox = "O2:0.21,N2:0.79"
        else:
            raise Warning("Oxidiser type not supported")
        if self._rde.fuel == "H2":
            self._rde.fu = "H2:1"
        else:
            raise Warning("Fuel type not supported")
```

C.4. Mass Flow Separation

When both the fuel and oxidiser flows are combined together, they are represented with a total mass flow and equivalence ratio. To once again separate these flows, the stoichiometric fuel to oxidiser ratio must be known, and can be added into the relevant section of the code. With the H2 and air combination this is approximated at 34.5. This mass flow separation function can be found in the Utils file.

The relevant section of code can be seen below.

```
                if prop_types[0] == "Air" and prop_types[1] == "H2":
                        fuel_to_ox_stoich = 1 / 34
```

C.5. Partially Stirred Reactor

The Partially Stirred Reactor (PaSR) model has a number of inputs that are specific to the fuel and oxidiser combination used. These inputs can be provided as separate inputs to the model, but should also be added into the *PaSR* function for completeness of the model.

The PaSR parameters are the effective viscosity at the right equivalence ratio (or the effective viscosities of the fuel and oxidiser components), the turbulent dissipation rate, the kinematic viscosity, and the laminar flame speed. The value and method of calculation of these parameters for the combination of H2 and air can be seen in the code below.

```
        if self._rde.oxidiser == "Air" and self._rde.fuel == "H2":
            if self._rde.v_eff is None:
                self._rde.v_eff = (8.9 * m1 + 18.46 * m2) / (m1 + m2) * 1e-6  #
                    Effective viscosity of mixture [Pa s]
            if self._rde.epsilon is None:
                self._rde.epsilon = 18  # Turbulent dissipation rate (see Wang.
                    etal_2021)
            if self._rde.v is None:
                self._rde.v = 0.1 * self._rde.v_eff * gas.density  # Kinematic
                    viscosity is factor * viscosity * density
            if self._rde.su is None:
                self._rde.su =  1.7 * gas.T/285 # Laminar flame speed (taken from
                    Combustion, Irvin Glassman, Appendix F)
                else:
                        print("Propellant combination is ", self._rde.oxidiser, ' and '
                            ,self._rde.fuel)
                        raise Warning("Combination of Propellants not supported")
```

D

Model Useage

This appendix described how the model should be used. There are three methods of running the model, and the ideal usage methods will depend on the application. When wanting to run the model a single time, or to play around with values to determine outcomes etc., the user interface method is the best to use. This interface can be seen in Figure D.1.

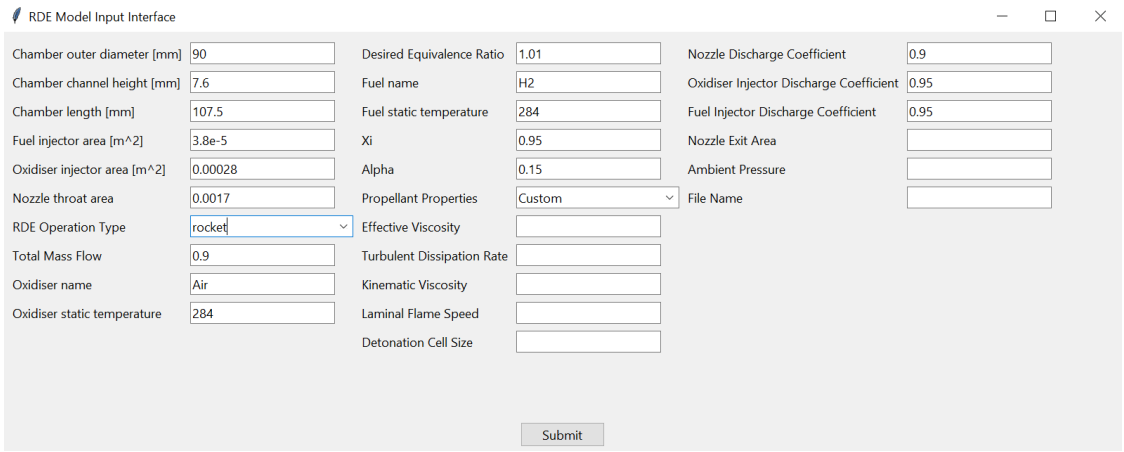

Figure D.1: The method of giving inputs to the model using the interface screen

However this interface does not store the input parameters, so when changing only a few parameters at a time, it may be better to type the input list directly into python. In this case, the basic code to run the model is shown below.

```
if __name__ == "__main__":
    inputs = [
        90,             # Chamber_outer_diameter
        7.6,            # Chamber_channel_height
        107.5,          # Chamber_length
        3.8E-05,        # Fuel_injector_area
        0.00028,        # Ox_injector_area
        1.01,           # Desired_equivalence_ratio
        0.0017,         # Nozzle_throat_area
        ['rocket',[0.9, "Air",284]], # Type of RDE operation ('rocket' or 'airbreathing')
        # With corresponding inputs, for rocket: [tot_mass_flow, ox_type, ox_static_temp]
        # ['rocket',[0.9, "Air",284]]
        # for airbreathing: [mach, altitude, inlet_area, mcf, prf]
        # ['airbreathing', [5, 12000, 0.003, 1, 1]]
        ["H2", 284],    # Fuel:
```

```
        # [fuel name , fuel_static temp]
        None,                   # Propellant prop.:
        # [effective viscosity, turbulent dissipation rate, kinematic viscosity,
            laminar flame speed, detonation cell size]
        0.95,                   # Xi
        0.1,                    # Alpha
        [0.9, 1, 0.85], # Cd's:
        # [Nozzle discharge coefficient, Oxidiser injector discharge coefficient, Fuel
            injector discharge coefficient]
        None,                   # Nozzle_exit_area
        None,                   # Ambient_pressure
        None,                   # File_name
        ]

    [Input, Geometry, Performance, GasProp] = run_rde_model(inputs)
```

Lastly, the model can be set to run multiple times, through a variety of input conditions. This can easily be implemented with the excel version of the input list, as seen in Figure D.2.

Model Number	1	2	3
Chamber Outer Diameter	90	90	90
Chamber Channel Height	7.6	7.6	7.6
Chamber Length	107.5	107.5	107.5
Fuel Injector Area	3.84845E-05	3.84845E-05	3.84845E-05
Oxidiser Injector Area	0.000282743	0.000452389	0.000452389
Equivalence Ratio	0.7	0.85	0.85
Nozzle Throat Area	0.001475543	0.001475543	0.001475543
RDE Operation	'rocket';0.3,'Air',284	'rocket';0.7,'Air',289	'rocket';0.7,'Air',289
Fuel	H2,293.0	H2,288.6	H2,309.2
Propellant properties			
Xi	0.95	0.95	0.95
Alpha	0.1	0.1	0.1
Cd	0.9,1,0.9	0.9,1,0.9	0.9,1,0.9
Nozzle Exit Area			
Ambient Pressure			
Output File Name	HF-033	HF-044	HF-045

Figure D.2: The method of giving inputs to the model using the excel input sheet

When running the RDE model multiple times, a code similar to what is shown below is used, where a try, except methodology is implemented inn case a warning is raised within one of the input sets. Aside from the output .txt results file, additional relevant outputs can be extracted and stored in an excel file if useful.

```
excel_file = pd.read_excel('Validation_Inputs.xlsx')
with open("Validation_results.txt", "w") as f:
    for i in range(10):
        inputs = list(excel_file[i+1])
        try:
            [Input, Geometry, Performance, GasProp] = run_rde_model(inputs)
                excpet:
                        print('Validation run ',inputs[16],' was unable to converge')

        print('completed calculation round', inputs[16])
```

Additionally, an example output to the model is shown below.

```
------------------------------------------------------------------------
                                                RDE Model
------------------------------------------------------------------------

PROPELLANTS
Fuel type                                :       H2
Oxidiser type                    :       Air
Equivalence ratio                :       1.01
Total mass flow                          :       0.9

```

```
GEOMETRY
Chamber outer diameter   :       0.09 [mm]
Chamber channel height   :       0.0076 [mm]
Chamber length                   :       0.1075 [mm]
Oxidiser injector area   :       0.00026599999999999996 [m^2]
Fuel injector area               :       3.61e-05 [m^2]
Nozzle throat area               :       0.00153 [m^2]
Nozzle exit area                 :       0.00084 [m^2]

MODEL INPUTS
Portion deflagration in detonation (alpha)       :       0.15
Portion heat loss in detonation (chi)            :       0.95

PERFORMANCE
Pressure gain                    :       -53.63 [%]
Combustion efficiency    :       0.78 [-]
Isp                                              :       160.15 [s]
Thrust                                   :       1413.97 [N]
Detonation velocity              :       1944.96 [m/s]

------------------------------------------------------------------------
                                        Thermodynamic Properties
------------------------------------------------------------------------
Station                                  :                                2
                     3.2             4                       8                          10
Static pressure                  [bar]                   16.34           4.33
                   6.34                      4.18                    1.0
Total pressure           [bar]                   16.34           16.3
           7.58                    7.58                    7.58
Static temperature       [K]                     284.0           194.44          2002.93
             1837.43         1365.92
Total temperature        [K]                     284.0           285.03          2078.2
              2080.03          2107.53
Static enthalpy                  [kJ/kg]                 -14.31          -145.52
           -92.39          -371.43         -1139.11
Total enthalpy           [kJ/kg]                 -14.31          -18.54          35.85
              38.99           86.04
Entropy                                  [kJ/kgK]                6.04
           7.7                     10.38           10.38           10.4
Mach no.                         [-]                     0                       1.51
                         0.54                    1.0                     1.99

Molar mass                       [g/mol]                 28.85           20.56
           23.57           23.57           23.57
Gamma                            [-]                     1.4                     1.41
                         1.26                    1.27                    1.29

------------------------------------------------------------------------
```

E

Model Verification

This appendix contains the background information needed for the verification of the model, found in chapter 7. The graphs for the sensitivity analysis for the PaSR can be found in section E.1. The graphs for the sensitivity analysis on the pressure decay curve can be found in section E.2.

E.1. PaSR Verification

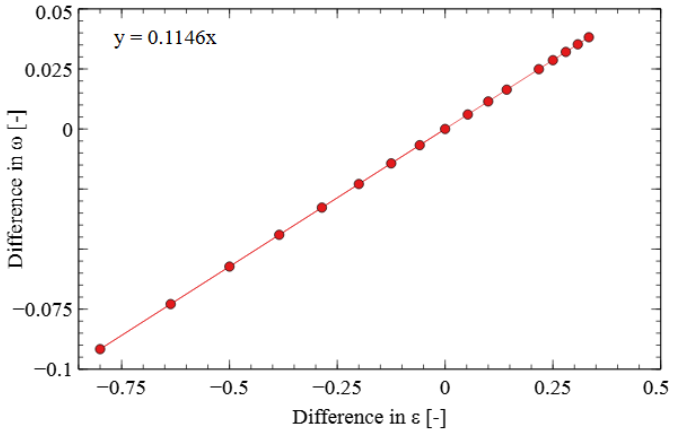

Figure E.1: The results of the sensitivity analysis on the effect of the turbulent dissipation rate on the factor ω

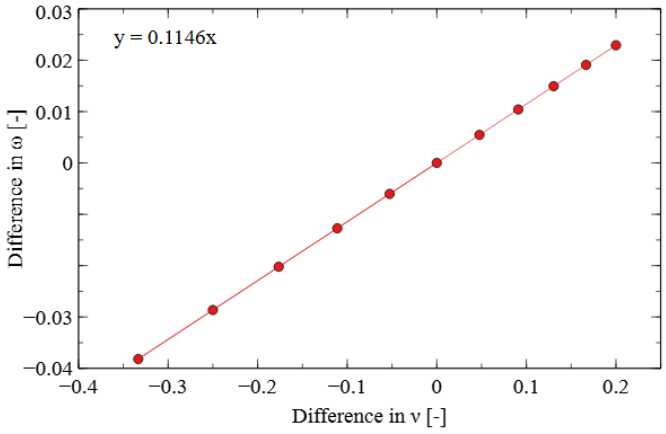

Figure E.2: The results of the sensitivity analysis on the effect of the kinematic viscosity on the factor ω

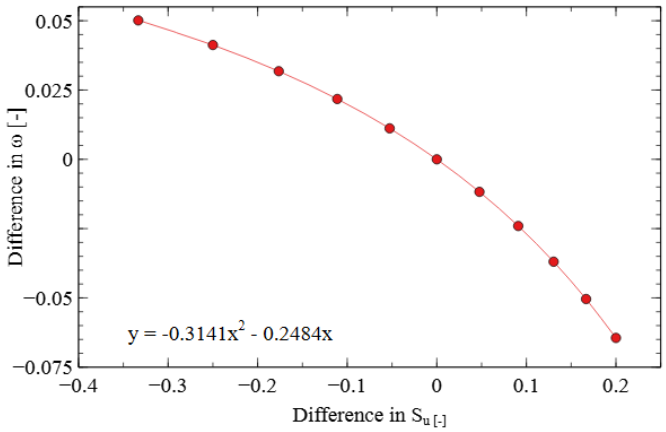

Figure E.3: The results of the sensitivity analysis on the effect of the linear flame speed on the factor ω

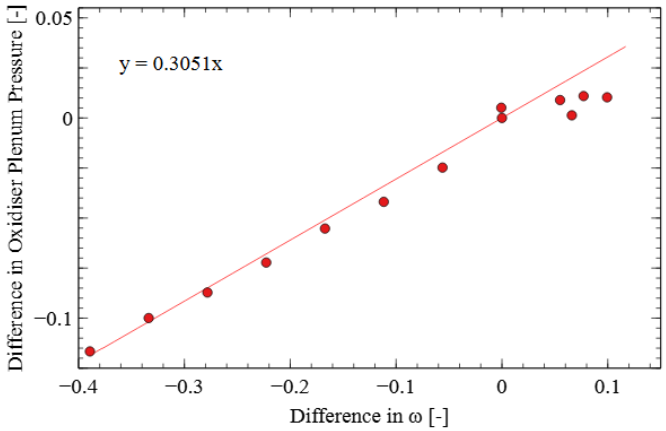

Figure E.4: The results of the sensitivity analysis on the effect of the factor ω on the oxidiser plenum pressure

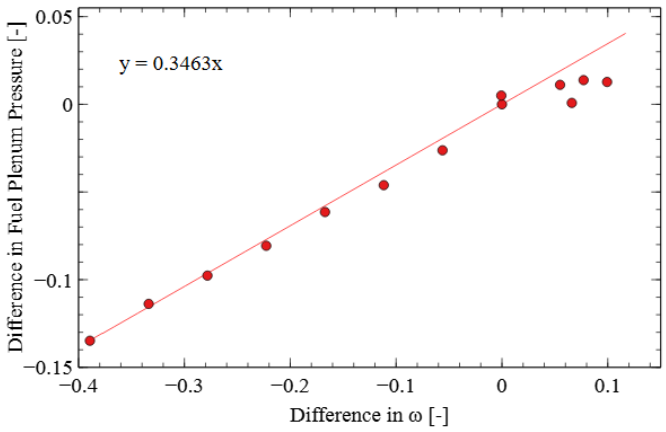

Figure E.5: The results of the sensitivity analysis on the effect of the factor ω on the fuel plenum pressure

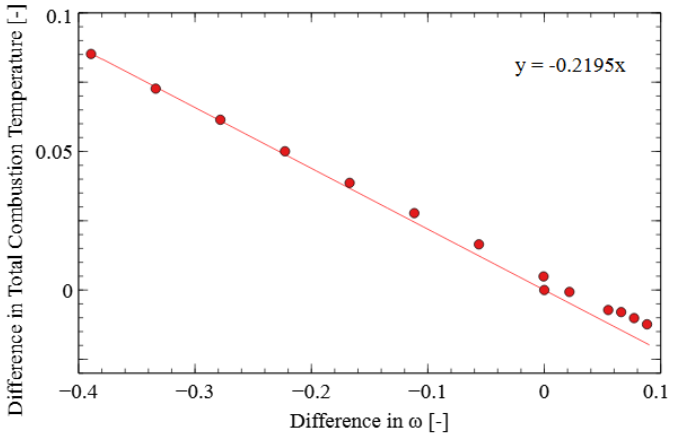

Figure E.6: The results of the sensitivity analysis on the effect of the factor ω on the total combustion temperature

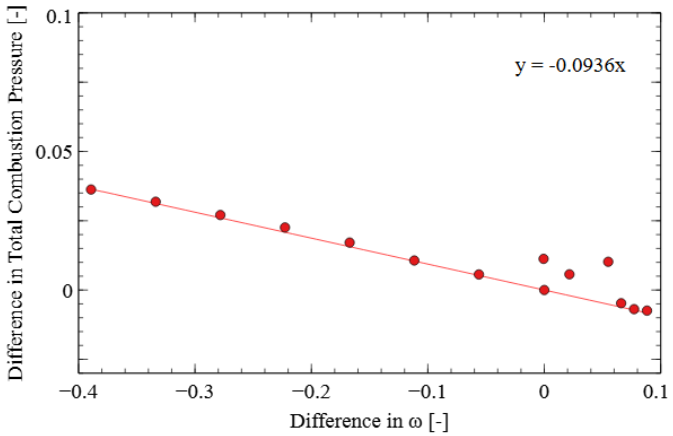

Figure E.7: The results of the sensitivity analysis on the effect of the factor ω on the total combustion pressure

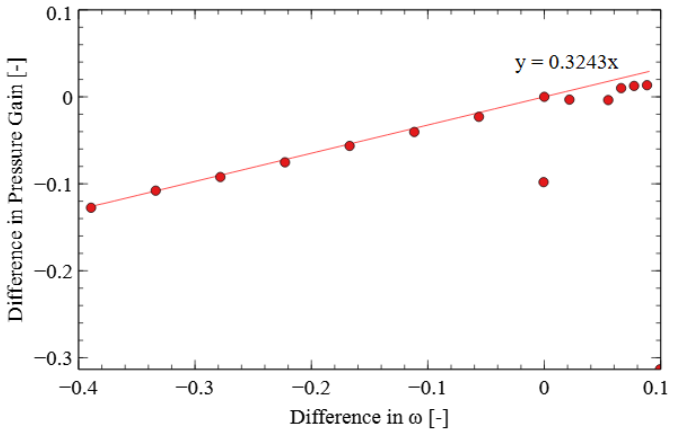

Figure E.8: The results of the sensitivity analysis on the effect of the factor ω on the pressure gain

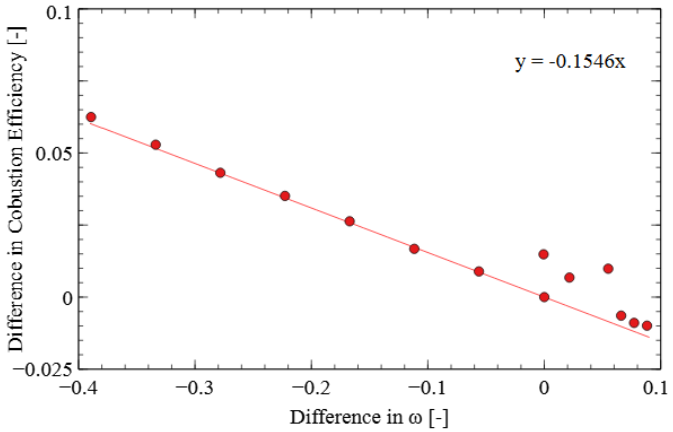

Figure E.9: The results of the sensitivity analysis on the effect of the factor ω on the combustion efficiency

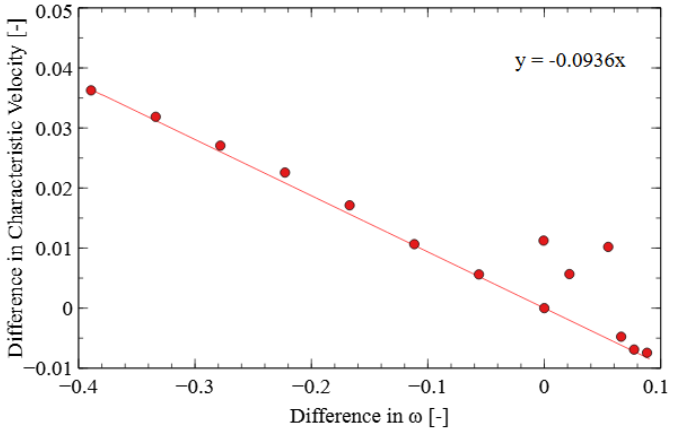

Figure E.10: The results of the sensitivity analysis on the effect of the factor ω on the characteristic velocity

Table E.1: The results of the combined sensitivity analysis, showing the absolute effect a 10% change in any of the three PaSR inputs has on the relevant RDE parameter.

PaSR Input	Parameter	Change in parameter [%]
Turbulent Dissipation Rate	Oxidiser Plenum Pressure	0.36
	Fuel Plenum Pressure	0.4
	Total Combustion Temperature	0.24
	Total Combustion Pressure	0.1
	Pressure Gain	0.37
	Combustion Efficiency	0.17
	Characteristic Velocity	0.1
Kinematic Viscosity	Oxidiser Plenum Pressure	0.36
	Fuel Plenum Pressure	0.4
	Total Combustion Temperature	0.24
	Total Combustion Pressure	0.1
	Pressure Gain	0.37
	Combustion Efficiency	0.17
	Characteristic Velocity	0.1
Laminar Flame Speed	Oxidiser Plenum Pressure	0.65
	Fuel Plenum Pressure	0.74
	Total Combustion Temperature	0.44
	Total Combustion Pressure	0.19
	Pressure Gain	0.67
	Combustion Efficiency	0.32
	Characteristic Velocity	0.19

E.2. Pressure Decay Curve Verification

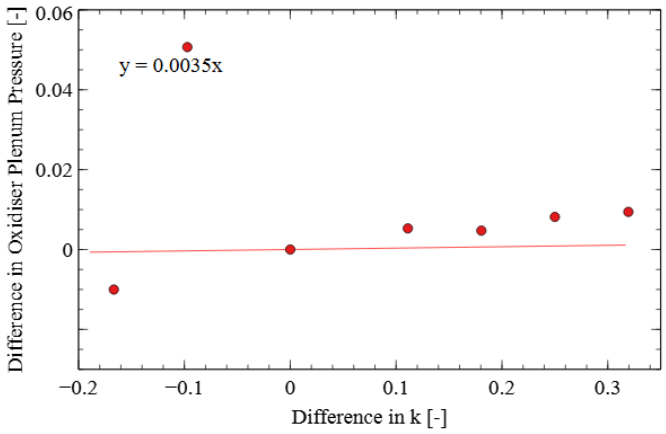

Figure E.11: The results of the sensitivity analysis on the effect of the factor k on the oxidiser plenum pressure

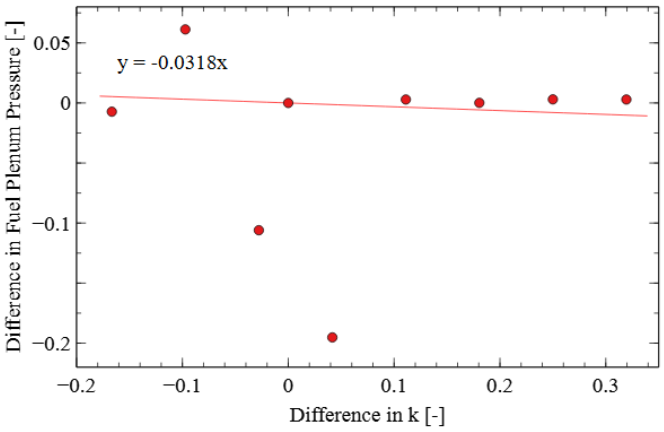

Figure E.12: The results of the sensitivity analysis on the effect of the factor k on the fuel plenum pressure

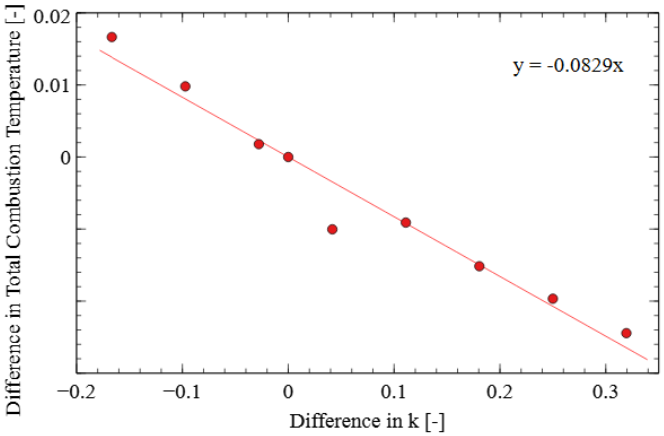

Figure E.13: The results of the sensitivity analysis on the effect of the factor k on the total combustion temperature

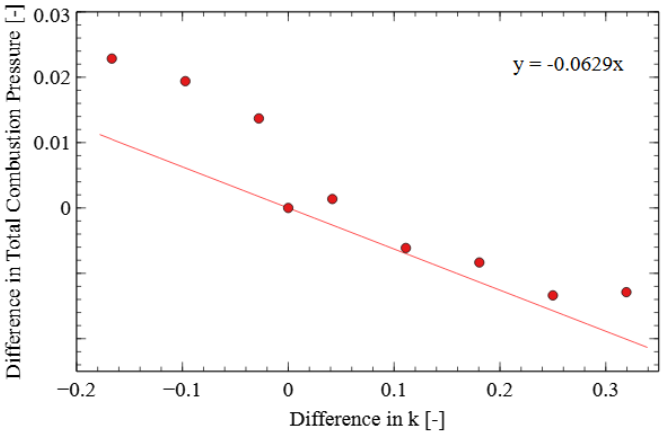

Figure E.14: The results of the sensitivity analysis on the effect of the factor k on the total combustion pressure

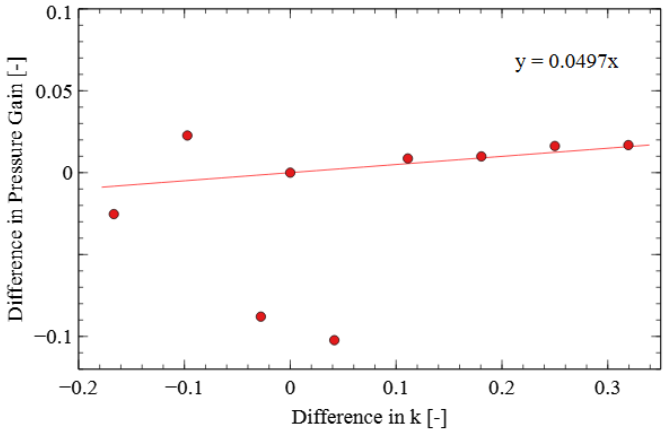

Figure E.15: The results of the sensitivity analysis on the effect of the factor k on the pressure gain

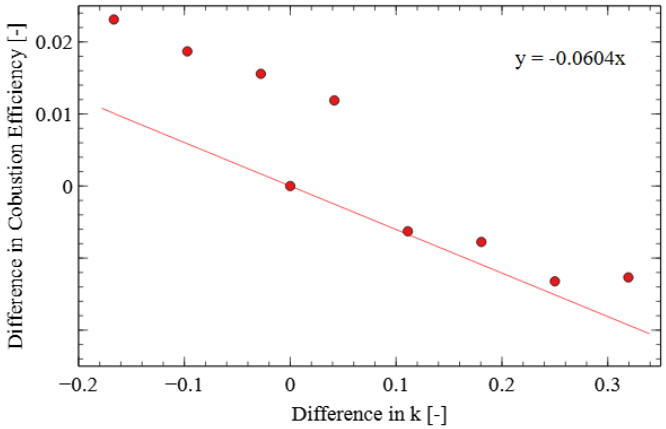

Figure E.16: The results of the sensitivity analysis on the effect of the factor k on the combustion efficiency

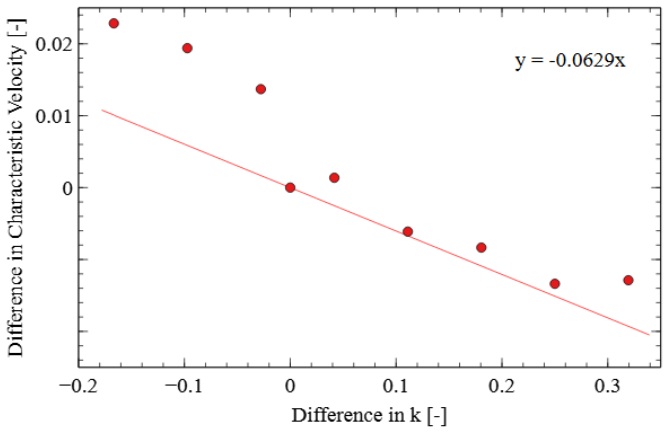

Figure E.17: The results of the sensitivity analysis on the effect of the factor k on the characteristic velocity

F

Model Validation

This section shows the remainder of the results of the validation that were not presented in chapter 7.

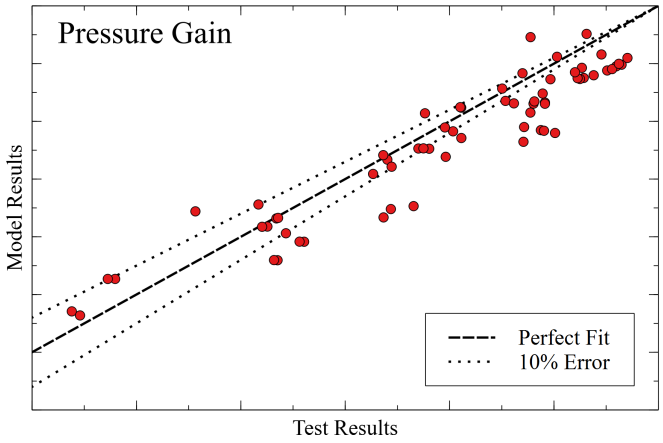

Figure F.1: The validation results showing the combustion efficiency resulting from test results compared to the model output for the selected runs

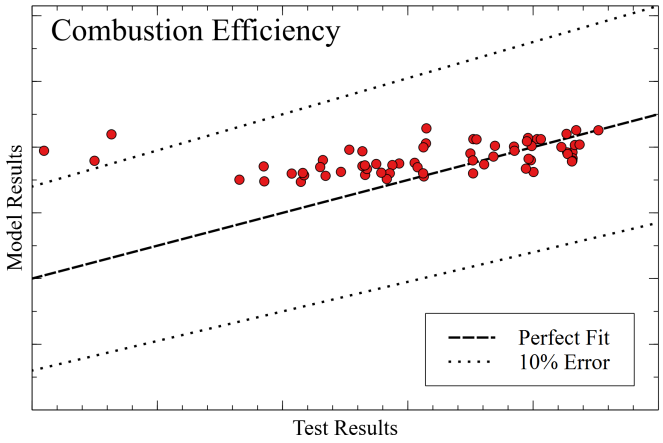

Figure F.2: The validation results showing the characteristic velocity resulting from test results compared to the model output for the selected runs

G

Additional Performance Assessment Plots

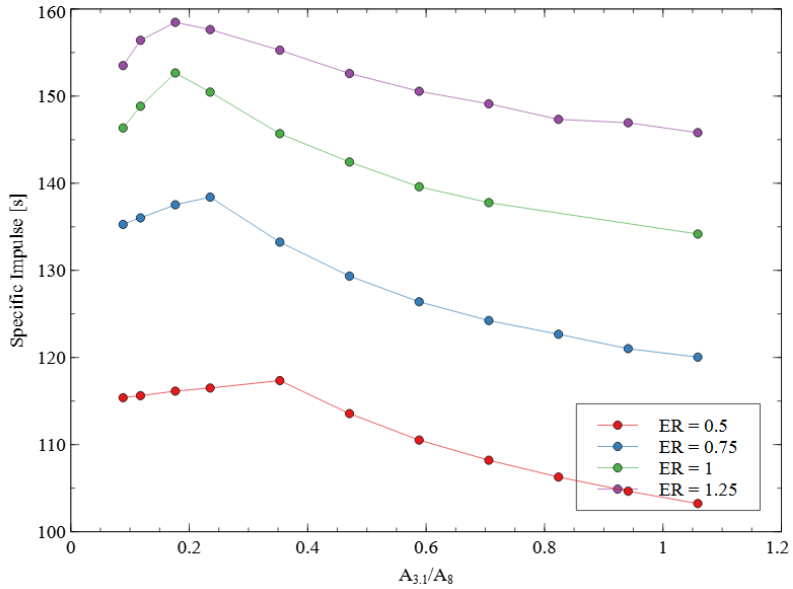

Figure G.1: The relationship between the area ratio, ($A_{3.1}/A_8$), and specific impulse of the RDE, with lines for different equivalence ratios.

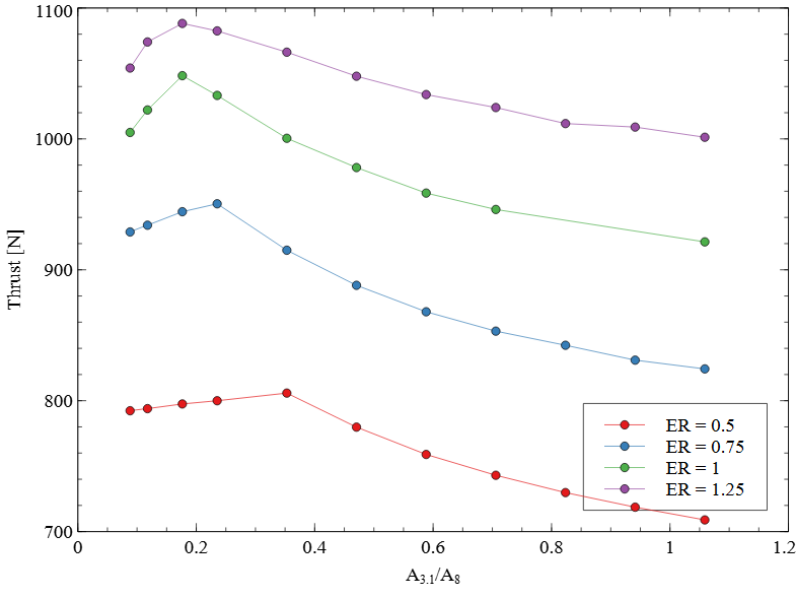

Figure G.2: The relationship between the area ratio, ($A_{3.1}/A_8$), and thrust of the RDE, with lines for different equivalence ratios.

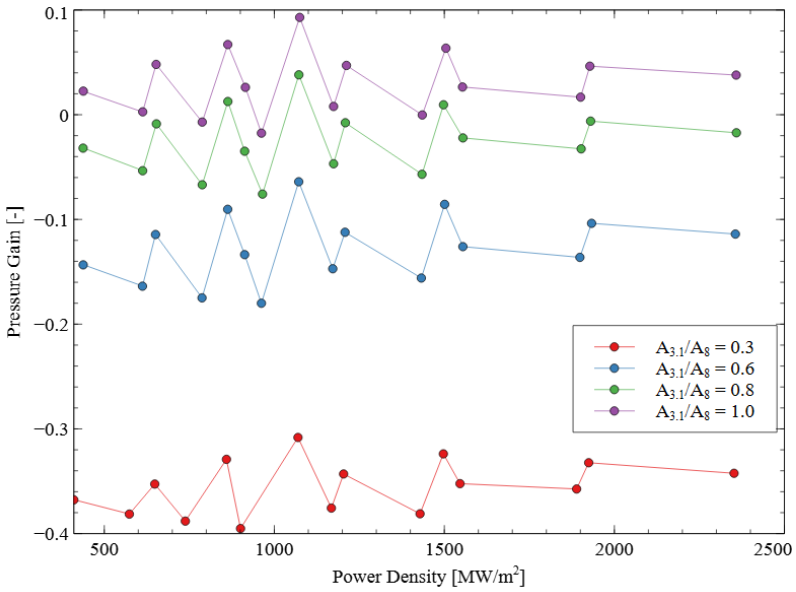

Figure G.3: The relationship between the power density, and the pressure gain of the RDE, with lines for different area ratios, ($A_{3.1}/A_8$).

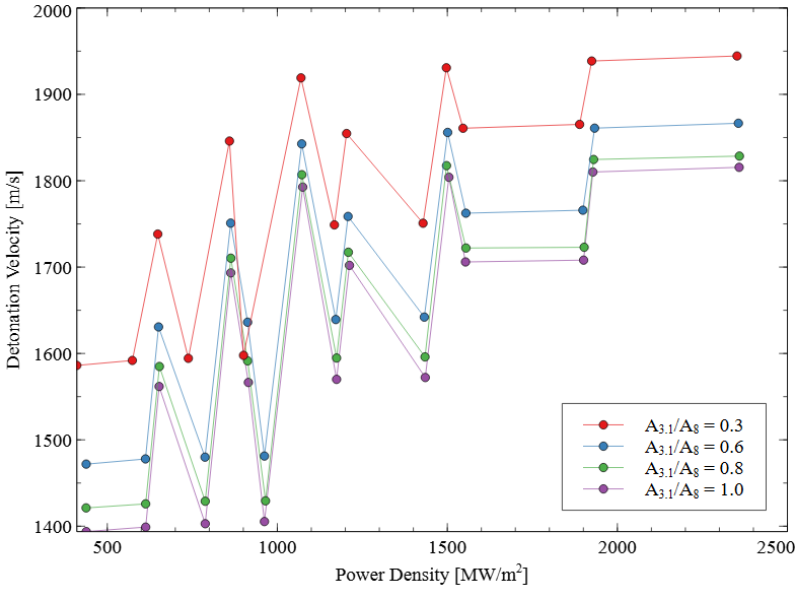

Figure G.4: The relationship between the power density, and detonation velocity of the RDE, with lines for different area ratios, $(A_{3.1}/A_8)$.